Universidad De Málaga

Escuela Técnica Superior de Ingeniería de Telecomunicación

Tesis Doctoral

PERFORMANCE OF SC-FDMA WITH DIVERSITY TECHNIQUES OVER LAND MOBILE SATELLITE CHANNEL

Autora

Jyoti Ramesh Gangane
Master in Electronics and Telecommunication
Master Universitario en TechnologiasÂ de Telecommunicacion

Directores

Mª Carmen Aguayo Torres y **Juan Jesús Sánchez Sánchez**
Doctores Ingenieros de Telecomunicación

Año 2016

Table of Contents

List of Tables

List of Figures

Acknowledgements

I would like to give the utmost gratitude to my thesis advisor, Dr. Mari Carmen Aguayo-Torres. She was kind enough to guide my thesis research during her busy schedules. She is my role model as a great engineer and teacher. Through numerous discussions and one to one meetings, I learned many technical and nontechnical things from her.

I am also thankful to my co-supervisor, Dr. Juan J. Sánchez-Sánchez for his valuable guidance and support during research and clearing my doubts. I want to thank Ph.D. co-ordinators of the University of Malaga, Spain, for their kind support and guidance during submission of the Ph.D. thesis.

I want express sincere thanks honourable president Prof. M. N. Navale, Dr. Sunanda Navale and Vice president H.R. Mr. Rohit Navale, and Mrs. Rachana, Sinhgad Technical Education Society, Pune, sponsoring me for Ph.D. I want to thank Dr. M. S. Gaikwad, Principal, and Vice principal, Dr. D. D. Choudhary, Sinhgad Institute of Technology, Lonavala for their kind support and guidance. I wish to express my special thanks to Dr. Sandeep Inamdar, for his recommendations to gain Erasmus Mundus Mobility for Life Scholarship.

I would also like to thank Dr. Janhavi Inamdar, Dr. Shankar Nawale, and Mr. Vilas Deotare, HOD ETC, SIT, Lonavala, for their amiable support and motivation during research work.

I am also grateful to my friends Dr. Javier Martinez, Dr. David Morales, Maribel Delgado, Francisco Blánquez-Casado for their help and support in Communicacion Moviles

Laboratory, at the University of Malaga, Spain. I am also thankful to all the teaching and nonteaching staff of ETC Dept., SIT, Lonavala.

Lastly, I would like to thank my Parents, Inlaws, and my husband Ramesh Gangane, daughter, Tejali for their strong support. Their loving and caring words were sources of encouragement to me, and I am deeply grateful to them.

Abstract

The major expansion seen in wireless technologies over last two decades is a direct result of the increasing demand for high data rate transmissions. Third Generation Partnership (3GPP) developed Long Term Evolution (LTE) mobile communication to meet high data rate requirement. Besides cellular communications, Land Mobile Satellite (LMS) systems is a significant part of the wireless systems. The LMS system provides services that are not feasible via Land Mobile Terrestrial (LMT) systems over a wide area of the network with low cost. Next generation of wireless systems is expected to be formed by the convergence of what now are considered independent systems.

The demand for high data rate results in significant Inter-Symbol Interference (ISI) for single carrier systems over bandwidth and power limited channels. Overcoming the time and frequency selective nature of the propagation channel requires the use of powerful signal processing techniques. Recent examples include different transmitter/receiver diversity techniques for high data rate transmissions as well as including multiple antennas at transmitter/receiver known as Multiple-Input Multiple-Output (MIMO). Multiple antenna communication technologies provide significant advantages over single antenna systems. These advantages include extended range, improved reliability in fading environments and higher data throughputs. In certain environments (such as the uplink of a mobile link) usually only one antenna is available at the transmission. Thus, only Single-Input-Single-Output (SISO) or Single-Input Multiple-Output (SIMO) transmissions are feasible.

Orthogonal Frequency-Division Multiplexing (OFDM) has been a more widely used modulation technique due to its robustness against frequency selective fading channels, scalability, and MIMO compatibility. However, it suffers from a high Peak-to-Average Power ratio (PAPR) which may be particularly troublesome in uplink cellular and satellite downlink transmissions as costly high-power linear amplifiers are needed for transmitting terminals.

Single Carrier Frequency-Division Multiple access (SC-FDMA) has become an alternative to OFDM techniques, specifically used as the uplink multiple access schemes in 3GPP LTE. It is able to reduce the PAPR in the transmission, resulting in a relaxation of the constraints regarding power efficiency needed in user terminals and satellite units. The SC-FDMA can be described as a version of OFDMA in which pre-coding and inverse pre-coding stages are included at the transmitter and receiver ends respectively, thus symbols are transmitted in time but after processing in the frequency. Even with the use of OFDMA or SC-FDMA, inter-symbol interference has to be compensated by equalization, which is usually performed in frequency domain.

The aim of this dissertation is to provide a mathematical analysis of the performance of SC-FDMA over land mobile satellite channel. For this purpose, the channel will be modelled as a shadowed Rice channel such that its Line Of Sight (LOS) follows Nakagami distribution. We first describe OFDMA and SC-FDMA multicarrier modulation techniques. Then we undertake an analysis of OFDMA and SC-FDMA based on enhanced complex noise at the detector stage. We evaluate the Bit Error Rate (BER) and spectral efficiency performance of SC-FDMA for different depths of shadowing. Finally, SC-FDMA performance with receiver diversity techniques, such as Maximal Ratio Combining (MRC) and Equal Gain Combining (EGC), is also evaluated.

Resumen

La expansión vista en las tecnologías inalámbricas durante las últimas dos décadas es el resultado directo de la creciente demanda de las transmisiones de datos a alta velocidad. La asociación Third Generation Partnership (3GPP) desarrolló el estándar Long Term Evolution (LTE) para cumplir los requisitos de alta velocidad de datos. Además de las comunicaciones celulares, los sistemas móviles terrestres por satélite (Land Mobile Satellite, LMS) son una parte importante de los sistemas inalámbricos. El sistema LMS proporciona servicios que no son factibles a través de sistemas terrestres a través de una amplia red con un bajo costo. Se espera que la próxima generación de sistemas inalámbricos sea formada por la convergencia de lo que ahora se consideran sistemas independientes.

La demanda de la alta velocidad de datos resulta en una importante interferencia entre símbolos (Inter-Symbol Interference, ISI) para los sistemas monoportadora en canales de ancho de banda y potencia limitada. Superar la selectividad en el tiempo y la frecuencia del canal de propagación requiere el uso de potentes técnicas de procesamiento de señales. Ejemplos recientes incluyen diferentes técnicas de diversidad de transmisión/recepción para alta velocidad de datos, así como el uso de múltiples antenas en el transmisor/receptor, en la técnica conocida como Multiple-Input Multiple-Output (MIMO). Estas tecnologías proporcionan ventajas significativas sobre los sistemas de antenas individuales que incluyen mejor fiabilidad en entornos de desvanecimiento y caudales de datos más altas. En ciertos entornos (tales como el enlace ascendente de un enlace móvil) únicamente una antena está disponible en la transmisión. Por lo tanto, sólo son factibles esquemas con entrada individual y salida única (Single Input Single Output, SISO) o transmisiones con entrada única y múltiples salidas (Single Input Multiple Output, SIMO).

La multiplexación por división ortogonal en frecuencia (Orthogonal Frequency-Division Multiplexing, OFDM) es una técnica de modulación ampliamente utilizada por su robustez

frente a la selectividad en frecuencia de los canales, su escalabilidad y su compatibilidad MIMO. Sin embargo, sufre de una alta relación de potencia de pico a promedio (Peak-to-Average Power Ratio, PAPR) que puede causar muchos problemas en el enlace descendente de las transmisiones por satélite y en el enlace ascendente de las comunicaciones celulares. La razón es que se necesitan amplificadores de alta potencia muy lineales, lo que resulta costoso energéticamente para la transmisión.

La técnica monoportadora con acceso múltiple por división de frecuencia (Single Carrier Frequency-Division Multiple Access, SC-FDMA) se ha convertido en una alternativa a OFDM que se utiliza específicamente en el enlace ascendente de LTE. SC-FDMA es capaz de reducir la PAPR en la transmisión, dando lugar a una relajación de las limitaciones en cuanto a la eficiencia de potencia necesaria en los terminales de usuario y las unidades satélite. SC-FDMA puede ser descrito como una versión de OFDMA en el que se incluyen una etapa de pre-codificación y de pre-codificación inversa en el transmisor y el receptor respectivamente. Así, los símbolos se transmiten en tiempo, pero después de ser procesados en la frecuencia. Incluso con el uso de OFDMA o SC-FDMA, la ISI tiene que ser compensada por la igualación, que normalmente se realiza en el dominio de frecuencia.

El objetivo de esta tesis es proporcionar un análisis matemático del comportamiento de SC-FDMA en un canal móvil terrestre por satélite (Land Mobile Satellite, LMS). Para este propósito, el canal se modela como un canal Rice sombreado tal que la línea de visión (Line of Sight, LOS) sigue la distribución de Nakagami. En primer lugar, se describen las técnicas de modulación multiportadora OFDMA y SC-FDMA. A continuación, se lleva a cabo un análisis de OFDMA y SC-FDMA basado en el ruido complejo recibido a la entrada del detector. Se evalúa la probabilidad de error de bit (Bit Error Rate, BER) de SC-FDMA para diferentes profundidades del desvanecimiento y de la diversidad de antena en el receptor. También se evalúa su eficiencia espectral para el canal LMS. Por último, se abordan las técnicas de diversidad y se evalúan las técnicas conocidas como Maximal Ratio Combining (MRC) y Equal Gain Combining (EGC).

Chapter 1

Introduction

1.1 Motivation

Orthogonal Frequency Division Multiplexing (OFDM) has become a very popular transmission technique for wireless communication for two main reasons: a) it provides a lower complexity solution in the presence of severe frequency selectivity at the transmission channel; b) it provides good spectral efficiency. OFDM has been adopted as physical layer technology for important broadband wireless interface standards, such as: IEEE 802.11/Wi-Fi [1], IEEE 802.16/WiMAX [2], 3GPP Long Term Evolution (LTE) downlink [3], as well as Digital Video Broadcasting-Second Generation Terrestrial (DVB-T2) [4].

Recently, OFDM has been also adopted in standards for communications that make use of satellite links, such as the standard for Digital Video Broadcasting-Satellite services to Handhelds (DVB-SH) [5]. The DVB-SH is a broadcast standard for delivering multimedia services over hybrid satellite/terrestrial networks to a variety of small mobile and fixed terminals with compact antennas. It has very limited directivity. In satellite channels, which are typically not highly frequency selective, the use OFDM is mainly motivated by the need to keep commonalities with the terrestrial systems. The Standard DVB-SH adopted OFDM transmission with the same signal format defined in Digital Video Broadcasting-Handheld (DVB-H) [6] for terrestrial systems in such a way that the satellite and terrestrial transmitters form a Single Frequency Network (SFN).

It is worth noting that for many years the application of OFDM has been considered unsuitable for satellite communication. An OFDM signal has high amplitude fluctuations

that produce a large Peak-to-Average Power-Ratio (PAPR). It makes OFDM sensitive to non-linear distortion caused by transmitter power amplifier. Hence transmit power amplifiers need to operate in with large Input Back Off (IBO) from their peak power, which leads to poor power efficiency. Several solutions have been suggested to reduce the impact of the signal distortion due to the non-linearities of the power amplifier such as the adoption of strong channel coding techniques in conjunction with the use of non-linear distortion compensation techniques [7] or the use of the so-called Constant Envelope OFDM (CE-OFDM) [8]. On the other hand, an interesting alternative is represented by using Single Carrier Frequency Division Multiple Access (SC-FDMA) signal format. SC-FDMA has been adopted in the up-link of the Long Term Evolution standard [3].

The SC-FDMA has been described as a single carrier transmission scheme with frequency domain equalization. Its performance is close to that of a multi-carrier system but with lower PAPR, which makes the user terminal more power efficient. Therefore, SC-FDMA transmission scheme is better candidate for satellite communication with respect to OFDM, also having the advantage of being compatible with OFDM-based transmitter-receiver. It also uses Cyclic Prefix (CP) and the equalization is performed in the frequency domain. The term cyclic prefix refers to the repetition of the end of the symbol at the beginning, which makes the linear convolution of the channel appearing as though it were circular convolution. Thus, it preserves this property in the part of the symbol after the cyclic prefix.

SC-FDMA can be seen as Discrete Fourier Transform (DFT) spread OFDM. It performs DFT spreading in the transmitter, previous to the Inverse Discrete Fourier Transform (IDFT) block. Using this DFT block, it spreads the energy of individual modulation symbols over a number of subcarriers in the DFT block. The main difference between OFDMA and SC-FDMA is the DFT and inverse DFT (IDFT) blocks at the transmitter and receiver, respectively.

There are two types of SC-FDMA on the basis of how DFT spread symbols are mapped on to the subcarriers in the IDFT block: Localized SC-FDMA (LFDMA) and Interleaved SC-FDMA (IFDMA). In Localized SC-FDMA, successive subcarriers are occupied by the DFT outputs of the input data resulting in continuos spectrum that occupies a small part

of the of the total available bandwidth. In case of interleaved SC-FDMA, the DFT outputs of input data are spread over the entire bandwidth [9].

To alleviate fading, many communication system make use of space diversity techniques [10]. Receiver diversity combining techniques such as Maximal Ratio Combining (MRC), Equal Gain Combining (EGC) and Selection Combining (SC) are commonly used to tone down the effect of multipath fading in. wireless communication systems. The maximum diversity gain takes place when diversity branches experience independent and identical fading. On the other hand, in reality, fading is not independent due to inadequate spacing between the antennas. In MRC, signals from different antenna elements are weighted and combined to make the most of the output Signal to Noise Ratio (SNR). In an EGC combiner, the output of different diversity branches are first co-phased to avoid signal cancellation and simply combined to give the resultant output.

The most commonly described performance indicator for digital transmission is Bit Error Rate (BER) under certainly employed modulation. In last few years, Quadrature Amplitude Modulation (QAM) is the most widely used constellation. However, quality of received signal in wireless communication system depends on many factors such as short-term fading, path loss exponent, lognormal shadowing, and noise. To improve system capacity, data rate and coverage reliability, the signal transmitted to and by a particular user can be continuously modified to track the signal quality variation through a process commonly referred to as Adaptive Modulation and Coding (AMC). Thus, it is possible to match the modulation scheme to the channel conditions for each user (at the expense, of course, of the need for feedback and certain throughput reduction due to signaling). Those users with good channel conditions are assigned with higher order modulation (e.g. 64 QAM) whereas the modulation order is lowered for users with worse channel conditions to keep the bit error rate under certainly given the target. In this case, spectral efficiency (as bits per second per Hertz) is the performance metric of interest.

The SC-FDMA transmission scheme performance has already motivated some studies over Land Mobile Satellite (LMS) channels [11]-[12]. In [11], a first attempt to evaluate the performance of an air interface similar to the uplink of the LTE-standard has been performed

to identify proper modifications and parameters optimization for the satellite scenario. A detailed comparison between SC-FDMA schemes versus OFDMA for a satellite uplink in S and K band have been presented in [12]. In particular, in [12] it is shown the performance sensitivity of the considered techniques to typical non-idealities of satellite such as inter block interference due to the not perfect synchronization among users and nonlinearities introduced by the High Power Amplifiers (HPAs). The study confirmed that the SC-FDMA transmission schemes is less sensitive to the amplifier non-linearity with respect to OFDMA.

All the previously described studies on SC-FDMA for satellite systems rely on simulation results of a specific transmission chain. The analysis difficulties due to the non-linear behaviour of the detection stage avoid the attempts to find expressions for SC-FDMA performance that could be easily evaluated. In [13], the author studied PAPR characteristics of SC-FDMA by using analytical and numerical methods. A BER performance study of SC-FDMA based on semi-analytical methods is presented in [14]. In [15], closed-form expressions for the BER of M-ary Quadrature Amplitude Modulation (M-QAM) SC-FDMA transmission on Nakagami-m fading channels are provided. Even fewer works can be found exploring the spectral efficiency reachable by SC-FDMA [13], and only a few attempts for AMC techniques on SC-FDMA can be found [16]. In [17], the author proposed a coded SC-FDMA for a satellite scenario. They also state that SC-FDMA spectral efficiency increases with respect to present second generation DVB interactive satellite system (DVB-RCS2) standard [17], which is based on single carrier system with a Joint Multi-User (JMU) estimation technique, and a Low-Density Parity Check (LDPC) coding scheme.

All these previous analytical or semi-analytical approaches have considered Rayleigh or Nakagami-m channels. However, for satellite communications, Loo's model [18] is most widely accepted and used extensively in the literature as LMS channel. This model assumes that the received signal envelope is described by a Rician model with logormal shadowing on the Line-of-Sight (LOS) component. Although the Rician-lognormal model provides good match to experimental data, its assumption results in complicated expressions for analytical performance evaluation. A new simple LMS channel model was proposed in [19] as a Rician channel where the amplitude of LOS component is assumed to follow a

Nakagami distribution. This Rician-Nakagami model is shown to provide a similar fit to the experimental data as the model in [18] but with less computational complexity and more mathematically tractability.

Bibliography consider different levels of fading for satellite communications, commonly named as light, average and heavy shadowing. Heavy shadowing is close to a simple Rayleigh channel, while light shadowing assumes a strong LOS along with weak multipath components. Average shadowing indicates Rician fading with about 4 dB Rice Factor.

In a wideband transmission, Inter Symbol Interfernce (ISI) appears due to the short symbol duration as compared to the multipath delay spread. The Power Delay Profile (PDP) of the multipath also defines correlation between channel responses at different subcarriers as ISI can be also seen as selectivity in the frequency domain. In case of frequency selectivity, equalization is needed, defined as any signal processing technique used at the receiver to alleviate the ISI problem caused by delay spread. Linear equalization techniques are generally simpler to implement compared to nonlinear mechanisms and avoids error propagation. Zero Forcing (ZF) equalizer is a type of linear equalization algorithm used in communication system, which applies the inverse of the frequency response of the channel. In Minimum Mean Square Error (MMSE) equalization, the main aim of the equalizer is to minimize the average mean square error (MSE) between the transmitted symbol and its estimate at the output of the equalizer. The ZF compensates completely the channel but can enhance noise, while MMSE reaches a compromise. Both OFDM and SC-FDMA techniques are able to cope with frequency selective channels by ZF or MMSE equalization performed in the frequency domain.

Although many works can be found in literature, those bounds of SC-FDMA performance over an LMS channel are unexplored yet. This dissertation aims at filling this gap by providing a semi-analytical approach to the BER and spectral efficiency evaluation. In particular, this work provides the statistical characterization of the enhanced noise at the detection stage for Interleaved SC-FDMA. Linear frequency domain equalizations such as ZF and MMSE are applied. The Rician-Nakagami model for LMS channel proposed in [19] has been considered in the analysis. Performance metrics under simulation are also given for

Localized SC-FDMA.

1.2 Contributions of this Dissertation

The contributions of this dissertaion are as follows:

- The bit error rate for OFDM and SC-FDMA over a shadowed Rice LMS channel model whose LOS follows Nakagami distribution is given.
- We present our study of the spectral efficiency when a frequency-domain equalizer is applied for OFDM and SC-FDMA transmission with adaptive modulation over light, average and heavy shadowed Rice LMS channel.
- SC-FDMA performance with receiver diversity techniques such as MRC and EGC is also analysed to study the convenience of including several antennae at the receiver.

1.3 Outline of the Dissertation

The following is the outline of the remainder of the thesis.

In Chapter 2 we describe OFDM multi-carrier modulation technique and compare it with Single Carrier Frequency Division Multiple Access.

Chapter 3 introduces channel models used under investigation. First we describe Rayleigh and Rice channel models, and then we discuss land mobile satellite channels. We also introduce frequency selectivity and two types of models are given: 1) Shadowed Rice with independent channel frequency response and 2) Correlated channel frequency response.

In Chapter 4 we describe SC-FDMA BER performance over different shadowing models, allocated subcarriers, and constellation sizes. Well known zero-forcing and minimum mean square error linear equalization techniques have been considered to cope with channel frequency selectivity. Both interleaved and localized subcarrier allocation for SC-FDMA have been analysed.

Chapter 5 is devoted to studying the spectral efficiency of SC-FDMA over different shadowing with linear equalization. First we present an overview of the adaptive modulation

techniques followed by the analysis of the spectral efficiency itself.

The SC-FDMA performance with receiver diversity techniques is carried out in Chapter 6 for different shadowing models.

Lastly, Chapter 7 presents a summary of the work and concluding remarks.

1.4 Related Publications

- J.R. Gangane, M.C. Aguayo-Torres and J.J. Sánchez-Sánchez, "Performance of SIMO MRC SC-FDMA over shadowed Rice Land Mobile Satellite channel," 3rd International Conference on Wireless Communications, Vehicular Technology, Information Theory and Aerospace and Electronic Systems (VITAE), pp. 1-5, Atlantic City, June 24-27, 2013.

- J. Gangane, M.C. Aguayo-Torres, J.J. Sánchez-Sánchez, and F.Blánquez-Casado, "Equal Gain Combining SC-FDMA Performance over Correlated Shadowed Rice Land Mobile Satellite Channel," The Ninth International Conference on Wireless and Mobile Communications (ICWMC), Nice, France, July 21-26, 2013.

- J.J. Sánchez-Sánchez, M.C. Aguayo-Torres, J.R. Gangane, and U. Fernández-Plazaola, "SC-FDMA BER Performance for MMSE Equalized Fading Channels," Chapter 3 in "Principles of 4G Wireless Communications," J.I. Agbinya, M.C. Aguayo-Torres, R. Klempous and J. Nikodem (editors), River Publishers, 2010.

- J.R. Gangane, M.C. Aguayo-Torres, J.J. Sánchez-Sánchez, "Maximal Ratio Combining SC-FDMA Performance over Correlated Rician Channels," Eighth International Conference on Wireless and Mobile Communications (ICWMC), Venice (Italy), June 24-29, 2012

- J.R. Gangane, M.C. Aguayo-Torres, J.J. Sánchez-Sánchez, S. Kate, "Link Level Performance of SC-FDMA over Land Mobile Satellite Rice Channel," 2012 IEEE International Conference on Computational Intelligence and Computing Research (ICCIC), Coimbatore, India December 18-20, 2012.

- J.R. Gangane, M.C. Aguayo-Torres, J.J. Sánchez-Sánchez, S. Wagh, " Equal Gain Combing (EGC) SC-FDMA Performance over Land Mobile Satellite (LMS) Channel," IEEE International Conference on Computational Intelligence and Computing Research (ICCIC), Coimbatore, India, December 18-20, 2012

- J.R. Gangane, M.C. Aguayo-Torres, J.J. Sánchez-Sánchez, U. Fernández-Plazaola, "SC-FDMA Performance over Rician Channel," Proceedings of 6^{th} IEEE International Conference on Broadband and Biomedical Communications (IB2Com), Melbourne, Australia, November 21-24, 2011.

Chapter 2

OFDM and SC-FDMA Fundamentals

2.1 Introduction

Nowadays, there is a need for high-speed transmission. To achieve high-speed data rate transmission over a wide bandwidth, the use of Multi-Carrier Modulation (MCM) is an attractive option [20]. The concept behind multi-carrier transmission is to allocate multiple subcarriers for conveying a large number of bits in parallel. The individual carriers have a narrow bandwidth, but the composite signal can have broad bandwidth. Some advantages of MCM are immunity to frequency selective fading and less susceptibility than single carrier systems to interference caused by impulse noise. It also shows an enhancement to minimize ISI. The main limitations of MCM include difficulty in synchronizing the carriers under marginal signal conditions, and the primary requirement is that amplification should be linear.

The MCM became an important modulation technique in Digital Video Broadcast-Terrestrial (DVB-T), or IEEE 802.11x and IEEE 802.16x series [21]. The best example of MCM transmission is Orthogonal Frequency Division Multiplexing (OFDM). The OFDM becomes Orthogonal Frequency Division Multiple Access (OFDMA) if different data signals travel through shared physical media. The main drawback of OFDM and OFDMA is that they have high PAPR [22]. To benefit the transmitter regarding power, a linear precoding stage is introduced to reduce the PAPR in a technique named as SC-FDMA.

The aim of this chapter is to provide some theoretical background of OFDM and

SC-FDMA transmission schemes. The brief information about OFDM is given in Sec. 2.2. We also discuss SC-FDMA in Sec. 2.3.

2.2 Orthogonal Frequency Division Multiplexing

In OFDM [22], the available bandwidth is divided into subcarriers that are orthogonal in the sense that the peak of one subcarrier coincides with the nulls of the other subcarriers, thereby avoiding the use of frequency guard bands and increasing spectral efficiency. The main advantage of OFDM is its behavior against adverse channel conditions, such as fading caused by multipath propagation, without complex equalization filters. Normally, as the bandwidth of the transmitted signal is less than the coherence bandwidth of the channel, the channel response in each carrier can be considered as flat. Thus, the channel can be modeled as a set of narrowband fading channel, one for each single subcarrier [22]. OFDM also provides multipath and interference tolerance in non-Line Of Sight (non-LOS) conditions.

The block diagram of an OFDM system transmitter and receiver is depicted in Figures 2.1 and 2.2, respectively. Not shown in the figure, the sequence of bits to be transmitted is mapped into a sequence of complex symbols according to the modulation scheme used, typically QAM. The complex symbols s are assigned to those orthogonal subcarriers and transmit them in parallel by employing an M-IDFT that produces an OFDM symbol in the time domain.

To eliminate temporal dispersion and ISI, a guard period has to be added. A CP of length greater than the channel response is added as a guard time to eliminate ISI [23]. Additionally, the prefix also helps to preserve the orthogonality among subcarriers, thereby avoiding inter-carrier interference as well.

The addition of the CP also transforms the linear convolution between the OFDM symbols in the time domain and the channel response into circular convolution. This circular convolution becomes, in the frequency domain, a point-wise multiplication between the compound symbol allocated in each subcarrier and the corresponding channel frequency response. Thereby, it is possible to perform the equalization in the frequency domain.

At the receiver, the CP is removed, and DFT operation converts the received signal into

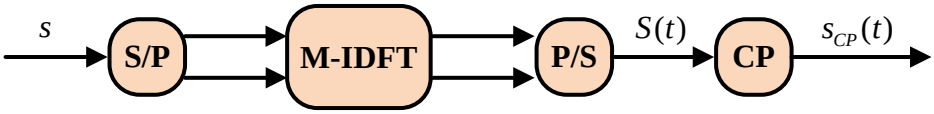

Figure 2.1: OFDMA Transmitter

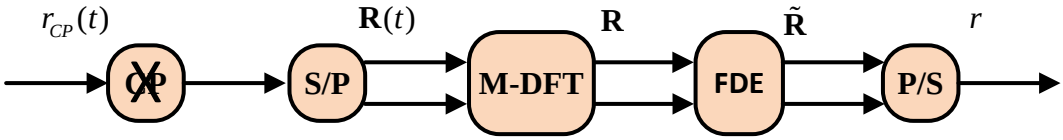

Figure 2.2: OFDMA Receiver

frequency domain. This noisy version of the transmitted signal is given to the frequency domain equalizer and finally to the detector for recovering the transmitted data.

2.3 Single Carrier Frequency Division Multiple Access

The SC-FDMA and OFDMA use the same transmitter and receiver blocks, being the main difference between them is the presence of DFT in the SC-FDMA transmitter and IDFT in the SC-FDMA receiver. Due to this reason, SC-FDMA is called as DFT-spread OFDMA. The DFT operation in SC-FDMA spreads the energy of one subcarrier over all allocated subcarriers before going to IDFT block [24]. The OFDMA waveform exhibits very high envelope fluctuations resulting in a high PAPR. Hence, signals with high PAPR need the highly linear power amplifier to reduce intermodulation distortion. However, SC-FDMA transmits the subcarriers sequentially rather than in parallel. Therefore, SC-FDMA signals have lower PAPR than OFDMA [25].

In SC-FDMA, the frequency-domain symbols are mapped on some subcarriers of the entire band. The subcarrier mapping in SC-FDMA can be interleaved or localized. In the Interleaved SC-FDMA (IFDMA) mode, the symbols are equally spaced across the entire channel bandwidth, and occupied subcarriers are equidistant. In the Localized SC-FDMA (LFDMA) mode, symbols are assigned to a group of adjacent subcarriers. Each mode has certain advantages and drawbacks.

The IFDMA introduces frequency diversity, reducing the possibility of simultaneous

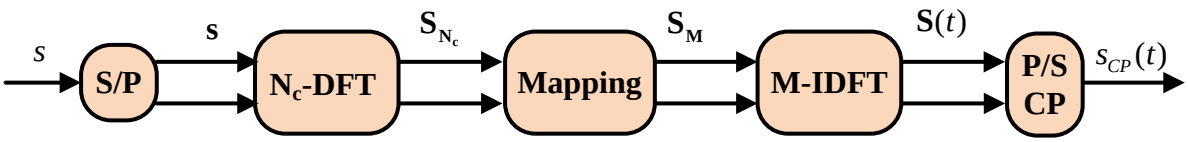

Figure 2.3: Transmission scheme in SC-FDMA

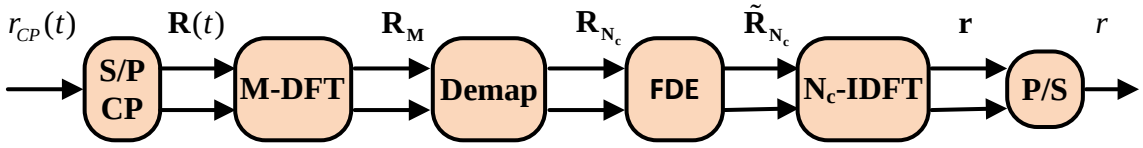

Figure 2.4: Reception scheme in SC-FDMA

deep fades at all allocated subcarriers. On the other hand, LFDMA allows using adaptive modulation techniques able to track channel variations.

Moreover, SC-FDMA can be seen as a precoded version of OFDM whose symbols travel in time. Processing in the frequency domain allows reduced power distortion. Also, SC-FDMA complexity focuses on the receiver side. Therefore, it is an appropriate technology for cellular uplink transmission and satellite downlink transmission, since complexity at the base station or the terrestrial receiver is not an issue. Both OFDMA and SC-FDMA techniques transmit the same amount of data symbols in the same period using the same bandwidth, and users are orthogonally multiplexed and demultiplexed in the frequency domain. However, SC-FDMA modulated symbols are transmitted sequentially over the air, and the final transmitted signal is a single carrier one.

Figures 2.3 and 2.4 show the transmission chain for SC-FDMA. As a previous step, the sequence of the bits to be transmitted are mapped into a constellation of complex symbols by using digital modulation techniques such as QAM. The resulting complex vector $\mathbf{s}$ of length N_c is pre-coded by means of a DFT operation before being mapped onto the subset of N_c allocated subcarriers. The pre-coded column complex vector $\mathbf{S}_{N_c}$ is obtained by multiplying with the unitary Fourier matrix $\mathbf{F}$ to perform the N_c-DFT operation as $\mathbf{S}_{N_c} = \mathbf{F}\mathbf{s}$.

The pre-coded sequence $\mathbf{S}_{N_c}$ is then mapped onto a different subset of allocated subcarriers per user, i.e., N_c out of the M subcarriers. As previously described, the

subset may consist of a group of adjacent, Localized SC-FDMA or Interleaved SC-FDMA subcarriers [9] and it is determined by the $M \times N_c$ mapping matrix $\mathbf{P}$ for which $\mathbf{P}_{i,j} = 1$ if the pre-coded symbol j is transmitted over the subcarrier i and zero otherwise. The bandwidth expansion factor is $U = M/N_c$, where M is the total number of subcarriers used for transmission and N_c is the number of allocated subcarriers.

The frequency-domain symbol is defined as $\mathbf{S}_M = \mathbf{P}\mathbf{S}_{N_c}$ and, consequently, non-allocated subcarriers are forced to zero. From this point on, transmission is similar to that of OFDMA, and an M-IDFT operation converts each frequency-domain symbol $\mathbf{S}_M$ into a time-domain symbol. These time domain symbols are transmitted sequentially after adding a cyclic prefix. The CP is inserted as the guard time, which prevents ISI due to multipath propagation. The length of CP is made longer than the maximum delay spread of the channel or duration of the channel impulse response. Since CP is the copy of the last part of the block, it converts discrete time linear convolution into discrete time circular convolution.

At the receiver end, the cyclic prefix is removed, and the received signal is converted into the frequency domain by taking DFT. After subcarrier demapping, equalization can be done by using ZF or MMSE. The MMSE is preferred over ZF due to robustness against noise. Later, symbols are converted back to the time domain by an N_c-IDFT, and the sequence is given to the detector.

2.4 Conclusions

In this chapter, we discussed SC-FDMA, a multiple access scheme that makes use of single carrier modulation, and orthogonal frequency division multiplexing. The main drawback of OFDM and OFDMA is that they have high PAPR. As SC-FDMA has low PAPR, it simplifies the transmitter circuit in the handset and reduces power consumption. The receiver structure with SC-FDMA is more complex than that with OFDMA.

Chapter 3

Wireless Channel Models

3.1 Introduction to Wireless Channel

The behaviour of a wireless communication system depends on the wireless channel environment. As compared to wired channel, the wireless channel is dynamic and unpredictable. So, to make an exact analysis of the wireless communication system is often complicated.

In wireless communication, radio propagation refers to the actions of radio waves when they travel from transmitter to receiver. During propagation, radio waves are mainly affected by three different modes of physical phenomena: reflection, diffraction, and scattering [26]. Reflection is the physical phenomenon that occurs when a propagating electromagnetic wave impinges upon an object. It makes the transmit signal power to be reflected back to its origin. Diffraction is the phenomena that occur when the radio path between the transmitter and receiver is blocked by a surface with sharp irregularities. The secondary waves generated by diffraction makes a path between the transmitter and receiver, even when an LOS path is not present. Scattering is a process that forces the radiation of an electromagnetic wave to deviate from a straight path by local obstacles. In short, the propagation of a radio wave is a complicated and less predictable process, the intensity of which varies with different environments at different instances. The deviation of the signal amplitude over time and frequency is called as fading. It is a unique characteristic of the wireless channel.

In this dissertation, the frequency selective Rayleigh and Rice fading channel models are based on simple satellite model defined in [27]. This chapter describes channel models to be

employed in the rest of the thesis.

3.2 Rayleigh and Rice Fading

3.2.1 Rayleigh Fading

Small-scale fading occurs due to small changes in position. It is often named it as Rayleigh fading since the signal envelope is often statistically characterized with a Rayleigh Probability Density Function (PDF). Rayleigh fading in the propagation channel is a major impairment in wireless communications and it significantly degrades the link performance.

The PDF for signal envelope in Rayleigh fading is given by

$$f_X(x) = \frac{x}{\sigma^2} exp\left(-\frac{x^2}{2\sigma^2}\right), x \geq 0 \tag{3.2.1}$$

Being σ the standard deviation of the underlying Gaussian distribution.

3.2.2 Rice Fading

In some environments, such as satellite communication, LOS between transmitter and receiver is present in the communication link. In this case, the amplitude gain is often described as a Rician distribution. It represents the envelope of a Gaussian signal whose average is different from 0.

The PDF of the Rice distribution is given by

$$f_X(x) = \frac{x}{\sigma^2} exp\left(-\frac{x^2 + c^2}{2\sigma^2}\right) I_o\left(\frac{xc}{\sigma^2}\right) x \geq 0 \tag{3.2.2}$$

Where $I_0(.)$ is the modified zeroth-order Bessel function of the first kind. The Rician factor K is defined as a ratio of the power present through the LOS path to the power contribution through non-LOS paths:

$$K = \frac{c^2}{2\sigma^2} \tag{3.2.3}$$

If there does not exist an LOS component (i.e., $K = 0$), Eq. (3.2.2) reduces to the Rayleigh PDF Eq. (3.2.1) as in the non-LOS environment. As K increases, Eq. (3.2.2) tends to be Gaussian PDF. It is assumed that $K = -40$ dB stands for a Rayleigh fading channel and $K > 15$ dB for a Gaussian channel.

3.3 Frequency Selectivity

3.3.1 Flat Fading Channels

It is said that a signal transmitted over a channel suffers flat fading if the coherence bandwidth of the channel is higher than the bandwidth of the signal. Therefore, all frequency components of the signal will experience the same magnitude of fading. The response of the channel is thus given by:

$$h(t, \tau) = a_i(t)\delta(\tau), \tag{3.3.1}$$

Where a_i is called amplitude of the channel, which may be Rayleigh or Rice distribution, t stands for time variability and τ for a delay.

3.3.2 Frequency Selective Channels

If the coherence bandwidth of the channel is smaller than the bandwidth of the signal then it is called frequency selective fading. The various frequency components of the signal, therefore, experience different fading. Channel is commonly modelled as a set of N uncorrelated taps, $a_k(t)$, each of them equivalent to the channel response of a flat fading channel. Finally the channel response for frequency selective channel is given by the well-known tapped-delay-line model:

$$h(t, \tau) = \sum_{k=1}^{L} a_k(t)\delta(\tau - \tau_k) \tag{3.3.2}$$

Where a_k is the variant amplitude of each echo, which may be Rayleigh or Rice distribution as explained in Sec. 3.2, t stands for time variability and τ for the delay.

Power Delay Profile (PDP) is the average intensity of a signal received through a multipath channel as a function of time delay, that is, the set of power averages of $a_k(t)$. In general, most powerful echoes are received first while power is decreasing with τ.

3.4 Single-Input Multiple-Output Channel Model

The multiple receiving antenna Single-Input Multiple-Output (SIMO) link is shown in Figure 3.1 for two antennas. The channel system with N_R antennas, i.e. diversity branches,

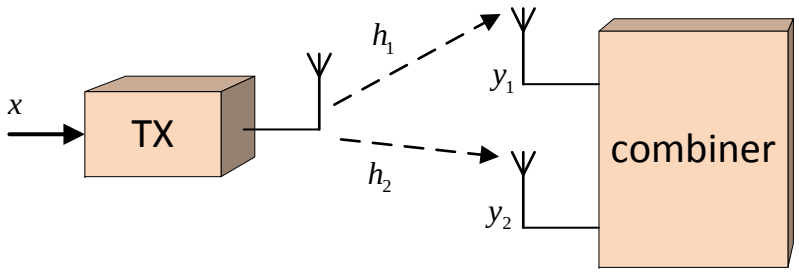

Figure 3.1: Receiver Diversity combining scheme.

at the receiver can be represented by the channel vector:

$$\mathbf{h} = [h_1,\ h_2, .., h_{N_R}]^T \tag{3.4.1}$$

Where h_j is the channel coefficient between the transmit antenna and the j^{th} receive antenna. Moreover, h_j can be described by multiple paths, as described in the previous section, that is, if there are L_j distinct paths from the transmitter to the receiver, the impulse response of this channel will be:

$$h_j(t, \tau) = \sum_{k=1}^{L_j} a_{k,j}(t)\delta(\tau - \tau_k) \tag{3.4.2}$$

With t standing for time variability and τ for the delay.

If there is less spacing between multiple antennas at receiver, then there exists certain correlation between antennas given by the correlation coefficient ρ. The values of ρ stand between 0 and 1. The value of $\rho = 0$ means no correlation between the antennas and $\rho = 1$ indicates perfect correlation, i.e., similar signal is received by both antennae.

The correlated channel model H is given as:

$$H = R_r^{1/2} H_w R_t^{1/2} \tag{3.4.3}$$

Where R_t is the correlation matrix, reflecting the correlation between the transmit antennas (i.e., the correlations between the column vector of H), R_r is the correlation matrix reflecting the correlation between receiver antenna (i.e., the correlation between the row vectors of H), and H_w denotes the i.i.d fading channel gain matrix. The diagonal entries of R_r and R_t are considered to be unity.

For SIMO the channel model H is simplified to:

$$H = R_r^{1/2} H_w \tag{3.4.4}$$

3.5 Satellite Channel Model

There are two types of propagation between a satellite and a mobile receiver, unshadowed and shadowed [28][29]. When the mobile receiver has an unobstructed LOS path to the satellite, it is called unshadowed propagation. In the case of shadowed propagation, the LOS path of the satellite is obstructed by terrain, vegetation, or human made structures.

The unshadowed signal received at the mobile receiver is composed of direct and diffuse components. The diffuse component is a phase incoherent multipath wave due to reflections and scattering from outside the first Fresnel zone of the vehicle of little variations with directions of arrival [30]. The direct LOS component is essentially constant.

The shadowed direct component can be modelled as the sum of attenuated LOS signal and a random forward scattered field.

Generally speaking, the available models for narrowband LMS channels can be placed into two categories: single model and mixture model. In the single model, the channel is characterized by a single statistical distribution, while a combination model refers to a combination of several statistical distributions. Single models are valid for stable conditions, where the channel statistics remain approximately constant over the period of interest in the small area. On the other hand, the mixture models are developed for nonstationary channels, where the signal statistics vary significantly over the observation interval. A list of proposed single and mixture models is given in [19]. Among the proposed models for LMS channels, the shadowed Rice model proposed originally by Loo [18] has found wide applications in different frequency bands such as the UHF-band, L-band, S-band, and Ka-band.

In this dissertation, an LMS model proposed in [19] is employed. This model can gather in a single distribution both for shadowed and unshadowed LMS channels by a different parameter set.

3.5.1 Shadowed Rice Land Mobile Satellite Channel Model

In an ideal land mobile satellite channel, there is a clear line of sight between the satellite and the land user, thus the envelope is a non-random constant. However, after multipath fading is caused by the weak scatter components propagated via different non-LOS paths, together with the non blocked LOS component, the envelope becomes a Rice random variable. Moreover, LOS shadow fading comes from the complete or partial blockage of the line of sight which makes the amplitude of the LOS component also a random variable. Finally, the low pass-equivalent complex envelope of the channel can be written as;

$$z(t) = A(t)\exp\left(j\alpha(t)\right) + B(t)\exp(j\alpha_0) \tag{3.5.1}$$

Where $\alpha(t)$ is the stationary random phase process of multipath fading with uniform distribution over $[0, 2\pi)$, while α_0 is the phase of the LOS component. The independent stationary random processes $A(t)$ and $B(t)$, which are also independent of $\alpha(t)$, represents the amplitudes of the scatter and the LOS components. As previously stated, we follow the LMS channel model described in [19], through which $A(t)$ and $B(t)$ follow Rayleigh and Nakagami distributions, respectively, as given bellow;

$$f_A(a) = \frac{a}{b_0}\exp\left(\frac{-a^2}{2b_0}\right) \tag{3.5.2}$$

$$f_B(b) = \frac{2m^m}{\Gamma(m)\Omega^m} b^{2m-1}\exp\left(\frac{-mb^2}{\Omega}\right) \tag{3.5.3}$$

Where $2b_0 = E[A^2]$ is the average power of scatter component, $\Gamma(\,)$ is the gamma function, $m = \dfrac{E\left[B^2\right]}{Var\left[B^2\right]} \geq 0$ is the Nakagami parameter with $Var\left[\,\right]$ as the variance, and $\Omega = E\left[B^2\right]$ is the average power of the LOS component.

The shadowed Rice probability density function (PDF) for the signal envelope $Z = |z(t)|$ in an LMS channel can be derived from:

$$P_Z(z) = E_B\left[\frac{z}{b_0}\exp\frac{(z^2+B^2)}{2b_0} I_0(\frac{Bz}{b_0})\right] \tag{3.5.4}$$

Where $E_B\left[\,\right]$ is the expectation with respect B, and $I_n(\,)$ is the n-th order modified Bessel's function of the first kind. Averaging [19] yields to:

$$f_Z(z) = \left(\frac{2b_0 m}{2b_0 m + \Omega}\right)^m \frac{z}{b_0}\, exp\left(-\frac{z^2}{2b_0}\right)\, {}_1F_1\left(m, 1, \frac{\Omega z^2}{2b_0(2b_0 m + \Omega)}\right) \tag{3.5.5}$$

The shadowed Rice PDF for the instantaneous power $|z(t)|^2$ can be then written as (Eq. (6) in [19]):

$$f_{Z^2}(q) = \left(\frac{2b_0 m}{2b_0 m + \Omega}\right)^m \frac{1}{2b_0} \exp\left(-\frac{q}{2b_0}\right) \, {}_1F_1\left(m, 1, \frac{\Omega q}{2b_0(2b_0 m + \Omega)}\right) \tag{3.5.6}$$

Different values of m are able to model distinct scenarios. While $m = 0$ corresponds to areas with complete obstruction of the LOS, any value $0 < m < \infty$ represents areas with partial obstruction of the LOS. The most common values considered for those parameters, which fully characterize the fading model, are presented in Table 3.1. Finally, the expressions of gamma $\Gamma(\,)$ and the confluent hyper geometric function ${}_1F_1(\,,\,,\,)$ can be found in [31].

Table 3.1: Parameters for considered fading channels [19].

Shadowing type	b_0	m	Ω
Light fading	0.158	19.4	1.29
Heavy fading	0.063	0.739	8.97×10^{-4}
Average fading	0.126	10.1	0.835

3.5.2 Channel Frequency Response Models

The channel frequency response, represented by the $M \times M$ diagonal matrix $\mathbf{H_M}$, is the Fourier transform of the variable impulse response of the channel. Two different models have been employed for dependence among the channel frequency responses at those allocated subcarriers, $\mathbf{h} = diag(\mathbf{P}^H \mathbf{H_M} \mathbf{P})$, with $\mathbf{P}$ is the mapping matrix as described in Sec. 2.3.

As first model, elements of $\mathbf{h}$ are assumed to be independent identically distributed random variables. Each element h_j follows the shadowed Rice distribution given by Eq. (3.5.5) and the PDF for the instantaneous power at each subcarrier $|h_j|^2$ can be then written as (Eq. (6) in [19]):

$$f_{|h_j|^2}(q) = \left(\frac{2b_0 m}{2b_0 m + \Omega}\right)^m \frac{1}{2b_0} exp\left(-\frac{q}{2b_0}\right) \, {}_1F_1\left(m, 1, \frac{\Omega q}{2b_0(2b_0 m + \Omega)}\right) \tag{3.5.7}$$

As the second model, a wideband LMS tapped delay line model is used. The first echo is considered to follow the narrow band shadowed Rice model while the rest are considered

to be Rayleigh distributed (i.e., LOS is present only in the first arrived path). Under this model, magnitude of **h** elements are easily shown to be also shadowed Rice. In this case, there exists certain correlation among elements of **h** which can be evaluated through the Fourier transform of the power delay profile. Specifically, the usual exponential power delay profile [27] has been considered. Thus, the scattered received power for l^{th} echo is as follows:

$$p_l = \frac{1}{\tau_{avg}} exp\left(-\frac{\tau_l}{\tau_{avg}}\right) \tag{3.5.8}$$

In the case of the rural environment, a typical value of τ_{avg} is less than $1\mu s$ and less than $2\mu s$ for a suburban area [32]. The value of τ_{avg} used within this thesis is $1.17\mu s$. Selected parameters in SC-FDMA should be such that for given time constant τ_{avg} most energy of the impulse response fits within the cyclic extension.

3.6 Conclusions

In this chapter, we discussed in brief about wireless channel models such as Rayleigh, Rice, and frequency selective fading. The channel models for SISO and SIMO with different antenna correlation has also been discussed. Finally, we described shadowed Rice LMS channel model based on Abdi's model, where LOS follows Nakagami distribution. The channel parameters for different shadowing such as light, average and heavy shadowing are tabulated.

Chapter 4

SC-FDMA BER Analysis over Shadowed Rice LMS Channel

4.1 Introduction

In this chapter, the performance of an SC-FDMA transmission over land mobile satellite channel is analyzed. We first consider zero forcing equalization in the frequency domain, which is applied to compensate the effects of the channel on the received signal. The analysis is emphasized on the noise term before the decision stage, and then we extended the study for MMSE equalization.

The analysis done under this chapter is derived under the assumption of independence among the frequency responses for the allocated subcarriers, which is validated through the simulations. We also consider correlation among subcarriers and BER is evaluated for Interleaved-SC-FDMA (IFDMA) and Localized SC-FDMA (LFDMA). We presented results for different shadowing such as light, average, and heavy shadowing. Presented results for heavy shadowing are consistent with the results presented in [15].

4.2 System Model

In this section, we describe the SC-FDMA transmitter-receiver scheme used for investigation. We use two different mapping schemes of SC-FDMA. First we generated random bits, these are modulated using either Binary Phase Shift Keying (BPSK), 4 Quadrature Amplitude Modulation (4QAM) or 16 Quadrature Amplitude Modulation (16QAM). These complex

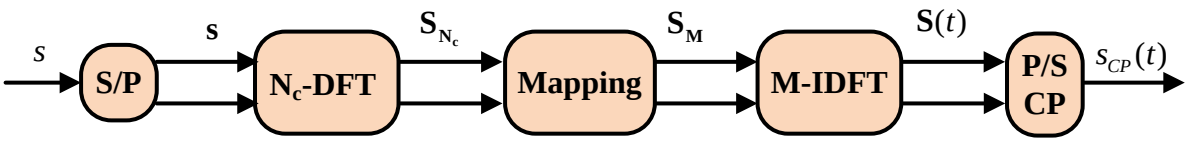

Figure 4.1: Transmission scheme in SC-FDMA

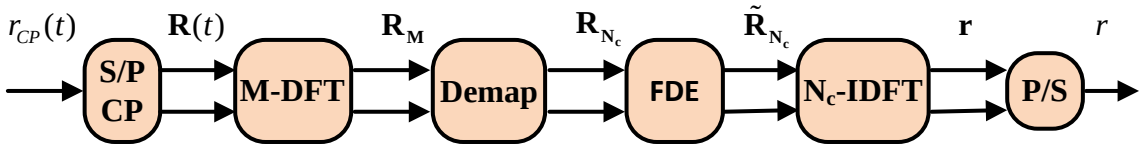

Figure 4.2: Reception scheme in SC-FDMA

symbols are transmitted using SC-FDMA transmission scheme. After passing through shadowed Rice channel, they are recovered at the receiver using zero forcing or minimum mean square error equalizer. The bit error rate is calculated and plotted using both simulations and numerical methods.

Figures 4.1 and 4.2, placed again for convenience, are the transmission and reception chain for SC-FDMA as presented in Chapter 2. As a previous step, the sequences of the bits to be transmitted are mapped into a constellation of complex symbols which in this chapter is considered to be fixed (e.g., 16QAM, 4QAM or BPSK). The resulting complex sequence $\mathbf{s}$ of length N_c is pre-coded by means of a discrete Fourier transform operation before being mapped onto the subset of N_c allocated subcarriers. The pre-coded column complex vector $\mathbf{S}_{N_c}$ is obtained by multiplying by the unitary Fourier matrix $\mathbf{F}$ to perform the N_c-DFT operation as $\mathbf{S}_{N_c} = \mathbf{F}\mathbf{s}$. Note that $\mathbf{F}\mathbf{F}^H = \mathbf{I}$ as each element in $\mathbf{F}$ is defined as $F_{j,k} = exp\{\frac{2\pi\imath}{N_c} j, k\}/\sqrt{N_c}$ where $\imath = \sqrt{-1}$ and j and k are the row and column indexes $\mathbf{F}^H$ is the Hermitian transpose of $\mathbf{F}$ as commonly noted. This step allows SC-FDMA complex symbols being transmitted sequentially rather than in parallel as in OFDMA.

The pre-coded sequence, $\mathbf{S}_{N_c}$, is then mapped onto a different subset of allocated subcarriers per user, i.e., N_c out of the M subcarriers in which the total system Bandwidth is divided. The subset may consist of a group of adjacent Localized (LFDMA) or Interleaved (IFDMA) subcarriers [9] and it is determined by the $M \times N_c$ mapping matrix $\mathbf{P}$ for which $\mathbf{P_{i,j}} = 1$ if the pre-coded symbol j is transmitted over the subcarrier i and zero otherwise.

The frequency-domain symbol is defined as $\mathbf{S}_M = \mathbf{P}\mathbf{S}_{N_c}$ and, consequently, non-allocated subcarriers are forced to zero. From this point on, transmission is similar to that of OFDMA: an M-IDFT operation converts each frequency-domain symbol $\mathbf{S}_M$ into a time-domain symbol; a cyclic prefix, whose length must be greater than the channel impulse response, is added to avoid ISI.

After transmission over the LMS channel (see SubSec. 3.5 for channel modelling), the cyclic prefix is suppressed and an M-DFT operation converts each time-domain symbol into a frequency-domain symbol $\mathbf{R}_M$ at the receiver (see Figure 4.2). After applying $\mathbf{P}^H$ for de-mapping, the signal at receiver $\mathbf{R}_{N_c}$ can be expressed as

$$\mathbf{R}_{N_c} = \mathbf{P}^H\mathbf{H}_M\mathbf{P}\mathbf{F}\mathbf{s} + \mathbf{P}^H\boldsymbol{\eta}_M \tag{4.2.1}$$

Where $\boldsymbol{\eta}_M$ is the noise vector whose entries are independent and identically distributed (i.i.d.) complex Gaussian $\mathcal{CN}(0, N_0)$. $\boldsymbol{\eta} = \mathbf{P}^H\boldsymbol{\eta}_M$ is formed by those noise samples at the allocated subcarriers. The channel frequency response is represented by the $M \times M$ diagonal matrix $\mathbf{H}_M$, whose characteristics are also described in SubSec. 3.5.

As in OFDM, the addition of the cyclic prefix in SC-FDMA also transforms the linear time domain convolution between the OFDM symbols and the channel response into a circular convolution. In the frequency domain, this circular convolution becomes a point-wise multiplication between the complex symbol allocated in each subcarrier and the corresponding channel frequency response. Thereby, it is possible to perform the equalization in the frequency domain by simply multiplying $\mathbf{R}_{N_c}$ by an $N_c \times N_c$ complex equalization matrix $\mathbf{W}$, defined as to accomplish zero forcing or minimum mean square error Frequency Domain Equalization (FDE) as described later. After FDE is performed, $\widetilde{\mathbf{R}}_{\mathbf{N_c}}$ yields

$$\widetilde{\mathbf{R}}_{\mathbf{N_c}} = \mathbf{W}\mathbf{R}_{N_c} = \mathbf{W}\mathbf{H}\mathbf{F}\mathbf{s} + \mathbf{W}\boldsymbol{\eta} \tag{4.2.2}$$

Where $\mathbf{H} = \mathbf{P}^H\mathbf{H}_M\mathbf{P}$ is a $N_c \times N_c$ diagonal matrix whose entries $\mathbf{h} = diag(\mathbf{H}) = [h_1 \dots h_{N_c}]$ are the channel frequency responses for each allocated subcarrier and $\boldsymbol{\eta} = \mathbf{P}^H\boldsymbol{\eta}_M$ is a vector whose elements are the corresponding complex noise values.

Before detection, an inverse pre-coding is performed by means of an N_c-IDFT

$$\mathbf{r} = \mathbf{F}^H \mathbf{R}_{N_c} = \mathbf{F}^H \mathbf{W}\mathbf{H}\mathbf{F}\mathbf{s} + \mathbf{F}^H \mathbf{W}\boldsymbol{\eta} \tag{4.2.3}$$

4.3 SINR analysis

From the previous section, we know that for SC-FDMA the effective noise at the entrance of the detector $\boldsymbol{\eta}$ is a combination of the received noise and the channel responses corresponding to the set of allocated subcarriers through the equalizing matrix $\mathbf{W}$ (see Eq. (4.2.2)). Moreover, if MMSE is applied, there also exists an interference component in the effective noise [33]. We describe those error terms in the next subsections for both, ZF and MMSE equalization techniques, for the specific case of transmission using SC-FDMA for shadowed Rice channels.

4.3.1 ZF FDE

Equalization in Eq. (4.2.2) could be performed with the aim of completely eliminating the inter carrier interference (Zero-Forcing equalization). In that case, $\mathbf{W}$ is applied as

$$\mathbf{W}^{ZF} = (\mathbf{H}^H \mathbf{H})^{-1} \mathbf{H}^H, \tag{4.3.1}$$

and the expression for the recovered symbol in frequency after FDE yields

$$\mathbf{r} = \mathbf{F}^H (\mathbf{H}^H \mathbf{H})^{-1} \mathbf{H}^H \mathbf{H}\mathbf{F}\mathbf{s} + \mathbf{F}^H (\mathbf{H}^H \mathbf{H})^{-1} \mathbf{H}^H \boldsymbol{\eta} \tag{4.3.2}$$

Hence, the expression for the k-th received symbol after ZF-FDE is given by

$$r_k = s_k + \sum_{j=1}^{N_c} \frac{F_{j,k}^*}{h_j} \eta_j = s_k + \sum_{j=1}^{N_c} \hat{\eta}_{j,k} = s_k + \tilde{\eta}_k \tag{4.3.3}$$

Where $\hat{\eta}_{j,k} = \dfrac{F_{j,k}^* \eta_j}{h_j}$. Thus, each received symbol is the result of adding an effective noise term $\tilde{\eta}_k$ to the original transmitted symbol.

As shown in Eq. (4.3.3), the effective noise in ZF-DFE is the result of adding an elementary noise term $\hat{\eta}_{j,k}$ for each allocated subcarrier. Each elementary noise term is equivalent to the enhanced noise in OFDM reception with ZF-FDE. Conditioned to the

channel frequency response $\mathbf{h} = [h_1 \dots h_{N_c}]$, the effective noise $\tilde{\eta}_k$ in Eq. (4.3.3) follows a complex Gaussian distribution with zero-mean and variance $\frac{N_0}{E_S}\beta^{ZF}$ with the random variable β^{ZF} defined [14] as

$$\beta^{ZF} = \frac{1}{N_c}\sum_{j=1}^{N_c}\frac{1}{|h_j|^2} = \sum_{j=1}^{N_c}\beta_j^{ZF} \tag{4.3.4}$$

Each term in the addition β_j is a random variable that depends on the fading channel. For the considered shadowed Rice channel, its PDF can be easily evaluated as

$$f_{1/X}(t) = \frac{1}{t^2}f_X\left(\frac{1}{t}\right) \tag{4.3.5}$$

Being $f_{|h_j|^2}(q)$ as given by Eq. (3.5.7), the above expression yields

$$f_{1/|h_j|^2}(s) = \left(\frac{2b_0m}{2b_0m+\Omega}\right)^m \frac{1}{2b_0}\frac{1}{s^2}exp\left(-\frac{1}{2b_0s}\right)\ {}_1F_1\left(m, 1, \frac{\Omega}{2b_0s(2b_0m+\Omega)}\right) \tag{4.3.6}$$

Simple transformation by a constant as

$$f_{X/a}(s) = af_X(as) \tag{4.3.7}$$

Would result in

$$f_{\beta_j^{ZF}}(s) = \left(\frac{2b_0m}{2b_0m+\Omega}\right)^m \frac{1}{2b_0}\frac{1}{N_cs^2}exp\left(-\frac{1}{2b_0N_cs}\right)\ {}_1F_1\left(m, 1, \frac{\Omega}{2b_0N_cs(2b_0m+\Omega)}\right) \tag{4.3.8}$$

If independence among channel frequency responses can be assumed, the Characteristic Function (CHF) of the addition in Eq. (4.3.4) can be written as

$$\Phi_{\beta^{ZF}}(\omega) = \left(\Phi_{\beta_j^{ZF}}(\omega)\right)^{N_c} \tag{4.3.9}$$

With the CHF of β_j given by

$$\Phi_{\beta_j^{ZF}}(\omega) = \int_0^\infty f_{\beta_j^{ZF}}(s)e^{\imath s\omega}ds \tag{4.3.10}$$

To the author's best knowledge, it is not possible to obtain an analytical expression for the CHF of β_j but only numerical calculation could be carried on, e.g. using of successive computations of Eq. (4.3.10). Later on, it is possible to evaluate the Cumulative Distribution

Function (CDF) of β^{ZF} using Gil-Peláez's inversion theorem expression [34] which can be written in this particular case as

$$F_{\beta^{ZF}}\left(\beta^{ZF}\right) = \frac{1}{2} - \frac{1}{2\pi}\int_0^\infty \left(\frac{\Phi_{\beta^{ZF}}(\omega)}{\imath\omega}e^{-\imath\beta^{ZF}\omega} - \frac{\Phi_{\beta^{ZF}}(-\omega)}{\imath\omega}e^{\imath\beta^{ZF}\omega}\right) d\omega \tag{4.3.11}$$

Once we have characterized β^{ZF}, we might use it to evaluate the instantaneous SNR conditioned to channel as they are related by the following expression

$$\gamma^{ZF} = \frac{E_S/N_0}{\beta^{ZF}} \tag{4.3.12}$$

4.3.2 MMSE FDE

In order to avoid ZF noise enhancement, the design of $\mathbf{W}$ can be accomplished under the MMSE criterion

$$\mathbf{W}^{MMSE} = \left(\frac{N_0}{E_S}\mathbf{I} + \mathbf{H}^H\mathbf{H}\right)^{-1}\mathbf{H}^H \tag{4.3.13}$$

Where E_S and N_0 are the signal and noise powers respectively. In this case, the recovered symbol is

$$\mathbf{r} = \mathbf{F}^H\left(\frac{N_0}{E_S}\mathbf{I} + \mathbf{H}^H\mathbf{H}\right)^{-1}\mathbf{H}^H\mathbf{H}\mathbf{F}\mathbf{x} + \mathbf{F}^H\left(\frac{N_0}{E_S}\mathbf{I} + \mathbf{H}^H\mathbf{H}\right)^{-1}\mathbf{H}^H\boldsymbol{\eta} \tag{4.3.14}$$

Each received symbol can be written as the transmitted symbol modified and contaminated by noise and interference.

$$r_k = T_{k,k}s_k + \sum_{\substack{l\neq k\\ l=1}}^{N_c} s_l T_{k,l} + \sum_{j=1}^{N_c}\frac{F_{j,k}^* h_j^*}{|h_j|^2 + N_0/E_S}\eta_j \tag{4.3.15}$$

The elements of the matrix $\mathbf{T} = \mathbf{F}^H\mathbf{W}^{MMSE}\mathbf{H}\mathbf{F}$ can be expressed as

$$T_{k,l} = \sum_{j=1}^{N_c}\frac{F_{j,k}^* F_{j,l}\,|h_j|^2}{|h_j|^2 + N_0/E_S} \tag{4.3.16}$$

Specifically, the term $T_{k,k}$, which multiplies the transmitted signal, is given by

$$T_{k,k} = \sum_{j=1}^{N_c}\frac{|F_{k,j}|^2\,|h_j|^2}{|h_j|^2 + N_0/E_S} = \frac{1}{N_c}\sum_{j=1}^{N_c}\frac{|h_j|^2}{|h_j|^2 + N_0/E_S} \tag{4.3.17}$$

Please, note that really $T_{k,k}$ is independent of k, that is, all symbols are received with the same power.

After compensating it, the transmitted symbol is obtained as

$$r_k = s_k + T_{k,k}^{-1} \sum_{\substack{l \neq k \\ l=1}}^{N_c} s_l T_{k,l} + T_{k,k}^{-1} \sum_{j=1}^{N_c} \frac{F_{j,k}^* h_j^*}{|h_j|^2 + N_0/E_S} \eta_j = s_k + \sum_{\substack{l \neq k \\ l=1}}^{N_c} \delta_{l,k} + \sum_{j=1}^{N_c} \tilde{\eta}_{j,k} \tag{4.3.18}$$

That is, the transmitted symbol is contaminated by the equivalent noise $\tilde{\eta}_k$ and the interference δ_k

$$r_k = s_k + \delta_k + \tilde{\eta}_k = s_k + \xi_k \tag{4.3.19}$$

The term ξ_k gathers the effects of noise and interference, which are inherently independent [14].

When the channel frequency response is such that $\frac{N_0}{E_S} \ll |h_j|^2$, the effect of the interference term decreases and the noise term is equal to that of ZF in Eq. (4.3.3).

The density of the noise $\tilde{\eta}_k$ conditioned to the channel frequency response $\mathbf{h} = [h_1 \dots h_{N_c}]$ is the addition of N_c terms, each one following a complex Gaussian distribution. Thus, the total equivalent noise follows also a complex Gaussian distribution

$$p\left(\tilde{\eta}_k/\mathbf{h}\right) \sim \mathcal{CN}\left(0, \sigma_{\tilde{\eta}}^2\right) \tag{4.3.20}$$

Whose variance $\sigma_{\tilde{\eta}}^2$, equal for all symbols, can be simply obtained by taking into account that $|F_{j,k}^*| = 1$ and that noise samples are independent as

$$\sigma_{\tilde{\eta}}^2 = \frac{N_0}{(T_{k,k})^2} \frac{1}{N_c} \sum_{j=1}^{N_c} \left(\frac{|h_j|}{|h_j|^2 + N_0/E_S} \right)^2 \tag{4.3.21}$$

Now, we are evaluating the interference component. Conditioned the channel frequency response, we can assume it also follows a complex circularly symmetric Gaussian distribution [14]:

$$p\left(\delta_k/h\right) \sim \mathcal{CN}\left(0, \sigma_{\delta}^2\right) \tag{4.3.22}$$

Please, note that this will only hold if transmitted symbols are independent and with equal energy E_S, and it will be more realistic as more subcarriers are used. In this case, σ_{δ}^2 can be

expressed as

$$\sigma_\delta^2 = \frac{E_S}{(T_{k,k})^2} \sum_{\substack{l \neq k \\ l=1}}^{N_c} |T_{k,l}|^2 \tag{4.3.23}$$

We can manipulate the expression as to write

$$\sigma_\delta^2 = \frac{E_S}{(T_{k,k})^2} \left(\sum_{l=1}^{N_c} |T_{k,l}|^2 - (T_{k,k})^2 \right) \tag{4.3.24}$$

or

$$\sigma_\delta^2 = E_S \frac{\frac{1}{N_c} \sum_{j=1}^{N_c} \left(\frac{|h_j|^2}{|h_j|^2 + N_0/E_S} \right)^2 - \left(\frac{1}{N_c} \sum_{j=1}^{N_c} \frac{|h_j|^2}{|h_j|^2 + N_0/E_S} \right)^2}{\left(\frac{1}{N_c} \sum_{j=1}^{N_c} \frac{|h_j|^2}{|h_j|^2 + N_0/E_S} \right)^2} \tag{4.3.25}$$

As noise and interference components are independent random variables, their sum can be modelled with another zero-mean complex Gaussian random variable whose variance, given by

$$\sigma_\xi^2 = \sigma_\delta^2 + \sigma_{\tilde{\eta}}^2 \tag{4.3.26}$$

Can be written as

$$\sigma_\xi^2 = \frac{\frac{N_0}{N_c} \sum_{j=1}^{N_c} \left(\frac{|h_j|}{|h_j|^2 + No/Es} \right)^2 + \frac{Es}{N_c} \sum_{j=1}^{N_c} \left(\frac{|h_j|^2}{|h_j|^2 + No/Es} \right)^2 - Es \left(\frac{1}{N_c} \sum_{j=1}^{N_c} \frac{|h_j|^2}{|h_j|^2 + No/Es} \right)^2}{\left(\frac{1}{N_c} \sum_{j=1}^{N_c} \frac{|h_j|^2}{|h_j|^2 + No/Es} \right)^2}. \tag{4.3.27}$$

We will name β^{MMSE} to

$$\beta^{MMSE} = \frac{1}{N_c} \sum_{j=1}^{N_c} \frac{1}{|h_j|^2 + N_0/E_S} = \sum_{j=1}^{N_c} \beta_j^{MMSE} \tag{4.3.28}$$

Please, note, that after this definition the range of variation for β^{MMSE} is limited to $0 \leq \beta^{MMSE} \leq \frac{E_s}{N_0}$.

Manipulating the equations, as

$$\frac{E_s}{N_c}\sum_{j=1}^{N_c}\left(\frac{|h_j|^2}{|h_j|^2+N_0/E_s}\right)^2=\frac{E_s}{N_c}\sum_{j=1}^{N_c}\left(\frac{|h_j|^2}{|h_j|^2+N_0/E_s}\frac{|h_j|^2}{|h_j|^2+N_0/E_s}\right) \tag{4.3.29}$$

$$=\frac{E_s}{N_c}\sum\left(\frac{|h_j|^2}{|h_j|^2+N_0/E_s}\left(1-\frac{N_0/E_s}{|h_j|^2+N_0/E_s}\right)\right) \tag{4.3.30}$$

$$=\frac{E_s}{N_c}\sum\left(\frac{|h_j|^2}{|h_j|^2+N_0/E_s}\right)-\frac{N_o}{N_c}\sum\left(\frac{|h_j|^2}{\left(|h_j|^2+N_0/E_s\right)^2}\right) \tag{4.3.31}$$

Then

$$\sigma_\xi^2=\frac{\frac{Es}{Nc}\sum\left(\frac{|h_j|^2}{|h_j|^2+No/Es}\right)-Es\left(\frac{1}{N_c}\sum_{j=1}^{N_c}\frac{|h_j|^2}{|h_j|^2+No/Es}\right)^2}{\left(\frac{1}{N_c}\sum_{j=1}^{N_c}\frac{|h_j|^2}{|h_j|^2+No/Es}\right)^2}. \tag{4.3.32}$$

Taking into account that

$$\frac{1}{N_c}\sum_{j=1}^{N_c}\left(\frac{|h_j|^2}{|h_j|^2+N_0/E_s}\right)=\frac{1}{N_c}\sum_{j=1}^{N_c}\left(1-\frac{N_0/E_s}{|h_j|^2+N_o/E_s}\right) \tag{4.3.33}$$

$$=\frac{1}{N_c}\sum_{j=1}^{N_c}1-\frac{1}{N_c}\sum_{j=1}^{N_c}\frac{N_0/E_s}{|h_j|^2+N_0/E_s}=1-\frac{N_0}{E_s}\beta^{MMSE} \tag{4.3.34}$$

We can write

$$\sigma_\xi^2=\frac{Es\left(1-\frac{No}{Es}\beta^{MMSE}\right)-Es\left(1-\frac{No}{Es}\beta^{MMSE}\right)^2}{\left(1-\frac{No}{Es}\beta^{MMSE}\right)^2}=Es\left(\frac{1}{1-\frac{No}{Es}\beta^{MMSE}}-1\right) \tag{4.3.35}$$

And, finally,

$$\sigma_\xi^2=E_S\frac{\frac{N_0}{E_S}\beta^{MMSE}}{1-\frac{N_0}{E_S}\beta^{MMSE}} \tag{4.3.36}$$

PDF of β_j^{MMSE} can be easily obtained by a procedure similar to that in previous section for ZF except that we have to use first

$$f_{X+K}(t)=f_X(t-K) \tag{4.3.37}$$

Thus

$$f_{|h_j|^2+N_0/E_S}(s)=\left(\frac{2b_0m}{2b_0m+\Omega}\right)^m\frac{1}{2b_0}exp\left(-\frac{s-N_0/E_S}{2b_0}\right)\,{}_1F_1\left(m,1,\frac{\Omega(s-N_0/E_S)}{2b_0(2b_0m+\Omega)}\right) \tag{4.3.38}$$

Using now Eq. (4.3.5)

$$f_{1/(|h_j|^2+N_0/E_S)}(s) = \frac{1}{s^2}\left(\frac{2b_0 m}{2b_0 m+\Omega}\right)^m \frac{1}{2b_0} exp\left(-\frac{\frac{1}{s}-N_0/E_S}{2b_0}\right) {}_1F_1\left(m,1,\frac{\Omega(\frac{1}{s}-N_0/E_S)}{2b_0(2b_0 m+\Omega}\right), \tag{4.3.39}$$

i.e.

$$f_{1/(|h_j|^2+N_0/E_S)}(s) = \left(\frac{2b_0 m}{2b_0 m+\Omega}\right)^m \frac{1}{2b_0}\frac{1}{s^2} exp\left(-\frac{1-sN_0/E_S}{2b_0 s}\right) {}_1F_1\left(m,1,\frac{\Omega(1-sN_0/E_S)}{2b_0(2b_0 m+\Omega)s}\right). \tag{4.3.40}$$

By using now Eq. (4.3.7) to divide by N_c

$$f_{\beta_j^{MMSE}}(s) = \left(\frac{2b_0 m}{2b_0 m+\Omega}\right)^m \frac{1}{2b_0}\frac{1}{N_c s^2} exp\left(-\frac{1-sN_c N_0/E_S}{2b_0 N_c s}\right) {}_1F_1\left(m,1,\frac{\Omega(1-sN_c N_0/E_S}{2b_0(2b_0 m+\Omega)N_c s}\right) \tag{4.3.41}$$

We can compare it to that simpler expression for ZF (also repeated here for convenience) and note that both are equivalent for $N_0 = 0$

$$f_{\beta_j^{ZF}}(s) = \left(\frac{2b_0 m}{2b_0 m+\Omega}\right)^m \frac{1}{2b_0}\frac{1}{N_c s^2} exp\left(-\frac{1}{2b_0 N_c s}\right) {}_1F_1\left(m,1,\frac{\Omega}{2b_0 N_c s(2b_0 m+\Omega)}\right) \tag{4.3.42}$$

As in the previous case, if independence among the channel frequency responses is assumed, the CHF of β^{MMSE} yields

$$\Phi_{\beta^{MMSE}}(\omega) = \left(\Phi_{\beta_j^{MMSE}}(\omega)\right)^{N_c} \tag{4.3.43}$$

With the CHF of β_j given by

$$\Phi_{\beta_j^{MMSE}}(\omega) = \int_0^\infty f_{\beta_j^{MMSE}}(s) e^{\imath s\omega} ds \tag{4.3.44}$$

To our best knowledge, it is not possible to obtain an analytical expression for the CHF of β_j but only numerical calculation could be carried on, e.g. by means of successive computations of Eq. (4.3.44). Later on, it is possible to evaluate the CDF of β^{MMSE} using Gil-Peláez's inversion theorem expression [34] which can be written in this particular case as

$$F_{\beta^{MMSE}}\left(\beta^{MMSE}\right) = \frac{1}{2} - \frac{1}{2\pi}\int_0^\infty \left(\frac{\Phi_{\beta^{MMSE}}(\omega)}{\imath\omega} e^{-\imath\beta^{MMSE}\omega} - \frac{\Phi_{\beta^{MMSE}}(-\omega)}{\imath\omega} e^{\imath\beta^{MMSE}\omega}\right) d\omega \tag{4.3.45}$$

We might later evaluate the SNR by using Eq. (4.3.36) as

$$\gamma^{MMSE} = \frac{E_s}{\sigma_\xi^2} = \frac{\frac{E_s}{N_0}}{\beta^{MMSE}} - 1 \tag{4.3.46}$$

Its CDF is also easy to evaluate from that of β^{MMSE} as

$$F_\gamma^{MMSE}(g) = Pr\left[\gamma^{MMSE} < g\right] = Pr\left[\frac{\frac{E_s}{N_0}}{\beta^{MMSE}} - 1 < g\right] = Pr\left[\beta > \frac{E_s/N_0}{g+1}\right] \tag{4.3.47}$$

Thus

$$F_\gamma^{MMSE}(g) = 1 - F_\beta^{MMSE}\left(\frac{E_s/N_0}{g+1}\right) \tag{4.3.48}$$

Note that, being the range of β^{MMSE} from 0 to E_s/N_0, $F_\gamma^{MMSE}(0) = 1 - F_\beta^{MMSE}(E_s/N_0) = 0$ as expected. For $g \to \infty$ it is clear that $F_\gamma^{MMSE}(g) = 1$.

In [14] a similar procedure was followed but with a slight different expression as they name

$$\sqrt{\alpha^{MMSE}} = \frac{1}{N_c}\sum_{j=1}^{N_c}\frac{|h_j|^2}{|h_j|^2 + N_0/E_S} \tag{4.3.49}$$

And from it, they evaluate the SNR conditioned to channel as

$$\frac{1}{\sqrt{\frac{1}{\alpha_{MMSE}}} - 1} \tag{4.3.50}$$

4.4 Numerical Results

As previously stated, the modulation scheme employed to convert bits into complex symbols given to the SC-FDMA system could be fixed to certain constellation or could track the quality of the received signal, that is, an Adaptive Modulation (AM) approach. In this chapter, fixed modulation schemes have been considered. Specifically, BPSK and square QAM performance in terms of BER has been evaluated.

BER can be evaluated as the average of the BER conditioned to β, that is,

$$BER \doteq \int BER(\beta) f_\beta(\beta) d\beta \tag{4.4.1}$$

Table 4.1: Simulation Parameters

Parameter	Value
Total number of subcarriers M	1024
Allocated subcarriers N_c	$1, 64$
Modulation scheme	BPSK, 4QAM, 16QAM
Equalizers	ZF, MMSE
Cyclic Prefix Length	144
Default E_s/N_0 (dB)	10
Δf	$15KHz$
τ_{avg} (Exponential PDP)	$1.17\mu s$

With $BER(\beta)$ evaluated from the bit error rate of QAM over AWGN channels [14]. For Gray coding and square M-QAM, it might be evaluated from [35] as

$$BER(\gamma) = \frac{2}{\sqrt{M}log_2\sqrt{M}} \sum_{k=1}^{log_2\sqrt{M}} \sum_{i=0}^{(1-2^{-k}(\sqrt{M}-1)} \left\{ (-1^{\lfloor \frac{i2^{k-1}}{\sqrt{M}} \rfloor} \left(\frac{i2^{k-1}}{\sqrt{M}} + \frac{1}{2} \right) Q\left(\sqrt{\frac{6(2i+1)^2}{2(M-1)}\gamma} \right) \right\} \tag{4.4.2}$$

By simply substituting γ by β as given Eq. (4.3.12) or Eq. (4.3.46) for ZF and MMSE FDE, respectively.

4.4.1 CDF of β

Two different approaches have been followed to evaluate the PDF of β depending on the channel model. For independent subcarrier responses, CDF of β can be evaluated numerically following the previously described procedure with Eq. (4.3.9) and Eq. (4.3.10) for ZF and their equivalent ones for MMSE. Results for CDF in this case are shown in Figures 4.3 and 4.4 for heavy and light shadowing, respectively, and average SNR 10 dB. When the exponential PDP given in Eq. (3.5.8) is assumed, certain correlation between channel responses at different subcarriers avoids using that the CHF of the addition is the product of those of each term, making the analysis infeasible. In this case, a semi-analytical approach has been taken from the values of $\mathbf{h}$, that of β has been evaluated by using Eq. (4.3.4) or Eq. (5.3.7) and, by using ergodicity condition, its CDF is evaluated from time histogram. Results in this case are shown in Figures 4.5 and 4.8. As expected, in all cases, β takes statistically

lower values that for light fading as fading is deeper for heavy shadowing.

From results for independent subcarriers, it is clear that for ZF equalization β could reach higher values due to the noise enhancement for low values of channel gain. By contrast, MMSE equalization forces the maximum value for β. It is also observed a completely different performance for ZF and MMSE equalization as the number of subcarriers N_c changes. With ZF equalizer, reducing the number of subcarriers N_c lower the value of the effective β^{ZF}, thus β values for OFDM ($N_c = 1$) are statistically lower. On the other hand, in case of MMSE equalizer, the effect is opposite.

The effect of correlation in frequency can be seen from comparison among Figures 4.3, 4.5, and 4.7 for heavy shadowing, and from Figures 4.4, 4.6, and 4.8 for light shadowing. Only slight differences are shown for MMSE. However, for ZF equalization the use of subcarriers with highly correlated responses, as in LFDMA, reduces the range for β. This is the result of the fact that for ZF equalization the most faded subcarrier is forcing its value. The more uncorrelated the responses, the higher the probability of having at least one subcarrier which is highly faded.

4.4.2 BER Results

Figures 4.9 and 4.10 show comparison of BER over light shadowed channel with ZF and MMSE equalizer. Heavy shadowing results are consistent with Rayleigh fading results. Result for AWGN channel is also shown for comparison. The BER has been numerically evaluated when possible and obtained as time averaging of the BER for the given SNR in another case.

As previously stated, in the case of ZF equalization, for an SC-FDMA transmission scheme the value of the SNR (γ) is always lower than that of OFDMA; that causes a BER worse in the former. In the case of MMSE equalization, the SC-FDMA BER for uncorrelated frequency responses is below OFDMA. The consequence of the CDF of β, frequency correlation for ZF improves BER, that is, BER for LFDMA is better than that of IFDMA. On the contrary, MMSE enhance is clear for independent subcarrier responses. These results are consistent with SC-FDMA performance over Rician channel [36].

In Figures 4.11 and 4.12 the effect of the number of allocated subcarriers is analyzed. It observed that for the higher number of allocated subcarriers, BER decreases in case MMSE equalizer is used. In the case of ZF equalizer, this increase does not improve the performance.

The BER performance of SC-FDMA over different shadowing is depicted in Figure 4.13. It is observed that for both with ZF and MMSE equalization light shadowing BER is below that of average and heavy shadowing. Obviously, this is due to its stronger LOS component.

Figure 4.14 shows the performance of different constellations over one selected scenario, that is of light shadowing with ZF equalizer. It is obvious that the higher the constellation size, the worse is the BER. This is of course true for all considered scenarios.

4.5 Conclusions

In this chapter we have analysed the performance of SC-FDMA for independent and correlated channel frequency responses. The OFDM BER response was compared to that of SC-FDMA over different shadowing. It is observed that OFDM BER results are lower than those of SC-FDMA with ZF equalization. In the case of MMSE equalizer, independence among channel frequency responses improves the BER compared to that of Interleaved SC-FDMA, Localized SC-FDMA and OFDM. Heavy shadowing results are consistent with Rayleigh fading results. Light shadowing results are equivalent to 5 dB Rice factor results of Rician channel.

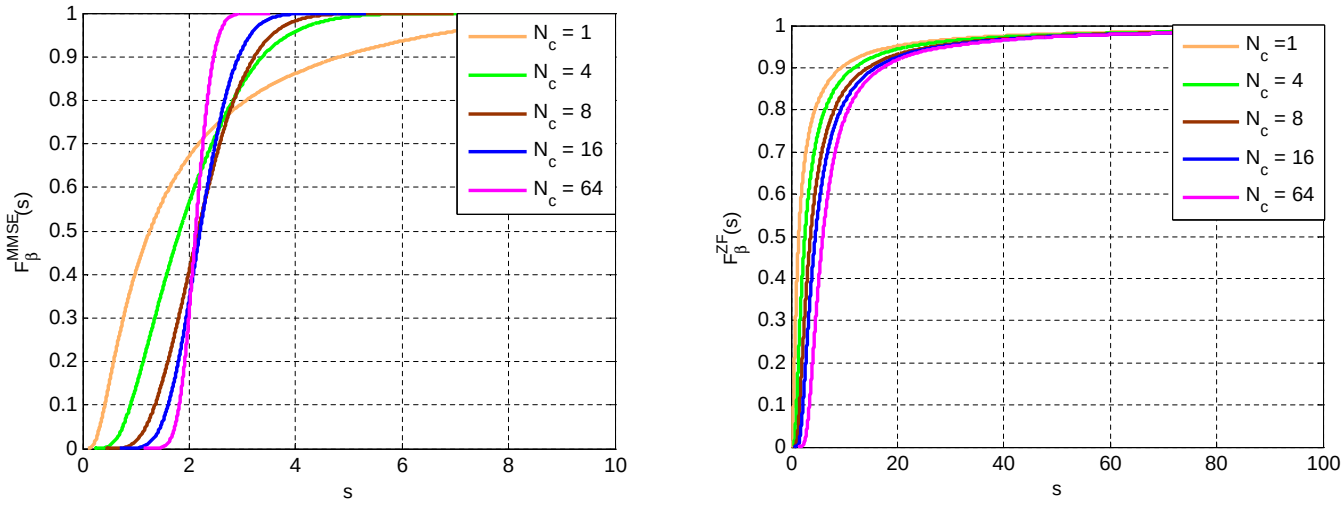

Figure 4.3: CDF of β for heavy shadowing with MMSE and ZF equalizer for uncorrelated responses at different subcarriers

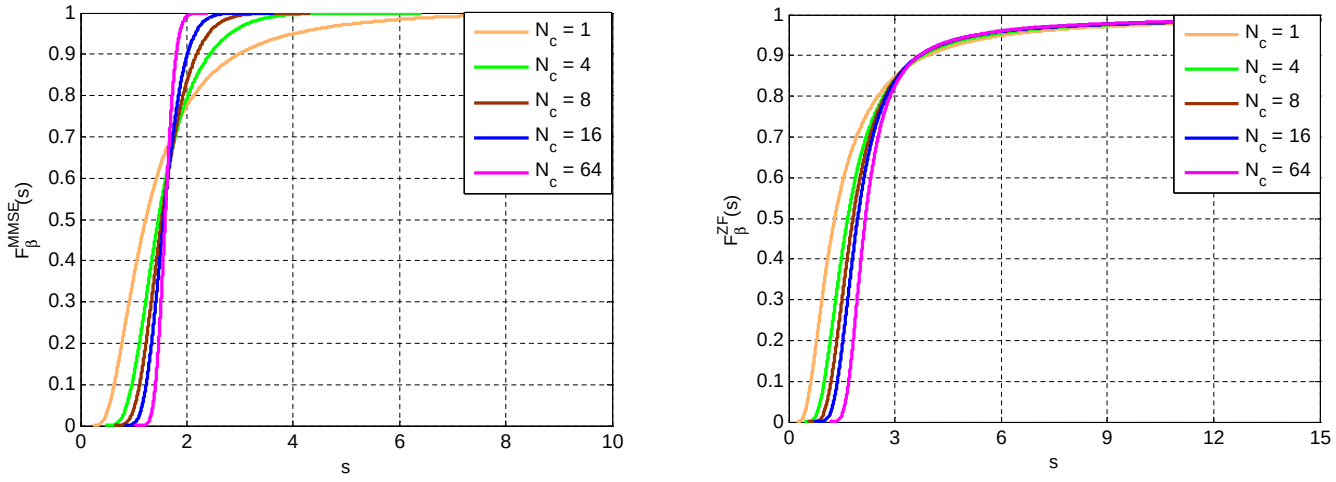

Figure 4.4: CDF of β for light shadowing with MMSE and ZF equalizer for uncorrelated responses at different subcarriers

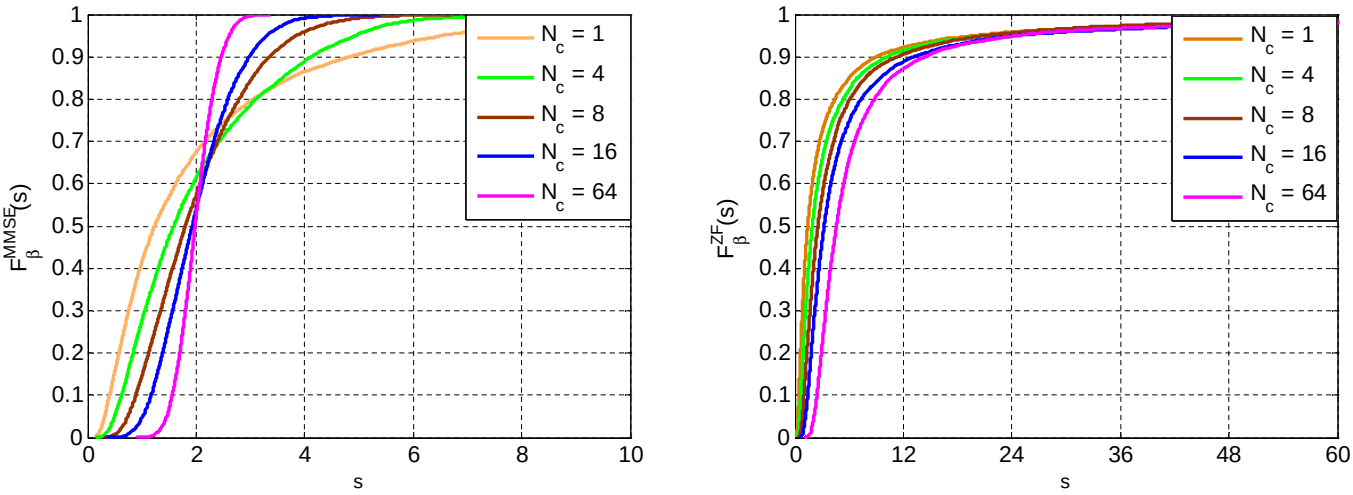

Figure 4.5: CDF of β for heavy shadowing with MMSE and ZF equalizer for correlated responses at different subcarriers and interleaved allocation (IFDMA)

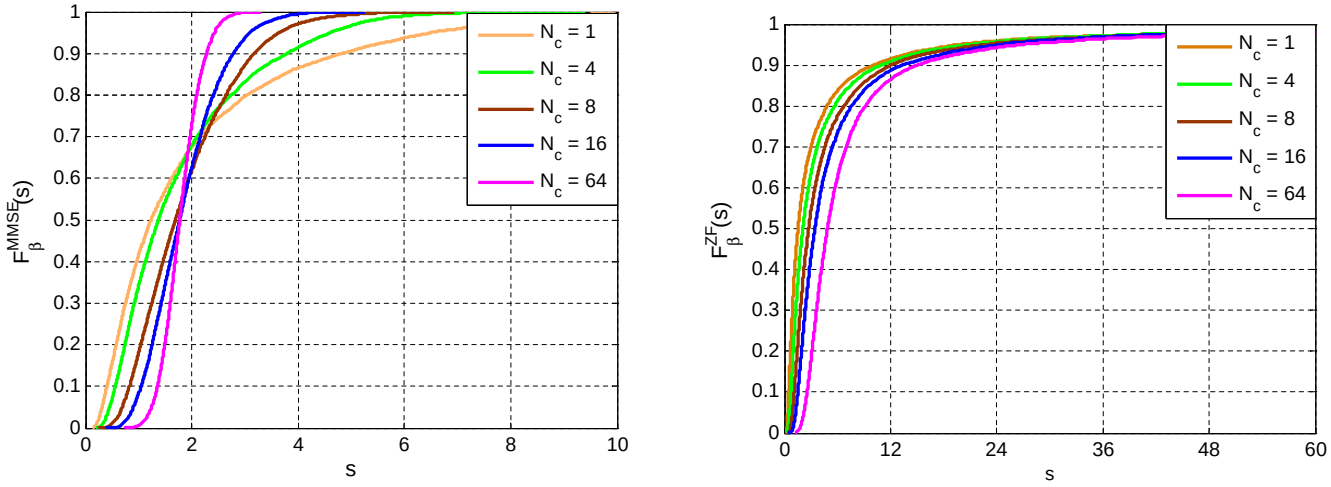

Figure 4.6: CDF of β for light shadowing with MMSE and ZF equalizer for correlated responses at different subcarriers and interleaved allocation (IFDMA)

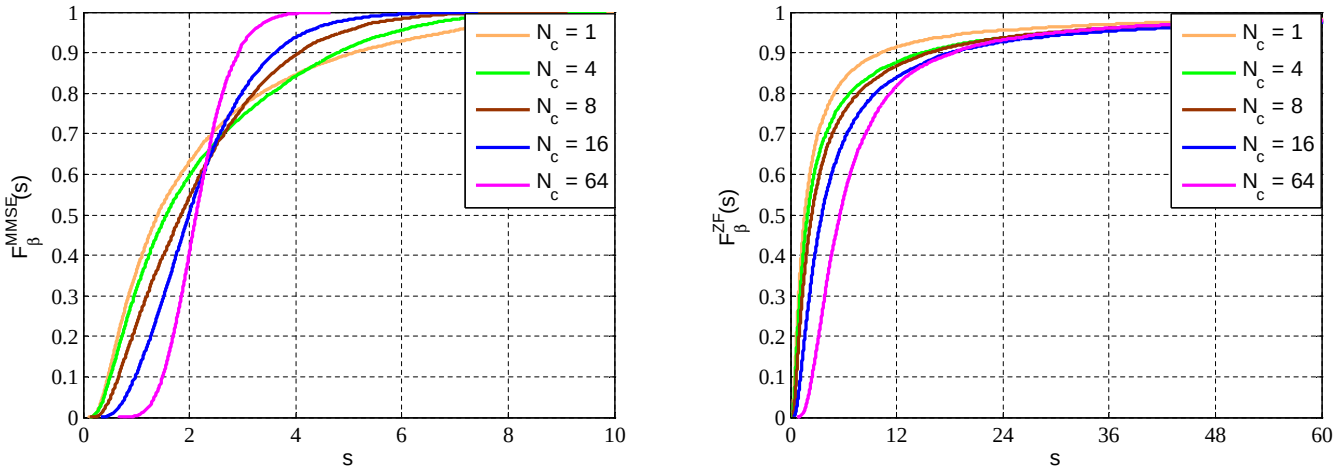

Figure 4.7: CDF of β for heavy shadowing with MMSE and ZF equalizer for correlated responses at different subcarriers and localized allocation (LFDMA)

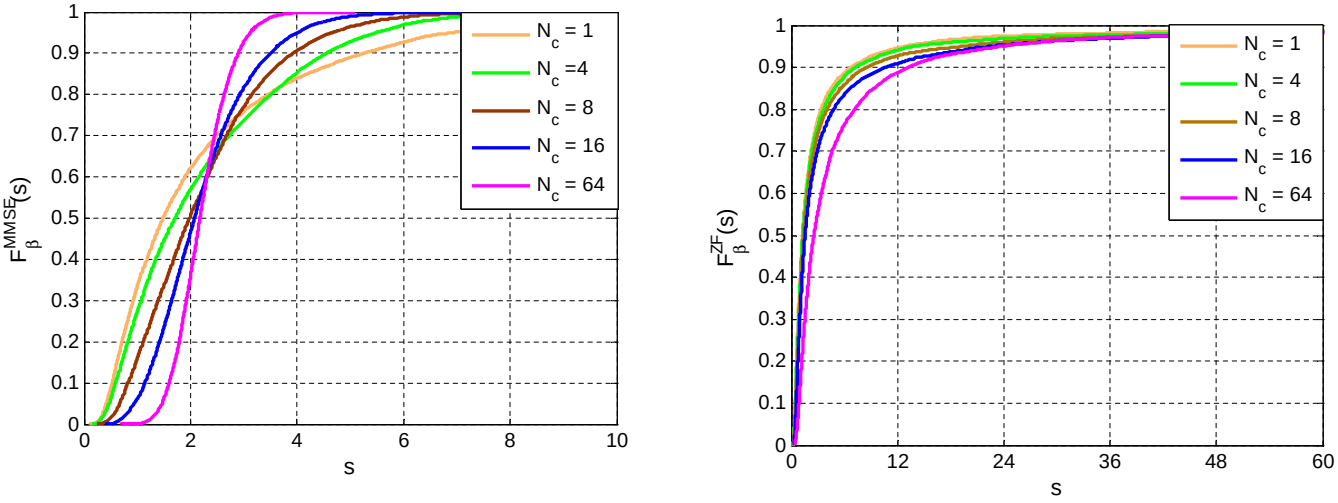

Figure 4.8: CDF of β for light shadowing with MMSE and ZF equalizer for correlated responses at different subcarriers and localized allocation (LFDMA)

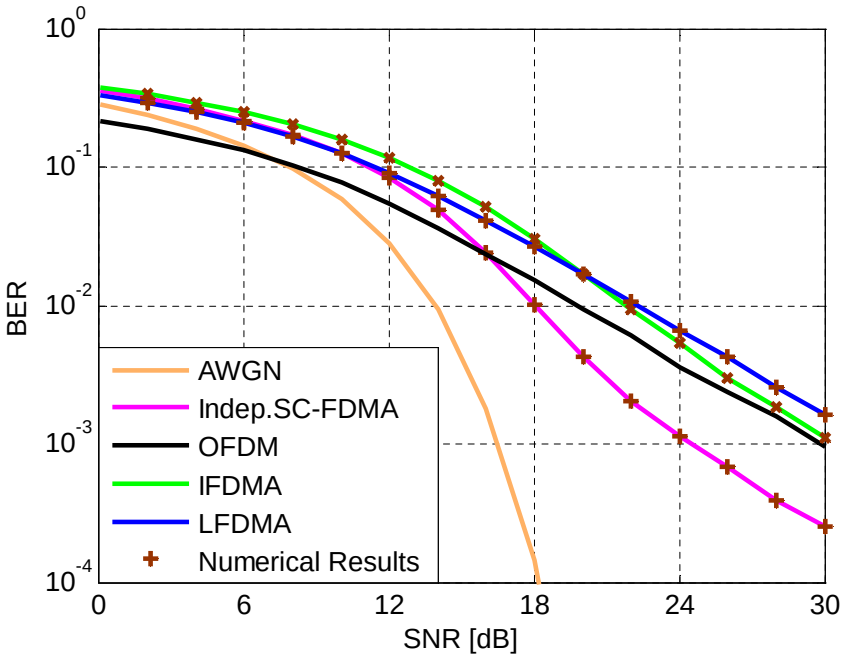

Figure 4.9: BER of OFDM, IFDMA, LFDMA, and independent SC-FDMA with 16QAM for light shadowing, $N_c = 64$ and ZF equalizer

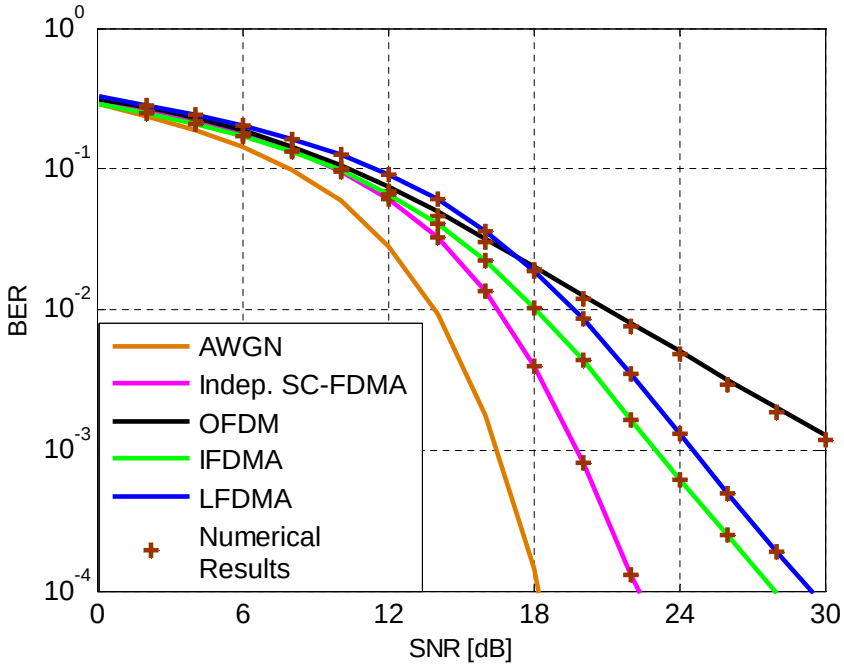

Figure 4.10: BER of OFDM, IFDMA, LFDMA, and independent SC-FDMA with 16QAM for light shadowing, $N_c = 64$ and MMSE equalizer

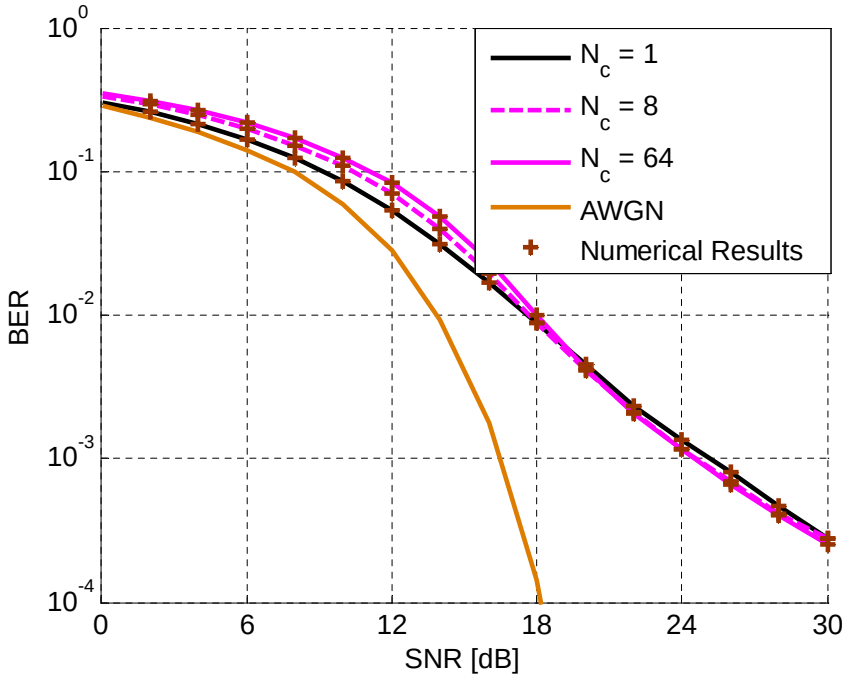

Figure 4.11: BER of OFDM, IFDMA, LFDMA, and independent SC-FDMA with 16QAM for light shadowing for different N_c and ZF equalizer

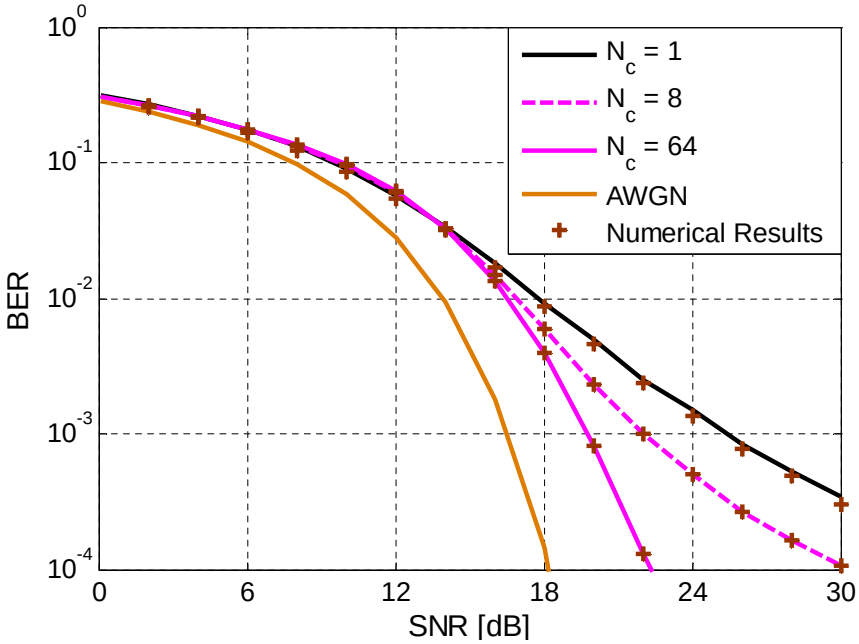

Figure 4.12: BER of OFDM, IFDMA, LFDMA, and independent SC-FDMA with 16QAM for light shadowing, for different N_c and MMSE equalizer

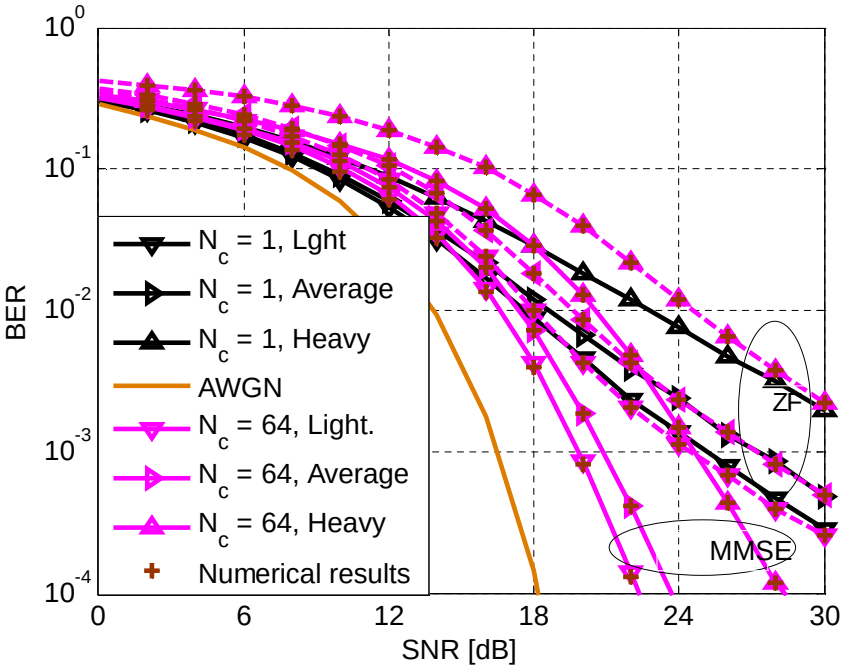

Figure 4.13: BER of independent SC-FDMA with 16QAM for different shadowing, ZF and MMSE equalizers

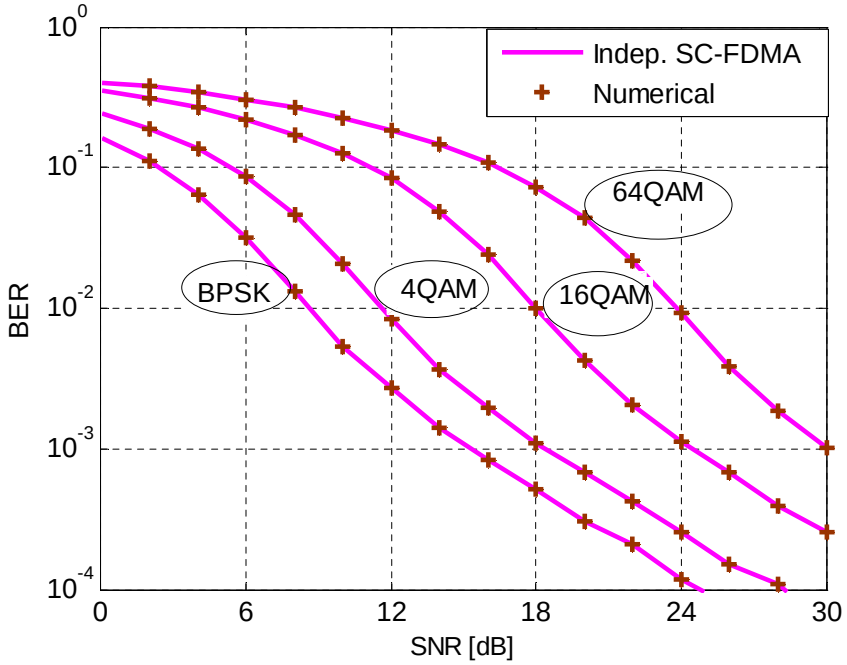

Figure 4.14: BER of independent SC-FDMA with different constellation size for light shadowing and ZF equalizer

Chapter 5

SC-FDMA Spectral Efficiency over Shadowed Rice LMS Channel

5.1 Introduction

Adaptive Modulation and Coding (AMC) technique is used in most current wireless systems to mitigate the time selective fading channel [37]. Adaptive modulation tracks the channel in such a way that when channel offers worse quality, more robust constellation/coding schemes are employed. On the other hand, if channel quality improves, transmission rate is increased at the expense of protection of sent bits.

In this chapter, we focus on the spectral efficiency of uncoded SC-FDMA transmission over shadowed Rice land mobile satellite channel in which LOS follows Nakagami distribution. Starting from the CDF of β calculated in the last chapter, the spectral efficiency is evaluated for different shadowing's using ZF and MMSE equalization.The spectral efficiency results of OFDM are also included for comparison.

5.2 Overview of Adaptive Modulation and Coding

We consider constant power and discrete rate adaptive modulation. In the following, we assume a set of constellations of size $R_0 = 0$, $R_1 = 2$, and $R_i = 2^{2(i-1)}, i = 2..N$.

As stated in the previous chapters, the instantaneous bit error rate for those constellations when used for SC-FDMA transmission are functions of the equivalent SNR (γ). Commonly, slow fading is assumed, that is, BER for the i-th constellation can be evaluated with an

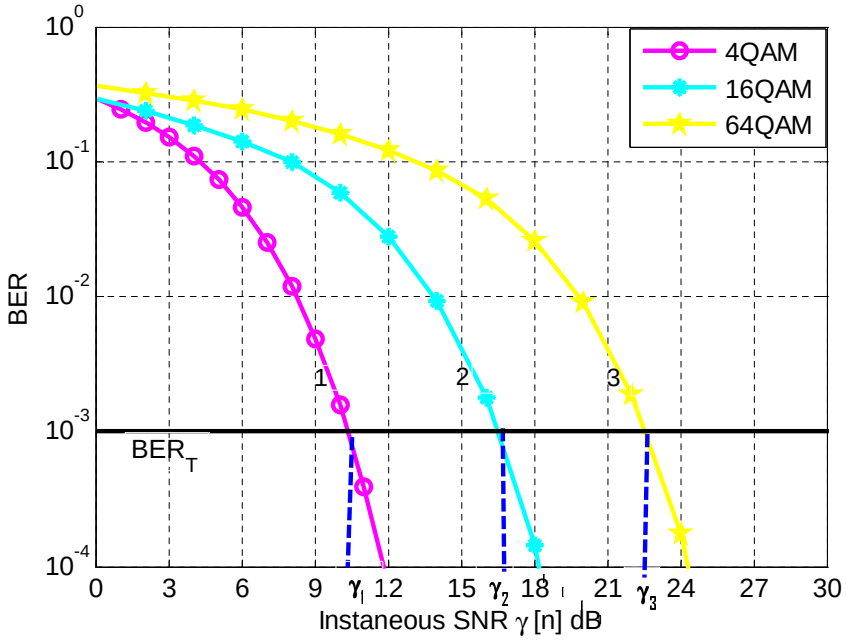

Figure 5.1: Examples of adaptive modulation regions for uncoded QAM

AWGN approach.

$$BER_i(\gamma) \approx BER_i^{AWGN}(\gamma) \tag{5.2.1}$$

Several criteria can be used to associate one constellation to each γ in adaptive modulation. The approach considered in this dissertation is discretizing the range of channel fade levels in such a way that the BER is always kept under a target, that is, $BER_i \leq BER_T$, being BER_T a design parameter. As shown in Figure 5.1, the range of γ is divided in to N fading regions $\Re_i = \{\gamma_i, \gamma_{i+1}\}$, $i = 0, 1, 2, ...N-1$ where $\gamma_0 = 0$ and $\gamma_N = \infty$. Within the fading region $\Re_i$, a certain QAM constellation with R_i bits/symbol is employed.

Switching thresholds $\{\gamma_i,\ i = 1, .., N-1\}$ are designed to maximize the spectral efficiency under that instantaneous BER constraints BER_T. Being BER_i monotonically decreasing, this finally means that at switching thresholds BER is exactly the target BER.

$$BER_i(\gamma_i) = BER_T \tag{5.2.2}$$

Whichever are the taken design criteria, the average spectral efficiency is written as

$$\frac{R}{B} = \sum_{i=1}^{L-1} \log_2 (M_i) \, Pr\{\gamma_{i-1} < \gamma \leq \gamma_i\} \tag{5.2.3}$$

Note that stricter BER_T values implies lower spectral efficiency values. For SNR values below a minimum threshold (i.e., in very poor channel conditions), there is an outage state in which there is no data transmission.

To perform adaptation, the instantaneous SNR γ has to be estimated at the receiver to determine the current fading region $\Re_i$ and, consequently, the transmit rate R_i. Both the average and the instantaneous SNR are supposed to be perfectly known and the receiver suggestion assumed to be fed back to the transmitter without delay nor errors.

5.3 Spectral Efficiency Analysis

In this section, the average spectral efficiency is evaluated for ZF and MMSE equalization.

5.3.1 ZF-FDE Analysis

As we obtained in previous chapter, instantaneous SNR at the receiver for SC-FDMA with ZF equalization is given by

$$\gamma^{ZF} = \frac{E_S}{\beta^{ZF} N_0} \tag{5.3.1}$$

where β^{ZF} is defined as

$$\beta^{ZF} = \frac{1}{N_c} \sum_{k=1}^{N_c} \frac{1}{|h_k|^2} \tag{5.3.2}$$

For OFDM the same expression is valid if N_c is set to 1. In both cases, the constellation corresponding to the i-th region is applied when the SNR is between the corresponding boundaries, that is

$$\gamma_i < \frac{E_s}{\beta^{ZF} N_0} < \gamma_{i+1} \tag{5.3.3}$$

We can rewrite the above the equation and the threshold for β^{ZF} becomes

$$\beta_{i+1}^{ZF} = \frac{1}{\gamma_{i+1}} \frac{E_S}{N_0} < \beta^{ZF} < \frac{1}{\gamma_i} \frac{E_S}{N_0} = \beta_i^{ZF} \tag{5.3.4}$$

where β_i^{ZF} and β_{i+1}^{ZF} are the modified thresholds. Please, note that they depend on E_s/N_0. The spectral efficiency can be averaged as

$$\frac{R}{B} = \sum_{i=1}^{N-1} \log_2(M_i) \left[F_{\beta^{ZF}}\left(\beta_i^{ZF}\right) - F_{\beta^{ZF}}\left(\beta_{i+1}^{ZF}\right) \right] \tag{5.3.5}$$

where N is the number of fading regions. Thus, in order to compute spectral efficiency values, we only require $F_{\beta^{ZF}}(\beta^{ZF})$ given by Eq. (4.3.11).

5.3.2 MMSE-FDE Analysis

For MMSE-FDE the value of SNR at the receiver is determined by Eq. (4.3.46) repeated here for convenience

$$\gamma^{MMSE} = \frac{E_s}{\sigma_\xi^2} = \frac{\frac{E_s}{N_0}}{\beta^{MMSE}} - 1 \tag{5.3.6}$$

where

$$\beta^{MMSE} = \frac{1}{N_c} \sum_{j=1}^{N_c} \frac{1}{|h_j|^2 + N_0/E_S} = \sum_{j=1}^{N_c} \beta_j^{MMSE} \tag{5.3.7}$$

The parameter β^{MMSE} decides the SNR and hence, the corresponding constellation to be used, that is

$$\beta_{i+1}^{MMSE} = \frac{\frac{E_S}{N_0}}{\gamma_{i+1}+1} < \beta^{MMSE} < \frac{\frac{E_S}{N_0}}{\gamma_i+1} = \beta_i^{MMSE} \tag{5.3.8}$$

with β_i^{MMSE} and β_{i+1}^{MMSE}, the modified thresholds that depend on the SNR.

The average spectral efficiency can be computed as

$$\frac{R}{B} = \sum_{i=1}^{N-1} \log_2(M_i) \left[F_{\beta^{MMSE}}\left(\beta_i^{MMSE}\right) - F_{\beta^{MMSE}}\left(\beta_{i+1}^{MMSE}\right) \right] \tag{5.3.9}$$

Again, in order to compute spectral efficiency values, we only require $F_{\beta^{MMMSE}}(\beta^{MMSE})$ given by Eq. (4.3.45).

5.4 Simulation Results and Discussion

In this section, we discuss the spectral efficiency results for OFDM, Independent SC-FDMA, Localized SC-FDMA, and Interleaved SC-FDMA and over different shadowing profiles.

Table 5.1: Switching thresholds of the SNR $\{\gamma_i\}$ for adaptive modulation and coding

$\gamma_i(dB)$	9 .7980	16.5290	22.5510	28.4170
$log_2(M_i)$	2	4	6	8

The spectral efficiency is calculated using Eq. (5.3.5) and (5.3.9) for ZF and MMSE, respectively. We consider the channel frequency responses, which are generated for each allocated subcarriers, to calculate the effective noise at the detector stage for ZF and MMSE equalizer. All the results presented were obtained for a fix $BER_T = 10^{-3}$, which has chosen as a reference value. Stricter BER target BER_T values implies lower spectral efficiency values. The set of switching thresholds $\{\gamma_i,\ i = 1, .., N-1\}$ are given in Table 5.1.

Figure 5.2 shows the spectral efficiency with ZF equalization over different shadowing profiles for independent subcarrier responses. The result for $N_c = 1$ refers to OFDM spectral efficiency. Equivalent results for MMSE are shown in Figure 5.3. It is observed that the noise amplification factor β is having low value for light shadowing as compared to average and heavy shadowing, so spectral efficiency is approaching close to OFDM. By observation of those figures, it is concluded that an increase in the number of allocated subcarriers reduces the spectral efficiency in SC-FDMA, whereas the spectral efficiency of OFDM is independent of this value (and equivalent to that of SC-FDMA with $N_c = 1$). The provided results for heavy shadowing are consistent with Rayleigh fading results [38].

It can be observed that SC-FDMA curves for spectral efficiency look like piecewise. This is more noticeable for light shadowing. The reason of this can be found in the behaviour of β PDF as shown for ZF equalization in Figure 5.4 and Figure 5.5 for 10 dB SNR over light and average shadowing channels, respectively. It can be observed that the PDF of β for $Nc = 64$ is very narrow, thus most values of β^{ZF} are concentrated in a unique fading region; so the same modulation scheme is applied under most instantaneous β^{ZF} values. In the case of OFDM ($N_c = 1$), β^{ZF} pdf is wider, occupying several fading regions. As a result of averaging, its spectral efficiency curve grows smoother [38].

Results for pdf of β^{MMSE} for $N_c = 64$ are shown in Figure 5.6. As described in previous chapter, its range is much shorter, but conversion into γ^{MMSE} finally results in similar ZF and MMSE performance, despite the different approaches to equalization, especially for high

SNR values.

The results of spectral efficiency for correlated subcarrier responses are depicted as shown in Figures 5.7 and 5.8 for IFDMA and LFDMA over light shadowing with ZF and MMSE equalizer respectively. Results for independent subcarrier responses and OFDM are kept for comparison. It is observed that spectral efficiency for LFDMA results with ZF equalizer is approaching to OFDM with less allocated subcarriers as the spectral efficiency increases when there is strong correlation among channel frequency responses. In fact, for flat fading channels in which the channel frequency response is the same for all subcarriers, β becomes the noise enhancement factor for OFDM. The same thing is observed for average shadowing with ZF and MMSE equalizer as shown in Figures 5.9 and 5.10. The results for heavy shadowing are shown in Figures 5.11 and 5.12. It is observed that spectral efficiency of independent subcarrier responses approaches to interleaved SC-FDMA, IFDMA. As in heavy shadowing the LOS component is weak, it is observed that the curves are lower compared to light shadowing. The existence of the strong line of sight component, as that of light fading, improves the performance through the weak multi-path component.

5.5 Conclusions

In this chapter, spectral efficiency for SC-FDMA has been calculated under ZF and MMSE equalization. The CDFs of β evaluated in the previous chapter were enough to evaluate it. It is observed that spectral efficiency of OFDM is better than that of Interleaved and Localized SC-FDMA while independent SC-FDMA spectral efficiency is approaching to OFDM spectral efficiency. Spectral efficiencies reached by ZF and MMSE equalizer look like similar. Moreover, the higher is the number of allocated subcarrier, the lower is the spectral efficiency.

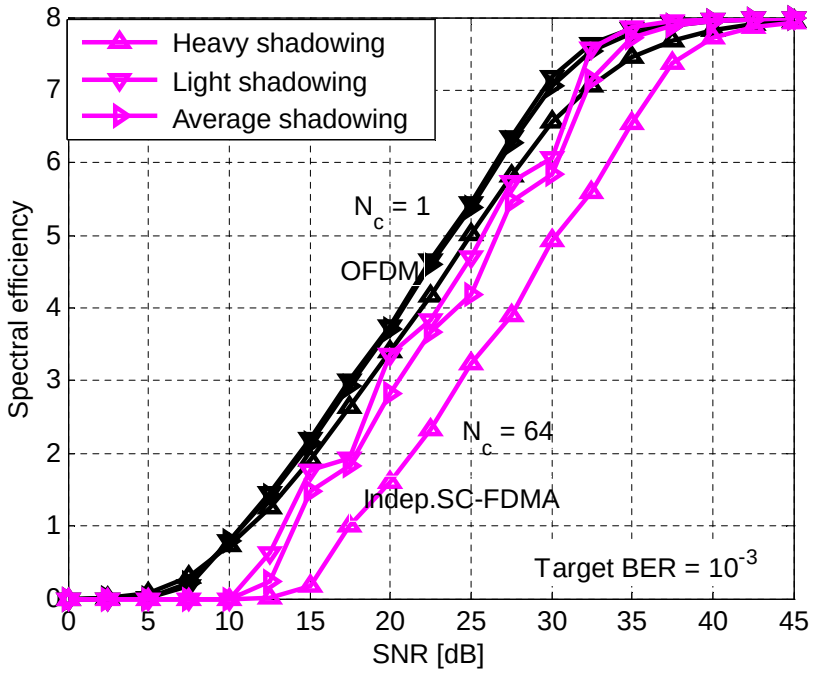

Figure 5.2: Spectral efficiency of OFDM and SC-FDMA for independent subcarrier responses over different shadowing profiles with ZF equalizer

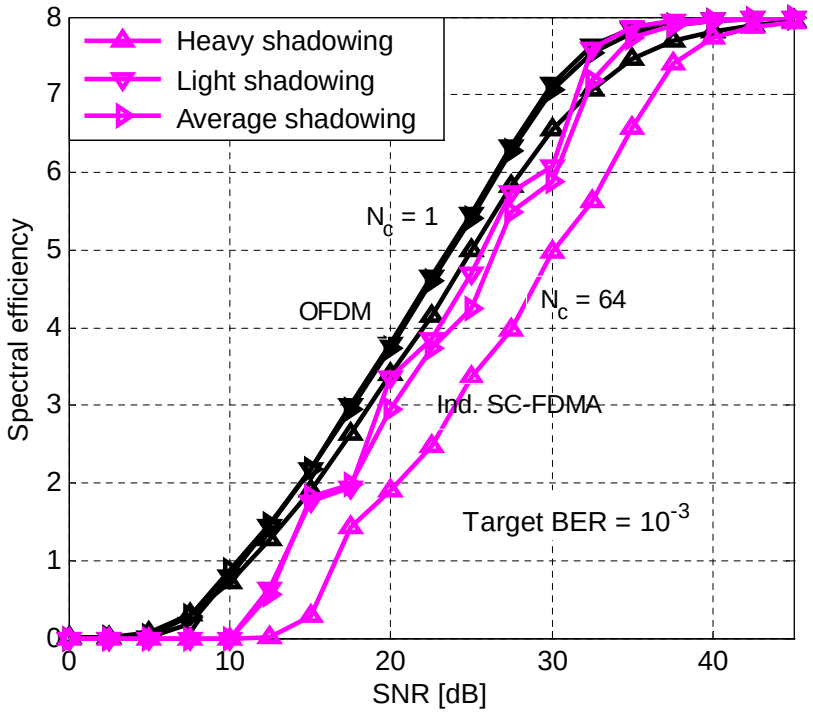

Figure 5.3: Spectral efficiency of OFDM and SC-FDMA for independent subcarrier responses over different shadowing profiles with MMSE equalizer

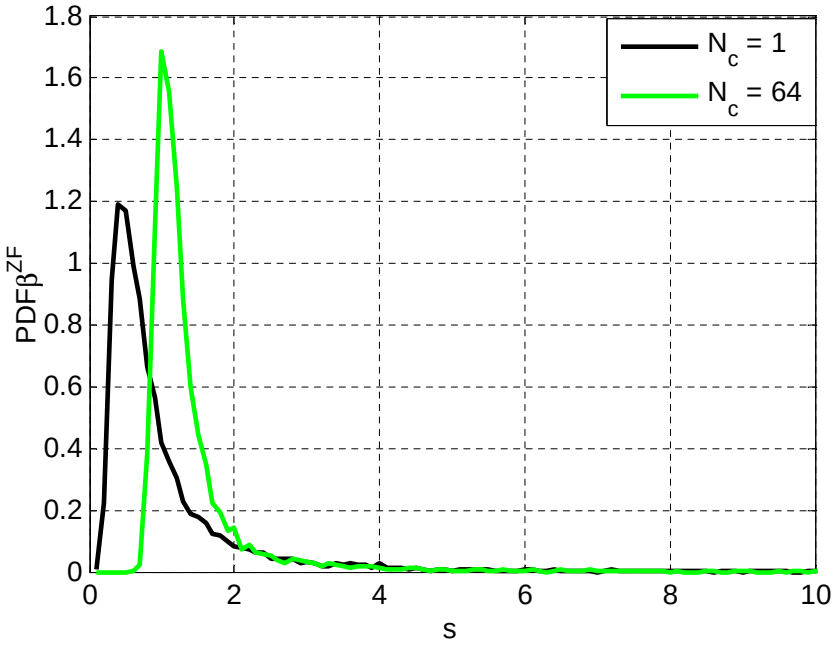

Figure 5.4: PDF of β^{ZF} under light shadowing for 10 dB SNR and different allocated subcarriers

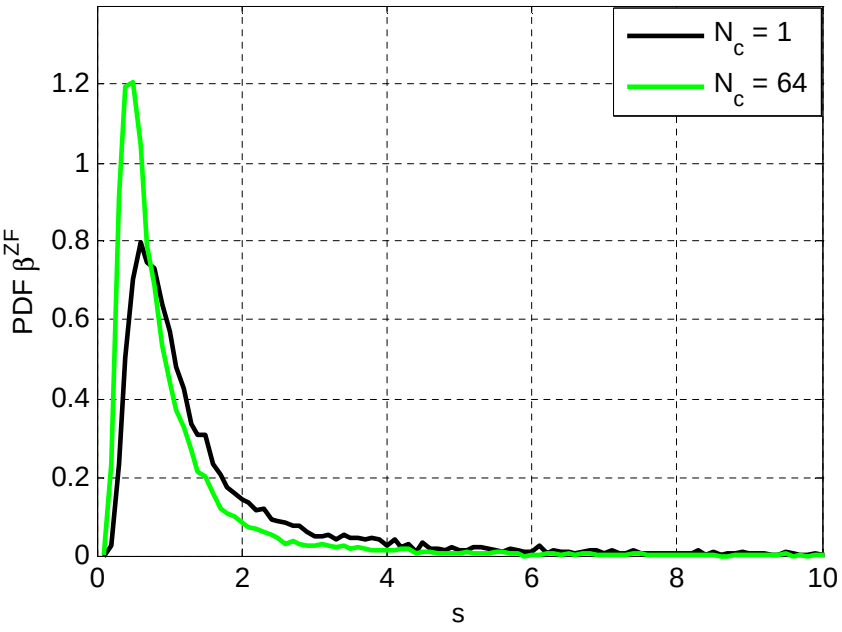

Figure 5.5: PDF of β^{ZF} under average shadowing for 10 dB SNR and different allocated subcarriers

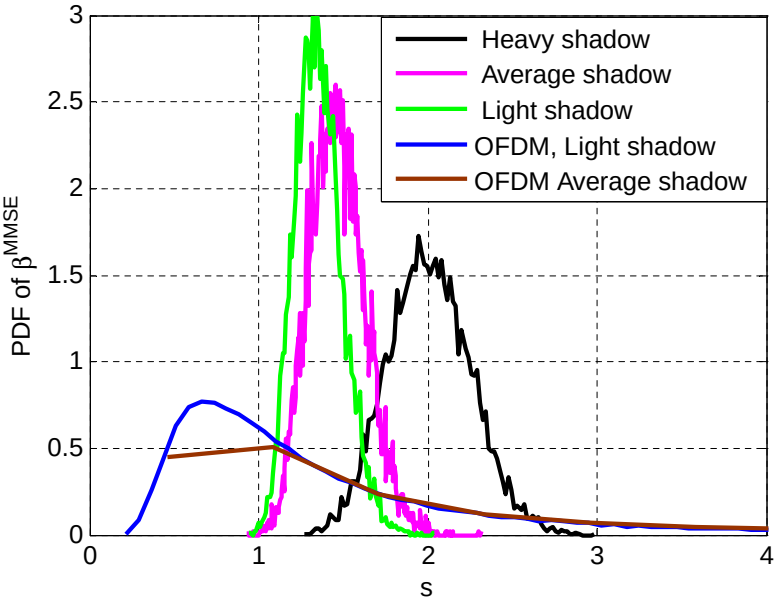

Figure 5.6: PDF of β^{MMSE} under different shadowing profiles for 10 dB SNR and 64 allocated subcarriers

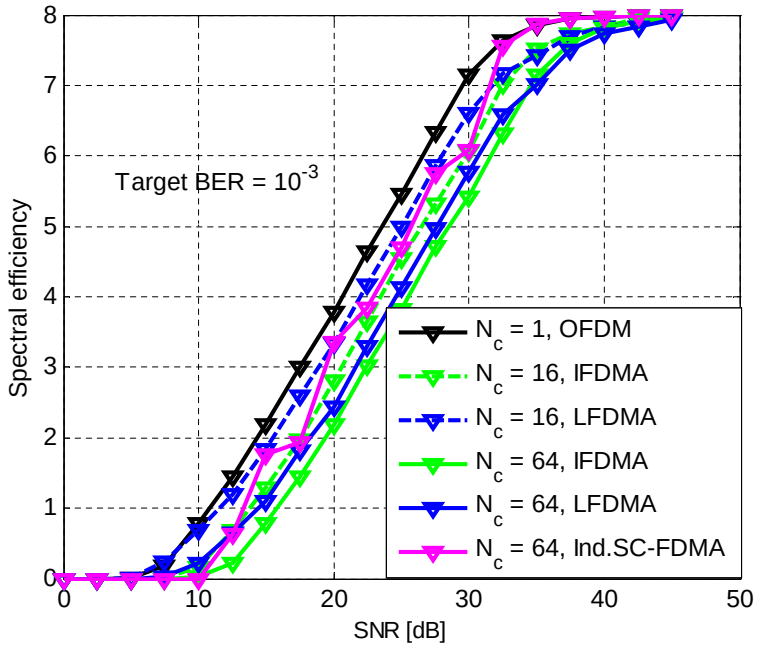

Figure 5.7: Spectral efficiency: OFDM, IFDMA, LFDMA and independent SC-FDMA for light shadowing with ZF equalizer

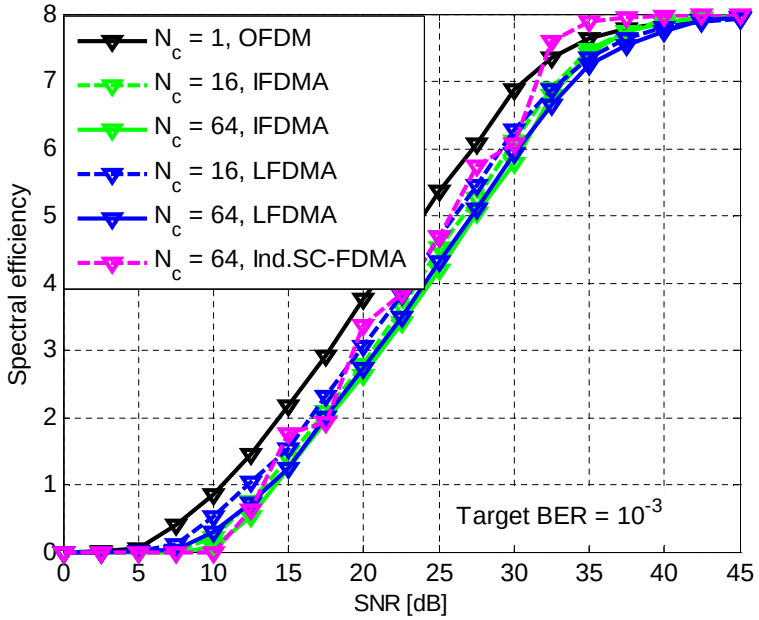

Figure 5.8: Spectral efficiency: OFDM, IFDMA, LFDMA and independent SC-FDMA for light shadowing with MMSE equalizer

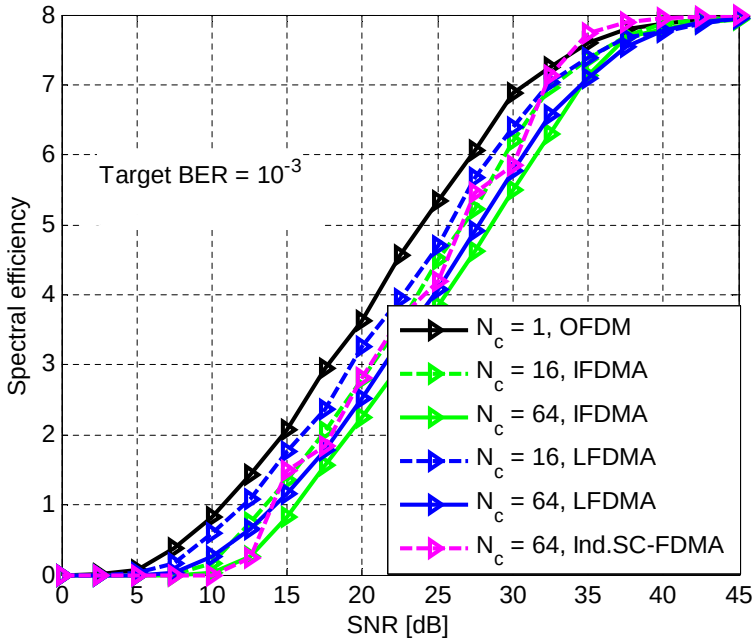

Figure 5.9: Spectral efficiency: OFDM, IFDMA, LFDMA and independent SC-FDMA for average shadowing with ZF equalizer

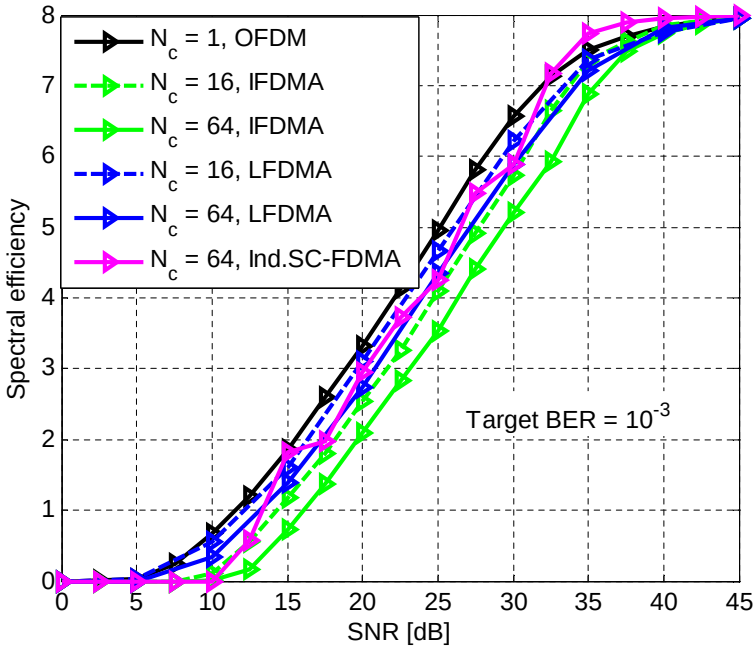

Figure 5.10: Spectral efficiency: OFDM, IFDMA, LFDMA and independent SC-FDMA for average shadowing with MMSE equalizer

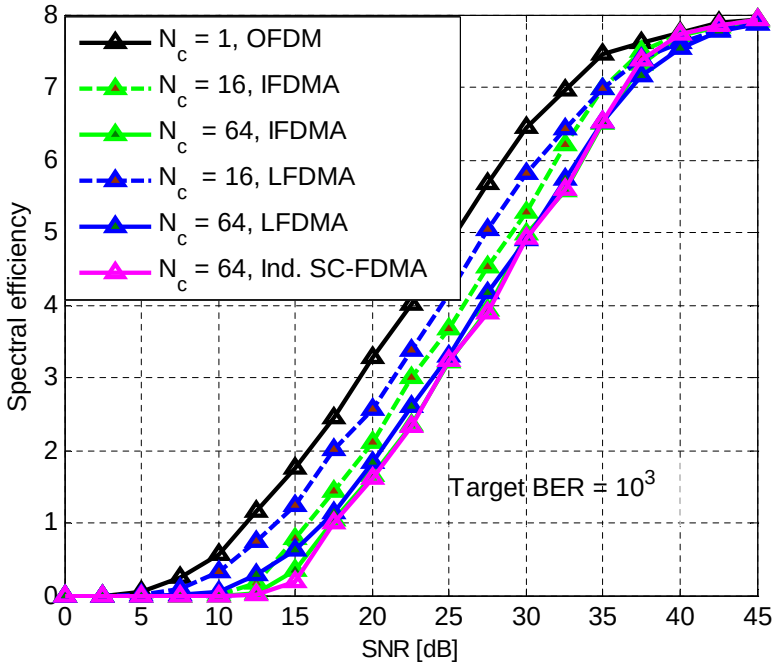

Figure 5.11: Spectral efficiency: OFDM, IFDMA, LFDMA and independent SC-FDMA for heavy shadowing, ZF

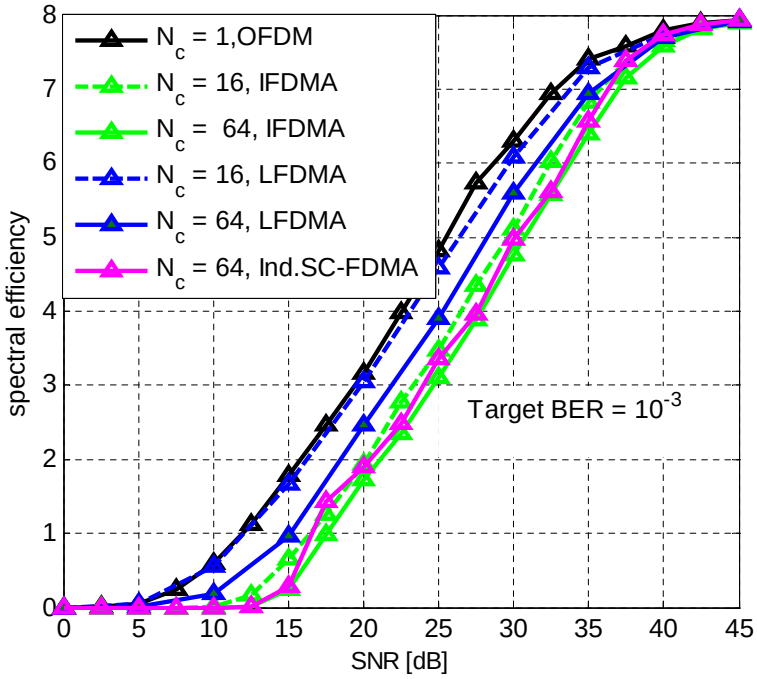

Figure 5.12: Spectral efficiency: OFDM, IFDMA, LFDMA and independent SC-FDMA for heavy shadowing, MMSE equalizer

Chapter 6

SC-FDMA Performance over Receiver Diversity Techniques

6.1 Introduction

As multimedia communication became increasingly popular, mobile communications are expected to support reliable high data rate transmissions. Multiple-Input Multiple-Output (MIMO) is seen as a technology to meet higher data rate and enhanced cell coverage. If there is a single antenna at the transmitter and multiple antennas at receiver, it is called Single-Input Multiple-Output (SIMO) system.

Multiple antenna techniques gathered much consideration in recent years as a way to considerably enhance communication link quality and communication capacity [39]. A MIMO system can contribute two types of gain: spatial diversity gain and spatial multiplexing gain [40]. Spatial diversity enhances the reliability of communication in fading channels, and spatial multiplexing gain raises the capacity by transmitting multiple streams of data in parallel through multiple spatial channels.

The different receiver diversity techniques can be used to combine the antenna signals at the receiver. It is a recognized technique to alleviate the performance degradation of multipath fading and co-channel interference in wireless systems. The analysis of transmitter and receiver diversity has been conducted over the last several decades to distinguish the performance of different diversity combining methods for various numbers of antennas and different fading distributions [41]. It also provides the entire resources of the array to service

a single user. These schemes enhance reliability by minimizing the channel fluctuations due to fading. It has assumed that different antennas receive different versions of the same signal. The chances of all these copies being in a deep fade are small.

In this chapter, we focus on the performance of SC-FDMA when multiple antennas are present at the receiver. Sec. 6.2 introduces the receiver diversity techniques studied in this dissertation. The Sec. 6.3 explains the system model, and Sec. 6.4 gives simulation results. Some conclusion remarks finish the chapter.

6.2 Receiver Diversity Techniques

Antenna diversity has recognized as space diversity or spatial diversity. It is one of several diversity schemes to make possible the use of two or more antennas to improve the quality and reliability of a wireless link. Generally in urban and indoor environments, there is no clear LOS between transmitter and receiver. Hence, the signal is reflected along multiple paths before at last being received. All of these different paths can introduce phase shifts, attenuations, time delays, and distortions that can destructively interfere with one another at the opening of the receiving antenna.

The multipath situations have mitigated by using antenna diversity. The reason is that multiple antennas offer a receiver several interpretation of the same signal. Each antenna will incident a different interfering environment. Thus, if one antenna is experiencing a deep fade, there may be a possibility that another has an enough signal. Individually such a system can provide a strong link. Diversity has mainly seen in receiving systems (diversity reception), the analogy is also true for transmitting systems (transmit diversity) as well.

There are three common techniques of receiver diversity: selection combining, maximal ratio combining, and equal gain combining. For all the three diversity techniques, the goal is to find a set of weights such that the impact of fading for a single user is minimized. The three techniques differ in how this weight vector is chosen. This dissertation work has focused on MRC and EGC techniques. In both, we assume that the receiver has the required knowledge of the channel fading vector $\mathbf{h}$.

Consider a receiver diversity system with N_R antennas as shown in Figure 3.1 and

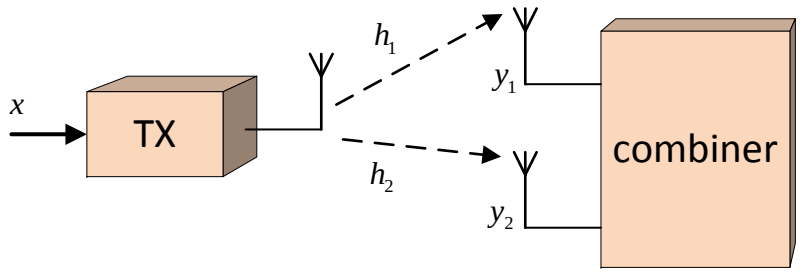

Figure 6.1: Receiver diversity combining scheme

repeated here, Figure 6.1 for convenience. The channel can be expressed as

$$\mathbf{h} = [h_1,\ h_2, .., h_{N_R}]^T \tag{6.2.1}$$

The correlation between the antennas is expressed by correlation coefficient ρ.

The received set of signals $\mathbf{R} = [R_1,\ R_2, .., R_{N_R}]^T$ is then given by

$$\mathbf{R} = \sqrt{\frac{E_s}{N_0}}\mathbf{h}x + \mathbf{n} \tag{6.2.2}$$

being x the unique transmitted signal at the single input. The vector $\mathbf{n}$ of noise AWGN samples and the transmitted symbol x are normalized in power. Each term of the received signal vector can be written as

$$R_n = \sqrt{\frac{E_s}{N_0}}h_n x + n_n. \tag{6.2.3}$$

Let γ_n be the instantaneous SNR for the n^{th} branch, which is given by:

$$\gamma_n = \frac{E_s}{N_o}|h_n|^2 \tag{6.2.4}$$

In SIMO systems, all branches are combined by a weighted sum

$$R^{COMB} = \mathbf{W}^T\mathbf{R} \tag{6.2.5}$$

where $\mathbf{W} = [W_1\ W_2\ ..W_{N_R}]^T$ is the weight vector. After some manipulation, the combined signal can be written as

$$R^{COMB} = [W_1\ W_2..W_{N_R}] \times \mathbf{R} = \sum_{n=1}^{N_R} W_n R_n \tag{6.2.6}$$

Which is decomposed as the addition of signal and noise parts as

$$R^{COMB} = \mathbf{W}^T \left(\sqrt{\frac{E_s}{N_0}} \mathbf{h} x + \mathbf{n} \right) = \sqrt{\frac{E_s}{N_0}} \mathbf{W}^T \mathbf{h} x + \mathbf{W}^T \mathbf{n} \tag{6.2.7}$$

Also written as

$$R^{COMB} = \sqrt{\frac{E_s}{N_0}} x \sum_{n=1}^{N_R} W_n h_n + \sum_{n=1}^{N_R} W_n n_n \tag{6.2.8}$$

Average power of the instantaneous signal and noise part in Eq. (6.2.8) are respectively given as

$$P_s = E_x \left[\left(\sqrt{\frac{E_s}{N_0}} \mathbf{W}^T \mathbf{h} x \right)^2 \right] = \frac{E_s}{N_0} |\mathbf{W}^T \mathbf{W}|^2 \tag{6.2.9}$$

And

$$P_z = E_n \left[\left(\mathbf{W}^T \mathbf{n} \right)^2 \right] = ||\mathbf{W}||^2 \tag{6.2.10}$$

Where $|| \cdot ||$ indicates norm of the vector. To write the expression, it has been taken into account noise and signal normalization.

From Eq. (6.2.9 and 6.2.10), the instantaneous SNR for the received signal can be written as

$$\gamma = \frac{P_s}{P_z} = \frac{E_s}{N_0} \frac{|\mathbf{W}^T \mathbf{h}|^2}{||\mathbf{W}||^2} \tag{6.2.11}$$

6.2.1 Maximal Ratio Combining (MRC)

Maximal ratio combining designs the weight vector in order to maximize SNR γ. Invoking the Cauchy-Schwartz inequality,

$$|\mathbf{W}^T \mathbf{h}|^2 \leq ||\mathbf{W}||^2 ||\mathbf{h}||^2. \tag{6.2.12}$$

Equality is only reached for a certain weight vector (except constants) which is just that designed for MRC [42]:

$$\mathbf{W}_{MRC} = \mathbf{h}^*. \tag{6.2.13}$$

SNR in the Eq. (6.2.11 is just maximized for the MRC weight vector $\mathbf{W}_{MRC}$ which yields:

$$\gamma^{MRC} = \frac{E_S}{N_o}. \tag{6.2.14}$$

SNR for any other weight vector is below this upper-bound.

The MRC process corrects the channel phase through conjugation and blends the received signals in the proper direction. Further, signals are amplitude scaled in such a way that stronger signals are more in-fluent in the final value. Later, the amplitude scaling step makes sure that the received sequence has the similar magnitude as the transmitted sequence. These steps together remove the channel effect and replace the equalizer.

6.2.2 Equal Gain Combining (EGC)

Equal gain combining simplifies the weight vector design by avoiding the amplitude scale of the received signal. The implementation complexity is low as compared to MRC. In an EGC combiner, all the diversity branches are first co-phased and then weighted equally before combining to give resultant output [43]. Co-phasing is still required to avoid signal cancellation.

The analysis of EGC performance can be found in [44] and shows similar performance to MRC. A complete summary of most of the linked work has presented in [41]. The Frequency-Domain (FD) amplify and forward single relay SC-FDMA performance with EGC is studied in [45].

6.3 SC-FDMA SIMO System Model

In this section, we discuss the transmission scheme for a SIMO SC-FDMA system. The two antenna signals are mixed using maximal ratio combining or equal gain combining technique.

Consider Figure 6.2 and Figure 6.3 system model with a single transmit antenna and N_R receive antennae, i.e. a SIMO $1 \times N_R$ system. Transmitter is kept from that presented in previous chapter.

As already described in Sec. 3.4, the frequency channel response at the j^{th} branch of the N_R diversity transmission chain can be represented by the channel vector $\mathbf{H}_j = [h_{i,j}]^T$, with $h_{i,j}$ the channel coefficient between the transmit antenna and the j^{th} receive antenna at the i^{th} subcarrier. The $\mathbf{H}_j$ follows any frequency response model as those described in previous chapter.

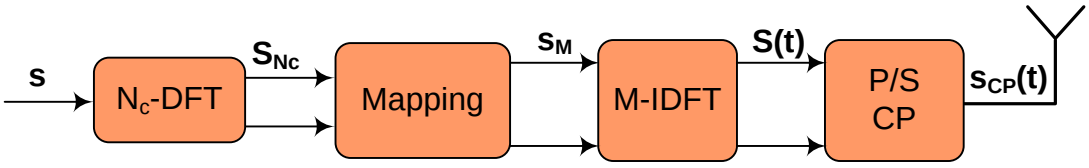

Figure 6.2: Transmission scheme in SISO SC-FDMA

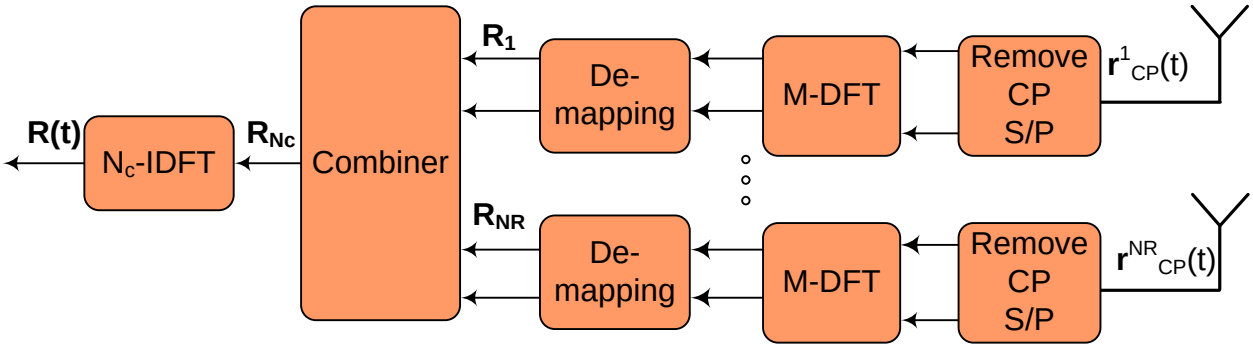

Figure 6.3: Reception scheme in SIMO SC-FDMA

The channel responses at each subcarrier can be written as a vector of the responses at each path, $\mathbf{h}_i = [h_{i,j}]^T$, $j = 1..N_R$, to be combined to exploit diversity at the receiver as shown in Figure 6.3. Perfect channel estimation and synchronization avoiding interference from other users are assumed. The cyclic prefix is suppressed and M point discrete Fourier transform (M-DFT) operation transfers the time domain symbol into a frequency-domain symbol at the receiver side. Later on, the demapping process is applied on received symbol at each antenna. The vector of received signals on the i^{th} subcarrier at all antennas $\mathbf{R}_i = [R_{i,j}]^T, j = 1..N_R$ can be expressed as

$$\mathbf{R}_i = \mathbf{h_i} s_i + \mathbf{n} \tag{6.3.1}$$

Where $\mathbf{n}$ is a noise vector whose entries are i.i.d. complex Gaussian $CN(0, N_0)$. The N_R signals at each subcarrier are frequency combined using the weight vector $\mathbf{W_i} = [W_{i,j}]$ and normalized to allow detection

$$R_i = \frac{\sum_{j=1}^{N_R} R_{i,j} W_{i,j}}{\sum_{j=1}^{N_R} |W_{i,j}|^2}. \tag{6.3.2}$$

Specifically, the result for MRC is obtained with the weight vector as the channel

conjugated $W_{i,j} = h^*_{i,j}$, thus the vector of signals at all subcarriers can be written as

$$R_i^{MRC} = \frac{\sum_{j=1}^{N_R} R_{i,j} h^*_{i,j}}{\sum_{j=1}^{N_R} |h_{i,j}|^2} \tag{6.3.3}$$

For EGC [46], the N_R signals are frequency combined by taking out the angle of the channel but with no modification in amplitude

$$R_i^{EGC} = \frac{\sum_{j=1}^{N_R} R_{i,j} \exp\left(-\jmath \cdot angle(h_{i,j})\right)}{\sum_{j=1}^{N_R} |h_{i,j}|} \tag{6.3.4}$$

6.4 Simulation Results and Discussion

In this section, we provide the results of SIMO maximal ratio combining and equal gain combining SC-FDMA performance in different scenarios. We also compare BER performance of SIMO MRC with single-input-single-output SC-FDMA with zero forcing and minimum mean square error equalization. The SIMO MRC SC-FDMA performance also has been studied for different correlation factor (ρ), for various antennae at receiver and number of allocated subcarriers.

The parameters used for channel modelling are depicted in Table 3.1. Simulation parameters for SIMO SC-FDMA are shown in Table 6.1.

Table 6.1: Simulation Parameters for SIMO SC-FDMA

Parameter	Value
Total number of subcarriers	1024
Allocated subcarriers (N_c)	1, 8, 16, 64
Modulation scheme	QPSK
Carrier Frequency	2.00 GHz
System Bandwidth	20.00 MHz
Channel Model	LMS with exponential PDP
Number of Antennas used	2 by default, 4
Diversity Techniques Used	MRC, EGC
τ_{avg}	1.17μs

6.4.1 Results and Discussion of SC-FDMA performance with MRC Diversity

Figures 6.4 and 6.5 compare SIMO and SISO BER performance over different shadowing scenarios for both IFDMA and LFDMA, respectively. All results are plotted for two receiving antenna, $N_R = 2$, except otherways said. In both cases, SIMO MRC performance is better than that of SISO IFDMA for both equalization techniques ZF and MMSE. The reason is that for SIMO MRC we have multiple antennas, and MRC combining technique can exploit their diversity as each signal arriving at receiver undergoes different fading. As in SISO, results with light shadowing are showing lower BER than with heavy shadowing because light shadowing is a Rice fading with 5 dB Rice factor. In the case of a Rician fading, the direct line of sight component is stronger than multipath component while the heavy shadowing is equivalent to Rayleigh fading.

The effect of different allocated subcarriers is depicted in Figures 6.6 and 6.7 for interleaved and localized SC-FDMA, respectively. An increase in allocated subcarriers results in certain gain in SNR for LFDMA, about 1dB from $N_c = 32$ to 64. The effect is similar to that for the single antenna at the receiver.

The effect of the different number of antennas at the receiver can be observed in Figures 6.8 and 6.9. As expected, BER improves with the increase in the number of antennae. However, it is shown that most gains were obtained for the use of two antennae as only BER improvement is slight for both shown shadowing.

All the previous results were plotted assuming independence among signals received at different antennae. We now compare the effect of correlation among antennas on BER performance for different shadowing. Figures 6.10, 6.12 and 6.14 show the BER performance of IFDMA for various correlation factor and different shadowing. Equivalent results for LFDMA can be found in Figures 6.11, 6.13 and 6.15. It is observed that the BER grows with higher correlation factor. The reason is that less diversity exists between antennas as correlation increases. However, certain correlation (up to 0.5 in light shadowing and 0.3 for average and heavy shadowing) does not affect the BER significantly.

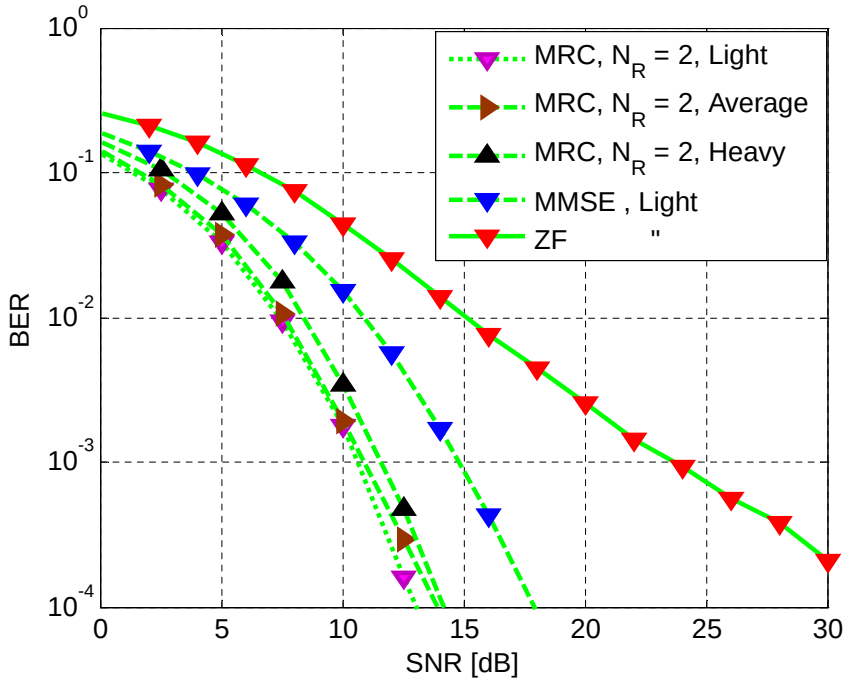

Figure 6.4: BER of SIMO and SISO IFDMA for QPSK, $N_c = 64$, over different shadowed channel

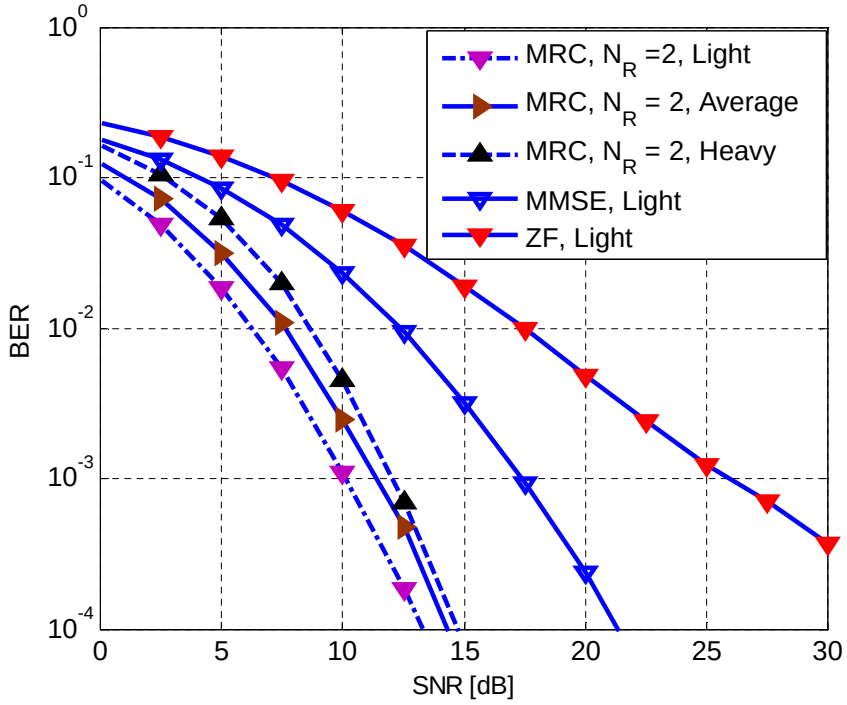

Figure 6.5: BER of SIMO and SISO LFDMA for QPSK, $N_c = 64$, over different shadowed channel

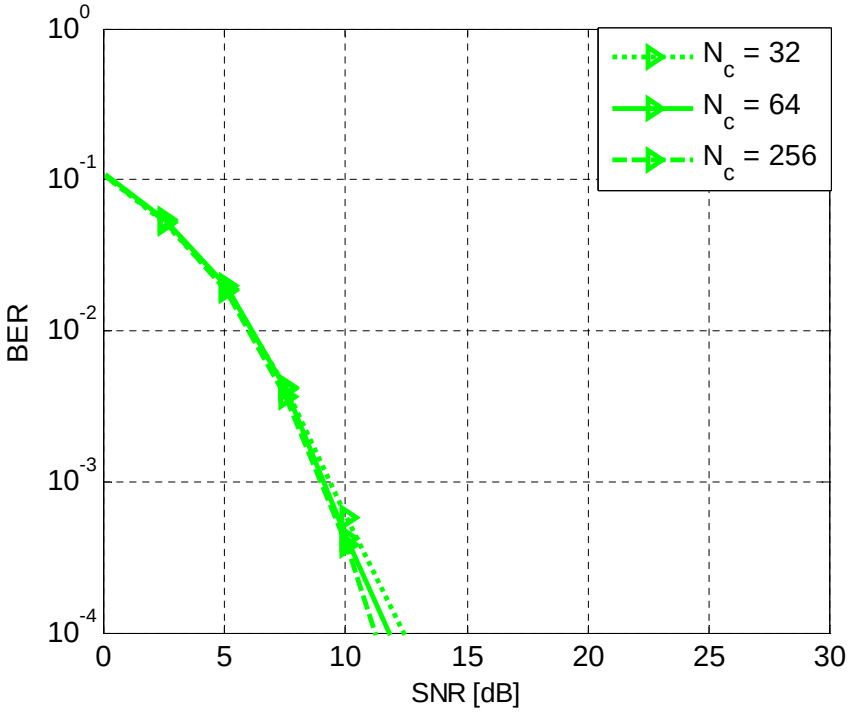

Figure 6.6: BER of SIMO MRC IFDMA with different N_c for QPSK over average shadowing

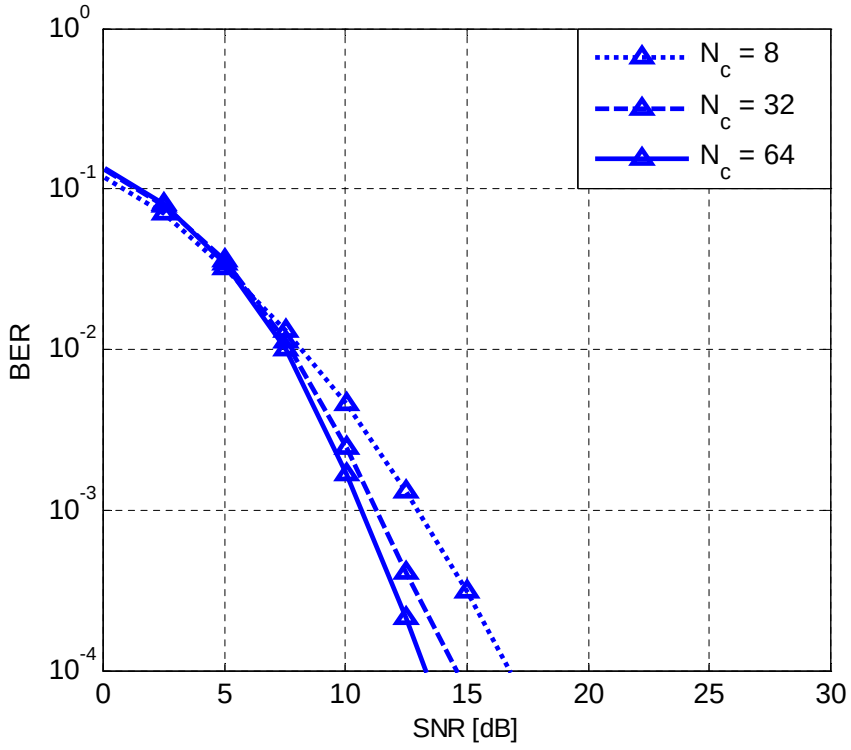

Figure 6.7: BER of SIMO MRC LFDMA with different number of N_c for QPSK over heavy shadowing

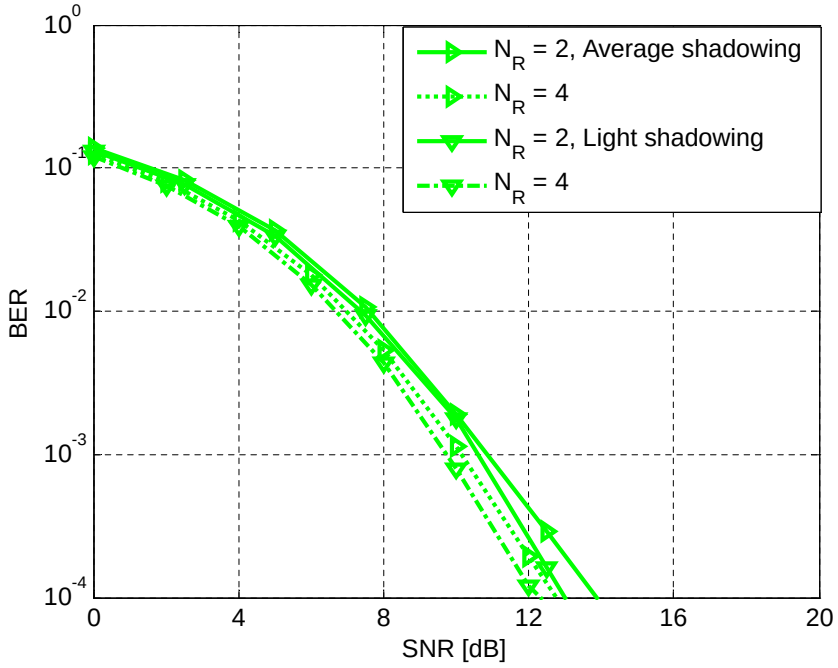

Figure 6.8: BER of SIMO MRC IFDMA with different N_R at the receiver for QPSK, $N_c = 64$, over average and light shadowing

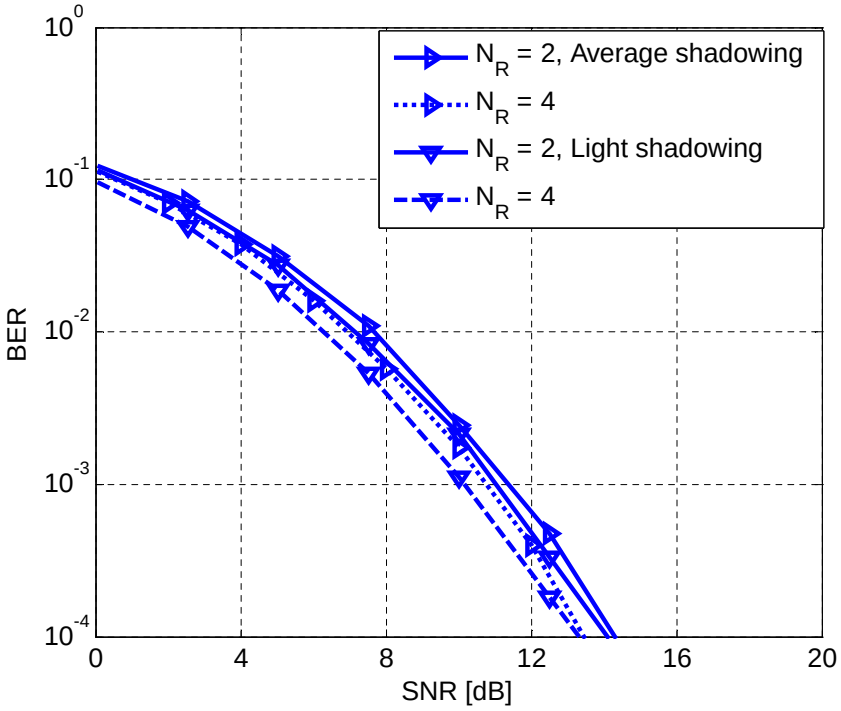

Figure 6.9: BER of SIMO MRC LFDMA with different N_R at the receiver for QPSK, $N_c = 64$, over average and light shadowing

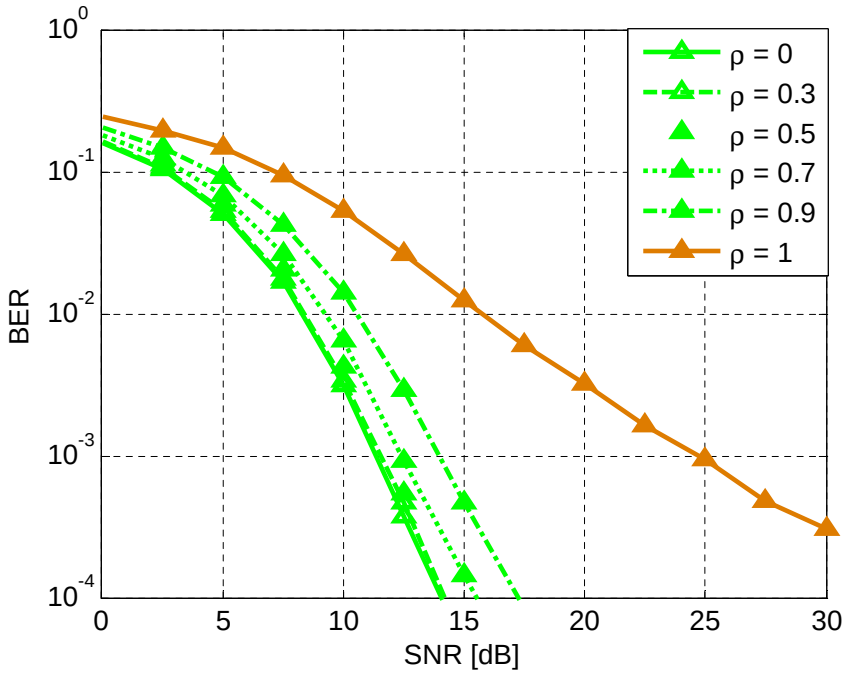

Figure 6.10: BER of SIMO MRC IFDMA with different ρ for QPSK, $N_c = 64$ over heavy shadowing

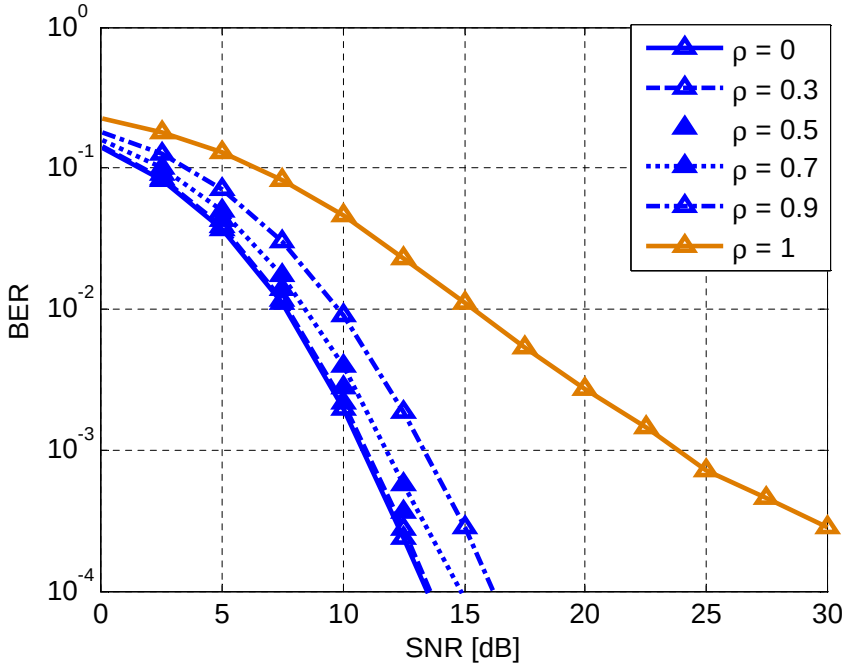

Figure 6.11: BER of SIMO MRC LFDMA with different ρ for QPSK, $N_c = 64$ over heavy shadowing

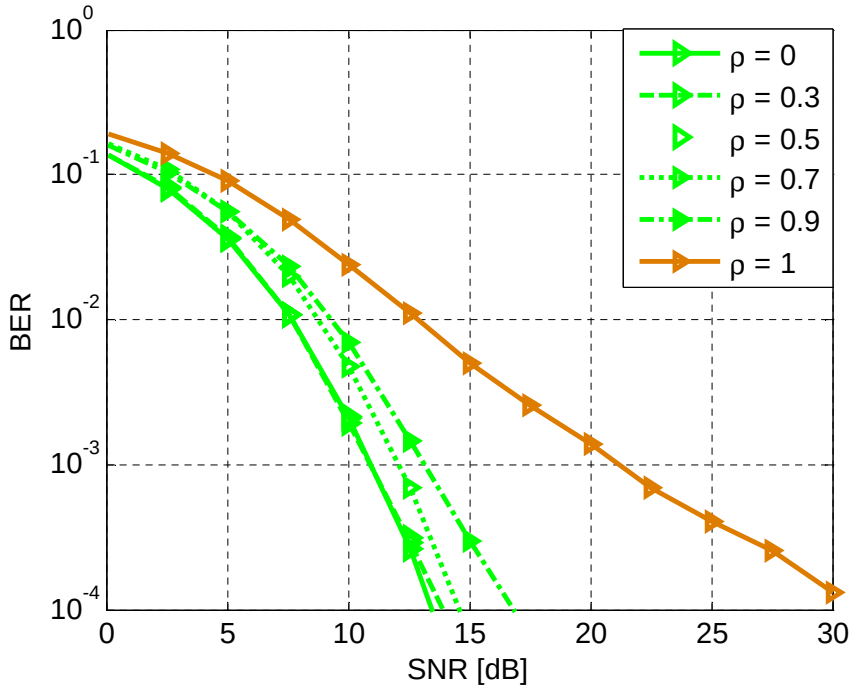

Figure 6.12: BER of SIMO MRC IFDMA with different ρ for QPSK, $N_c = 64$ over average shadowing

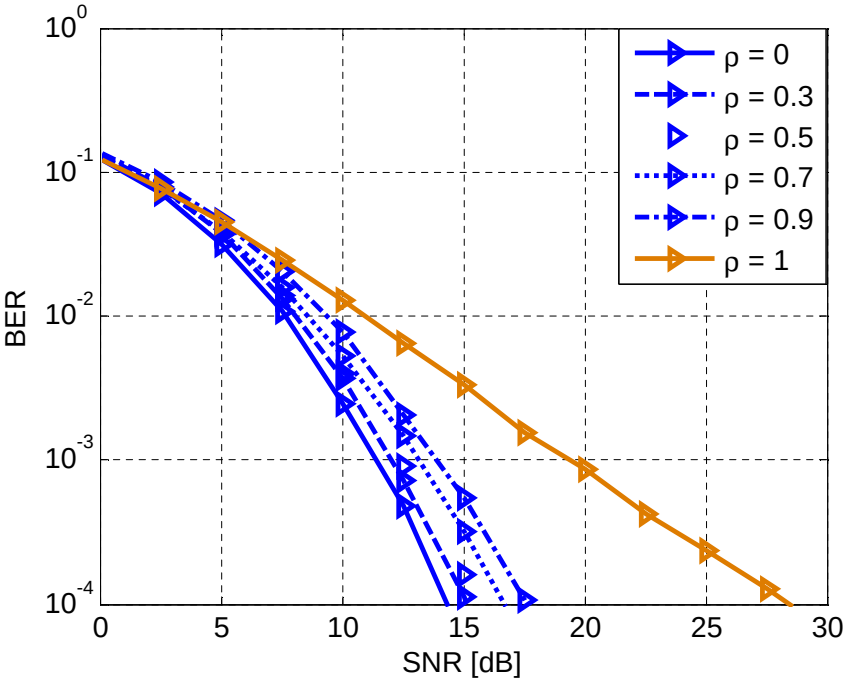

Figure 6.13: BER of SIMO MRC LFDMA with different ρ for QPSK, $N_c = 64$ over average shadowing

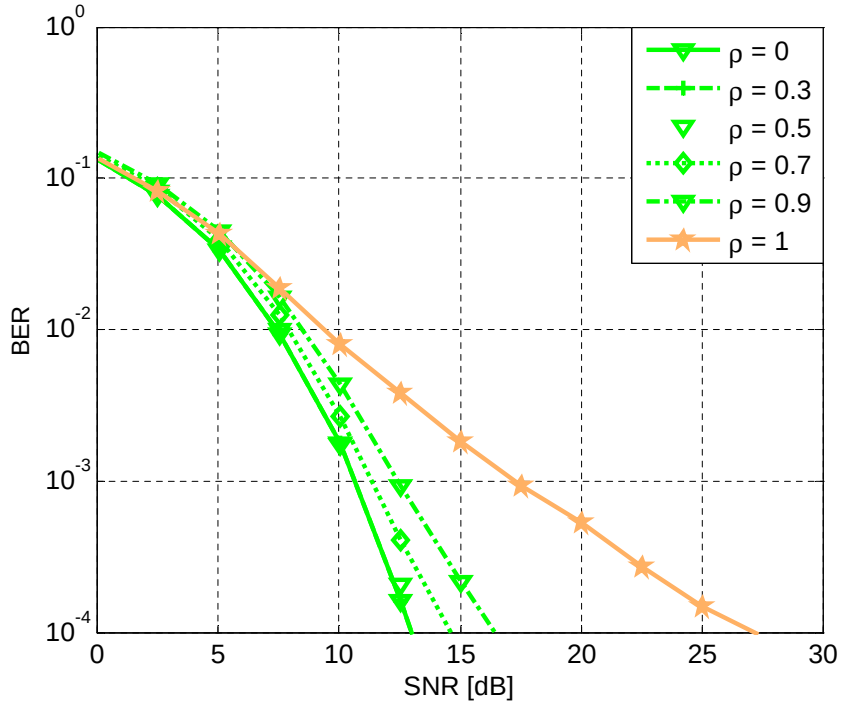

Figure 6.14: BER of SIMO MRC IFDMA with different ρ for QPSK, $N_c = 64$ over light shadowing

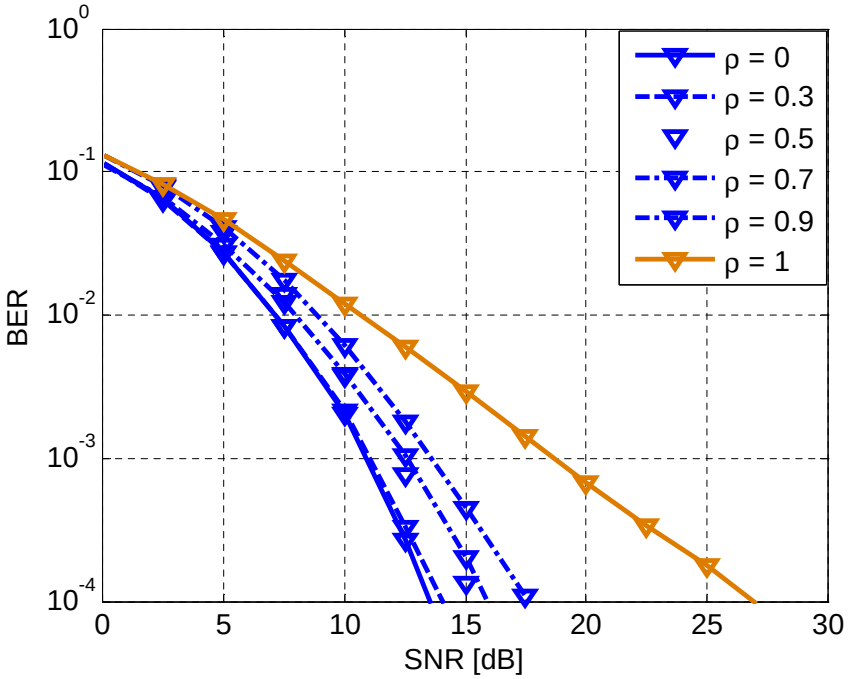

Figure 6.15: BER for SIMO MRC LFDMA with different ρ for QPSK, $N_c = 64$ over light shadowing

6.4.2 Results and Discussion of SC-FDMA Performance with EGC Diversity

In this section, we have investigated SC-FDMA performance for equal gain combining diversity over correlated shadowed Rice LMS channel. Figures 6.16 and 6.17 show the comparison of BER performance of SISO and SIMO 1×2 for IFDMA and LFDMA, respectively. As for MRC, it is observed that BER is lower with SIMO system as compared to SISO system with MMSE and ZF equalizer. Although in EGC all signals are co-phased to avoid signal cancellation, each diversity signal branch is weighted with the same factor, whatever may be the signal amplitude. As a result, the average SNR improvement of EGC is typically about 1 dB worse than that of MRC. On the other hand, implementation complexity is lower compared to that of MRC as only channel phase has to be estimated and compensated. A comparison between BER performance of both diversity techniques is shown in Figures 6.18 and 6.19 for interleaved and localized SC-FDMA, respectively.

For different number of antennae, the BER performance of IFDMA and LFDMA is depicted in Figures 6.20 and 6.21. As expected, with increased number of antennae at the receiver, BER lowers although improvement is only slight compared to that of using two antennae instead of a SISO scheme. Different allocated subcarriers is shown in Figure 6.22.

The comparison of IFDMA BER for different shadowing and with different correlation factor is shown in Figure 6.23. As explained with MRC IFDMA results, here also we observe with growing BER with antenna correlation, but influence below 0.5 is not great.

6.5 Conclusions

In this chapter, we studied the MRC and EGC receiver diversity techniques. Results for MRC are better (about 1 dB) compared to those in EGC at the expense of higher complexity. It is observed that the results of IFDMA are better as compared to LFDMA in all kind of shadowing because subcarriers are distributed over entire bandwidth while with LFDMA they are adjacent to each other, so the correlation between them is high. Note that for a correlation between antenna signals below $\rho = 0.5$ the performance degradation is negligible.

Moreover, the most diversity gain is obtained by using two antennae.

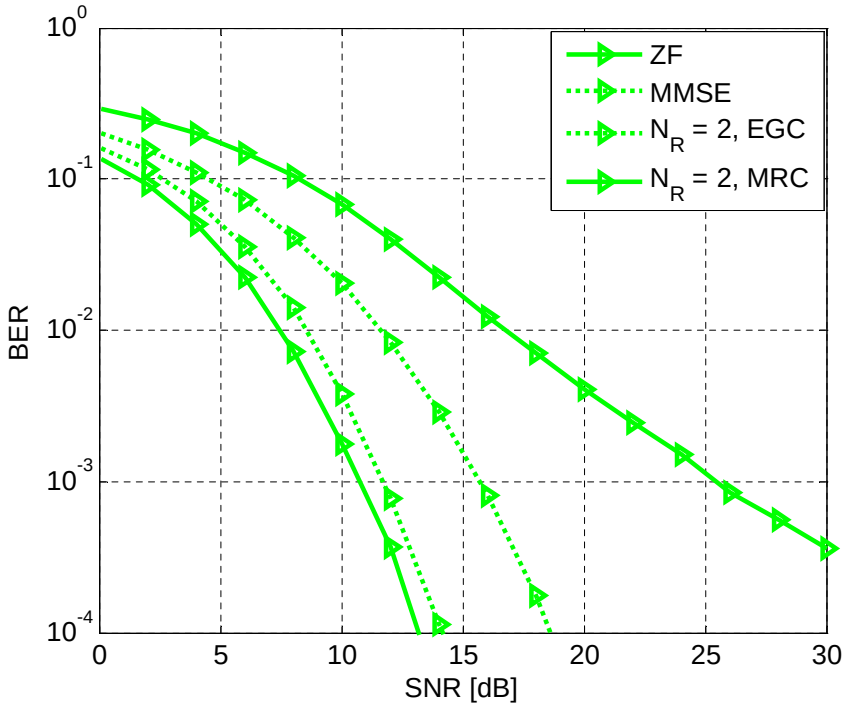

Figure 6.16: BER of SIMO EGC, MRC and SISO ZF, MMSE for IFDMA with QPSK, $N_c = 64$, over average shadowing

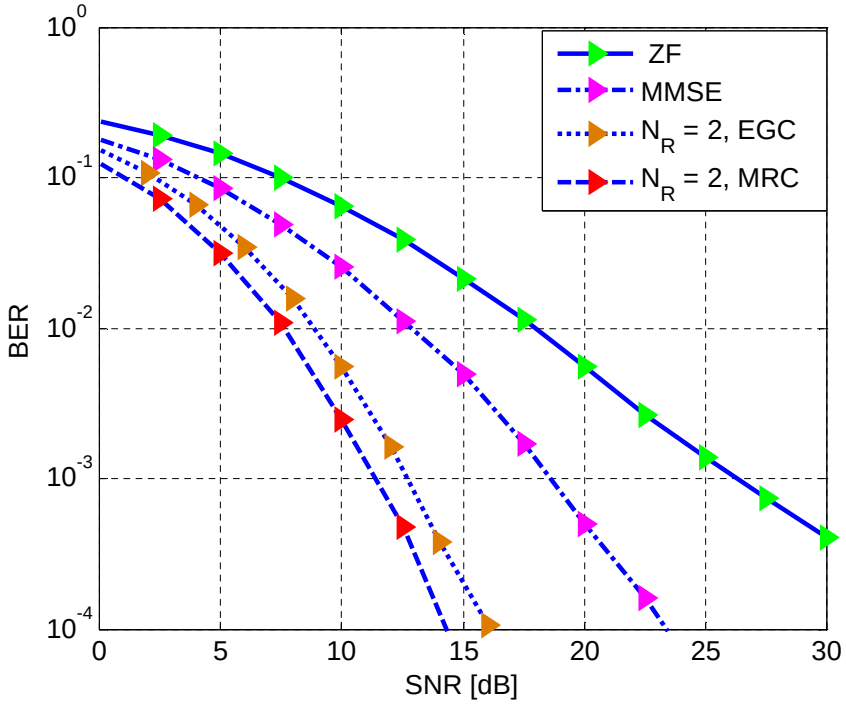

Figure 6.17: BER of SIMO EGC, MRC and SISO MMSE, ZF for LFDMA with QPSK, $N_c = 64$, over average shadowing

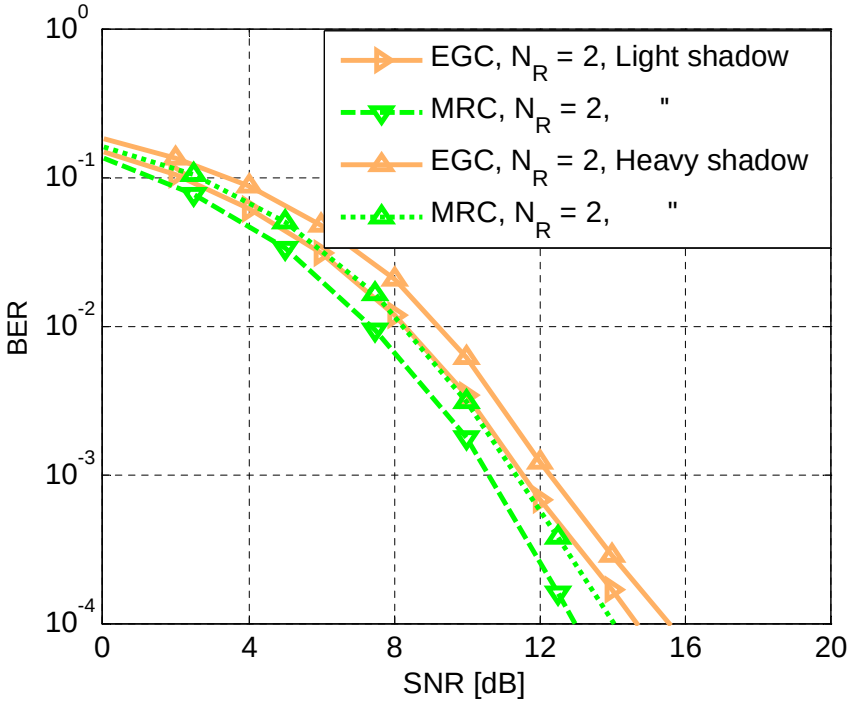

Figure 6.18: BER of SIMO EGC and MRC for IFDMA with QPSK, $N_c = 64$, over different shadowed channels

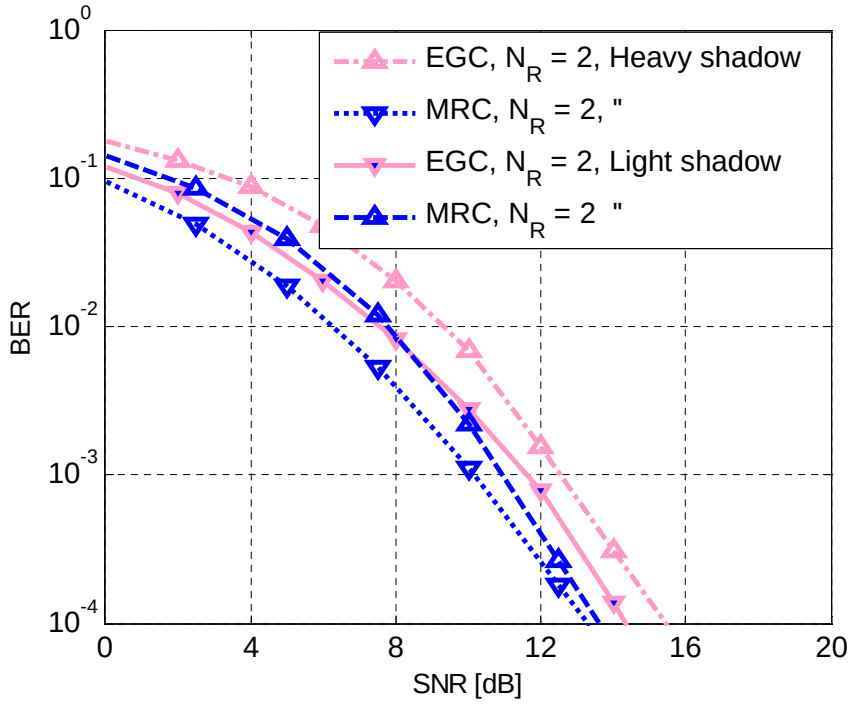

Figure 6.19: BER of SIMO EGC and MRC for LFDMA with QPSK, $N_c = 64$, over different shadowed channels

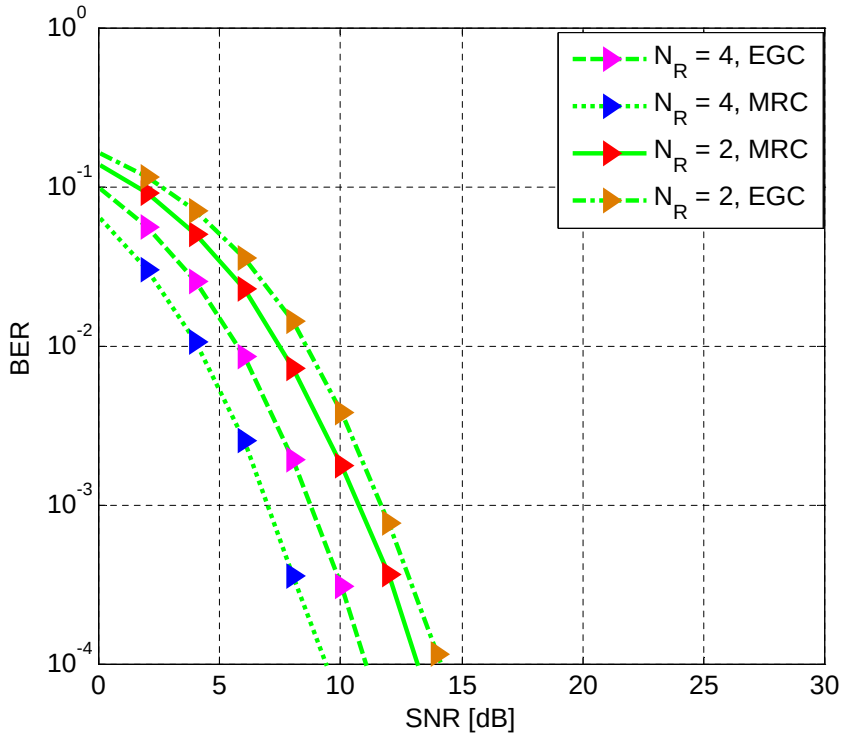

Figure 6.20: BER of IFDMA with different N_R, QPSK, $N_c = 64$, for average shadowing

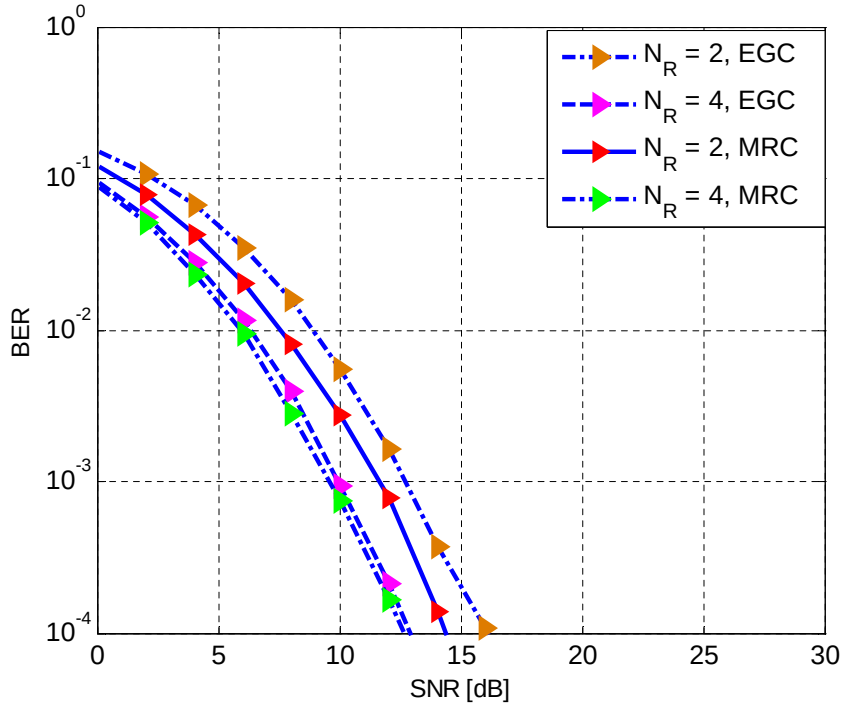

Figure 6.21: BER of LFDMA with different N_R, QPSK, $N_c = 64$, for average shadowing

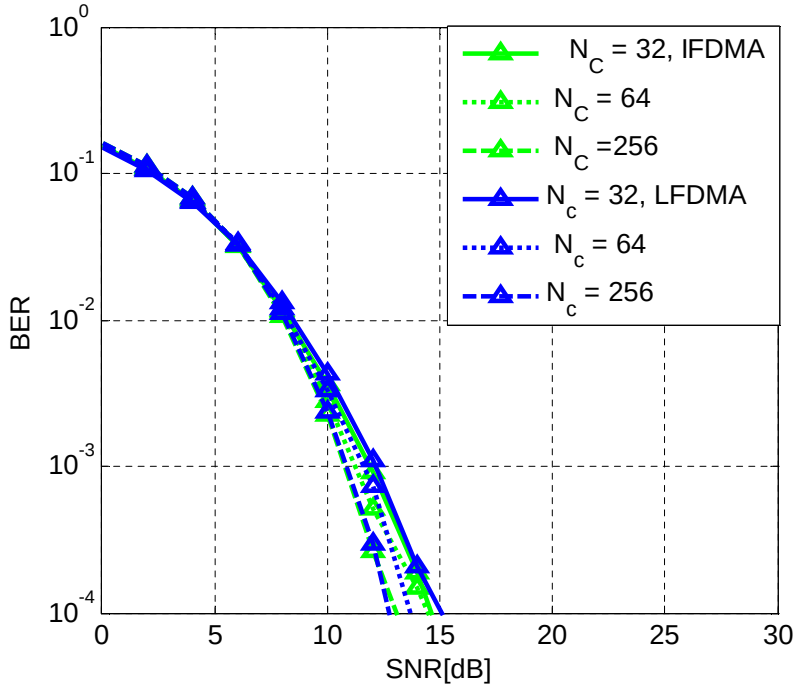

Figure 6.22: BER of SIMO EGC IFDMA and LFDMA with different number of allocated N_c for QPSK over heavy shadowing

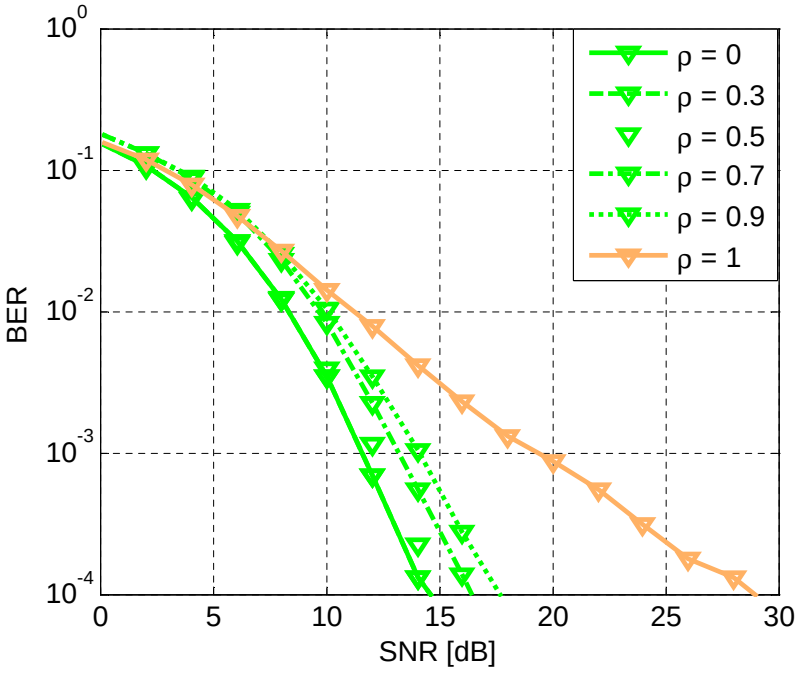

Figure 6.23: BER of SIMO EGC IFDMA with different ρ for QPSK and $N_c = 64$ over light shadowing

Chapter 7

Conclusions and Future Scope

In this Thesis, we have analysed the bit error rate performance of Independent SC-FDMA, Interleaved SC-FDMA, and Localized SC-FDMA for shadowed Rice land mobile satellite channel, where the line of sight follows Nakagami distribution. We considered three cases for shadowed Rice channel; light, average and heavy shadowing.

The BER performance has been calculated for independent and correlated channel frequency responses. In the event of independent SC-FDMA, BER is lower for light shadowing as compared to average and heavy shadowing. This is because light shadowing is equivalent to 5 dB Rician fading. We also observe that results are better with MMSE equalizer. The BER performance has also compared with different allocated subcarriers and modulation schemes. It has been found that with higher allocated subcarriers BER is lower for MMSE equalization. Equivalently, higher spectral efficiency can be exploited.

The performance of SC-FDMA with maximal ratio combining and equal gain combining has been also studied for IFDMA and LFDMA. The performance degrades for higher correlation between the antennas while it improves with more antennae at receiver.

In the final chapter, we give a brief summary of the previous chapters in which we emphasize the most significant insight. We also provide some future scope lines.

7.1 Synthesis of Dissertation

An outline of the dissertation is as follows. We provide Chapter 1 to introduce motivation of the work which is to provide SC-FDMA SISO and SIMO performance and SC-FDMA

transmission spectral efficiency for shadowed Rice LMS channel. We provide a description of physical layer radio interface technologies, OFDM, and SC-FDMA. We discussed emphasizing the similarities and differences between them in Chapter 2. In Chapter 3, we have talked about the wireless channel and different fading models. We give details about shadowed Rice LMS channel whose LOS follows Nakagami distribution.

In Chapter 4, we study SISO SC-FDMA performance for shadowed Rice LMS channel. SC-FDMA performance has been considered for different constellation size and different allocated subcarriers with ZF and MMSE equalization at the receiver side. SC-FDMA results has been compared to those of OFDM over channels with light, average and heavy shadowing.

In Chapter 5, we study the analysis of the spectral efficiency of SC-FDMA transmission of shadowed Rice LMS channel for ZF and MMSE equalization. We compare SC-FDMA spectral efficiency for independent frequency channel responses at the allocated subcarriers and correlated channel frequency responses. We also compare IFDMA and LFDMA spectral efficiency to that of OFDMA.

In Chapter 6, we study SC-FDMA performance with receiver diversity techniques, maximal ratio combining and equal gain combining over LMS channel.

7.2 Contributions

The main purpose of this thesis is the analysis of an SC-FDMA systems for shadowed Rice land mobile satellite channels regarding BER, spectral efficiency, and receiver diversity techniques. The obtained results has been compared to those of OFDM. This comparison allows us to determine the difference in performance between both technologies. Other contributions made during the development of this thesis are listed below:

- BER performance of SC-FDMA and OFDMA for shadowed Rice LMS channel with independence among channel frequency response and correlated channel frequency responses.

- Spectral efficiency of SC-FDMA and OFDMA transmission for shadowed Rice LMS

channel with adaptive modulation and coding.

- SC-FDMA performance with receiver diversity techniques for shadowed Rice LMS channel. The receiver diversity techniques used are maximal ratio combining and equal gain combining.

7.3 Future Scope

The results of this dissertation give interesting directions for future work. Some of them are as follows:

- SC-FDMA performance for shadowed Rice LMS channel where LOS follows a log-normal distribution.
- SC-FDMA performance with multiple antennae at transmitter and receiver for shadowed Rice LMS channel
- SC-FDMA transmit diversity with shadowed Rice LMS channel
- SC-FDMA performance for multi-state LMS channel model
- SC-FDMA performance with Massive MIMO
- SC-FDMA channel capacity with LMS channel

Appendix A

Rendimiento de SC-FDMA con técnicas de diversidad para canales móviles satelitales

A.1 Introducción

La modulación por división en frecuencias ortogonales (OFDM, Orthogonal Frequency Divison Multiplexing) se ha convertido en una técnica muy popular para la transmisión en canales móviles por dos razones: a) proporciona una solución menos compleja en canales con selectividad en frecuencia; b) proporciona buena eficiencia espectral. OFDM ha sido adoptada como tecnología de capa física por varios estándares inalámbricos como IEEE 802.11/Wi-Fi [1], IEEE 802.16/WiMAX [2], 3GPP Long Term Evolution (LTE) en el enlace descendente [3], y la televisión digital terrestre (Digital Video Broadcasting-Second Generation Terrestrial, DVB-T2) [4]. Recientemente, también ha sido elegida en estándares que hacen uso de enlaces por satélite (Digital Video Broadcasting-Satellite services to Handhelds, DVB-SH) [5]. En enlaces por satélite, que habitualmente no son muy selectivos en frecuencia, el uso de OFDM se debe principalmente a la necesidad de mantener tecnologías similares con los sistemas terrestres.

Durante muchos años, se ha considerado que OFDM no es apropiada para las comunicaciones por satélite. La razón son sus fluctuaciones de amplitud, que producen una razón entre potencia de pico y potencia media (Peak-to-Average-Power-Ratio, PAPR) elevada, lo que hace OFDM sensible a la distorsión no lineal causada por los amplificadores

de potencia. Una alternativa interesante a OFDM es la técnica de acceso múltiple por división en frecuencia de portadora única conocida en ingls como Single Carrier Frequency Division Multiple Access (SC-FDMA) que ha sido adoptada en el enlace ascendente de la cuarta generación de comunicaciones móviles Long Term Evolution (LTE) [3].

SC-FDMA se describe como un esquema de frecuencia única con igualación en el dominio de la frecuencia. Su rendimiento es similar al de OFDM pero con una PAPR menor, lo que hace más eficiente el terminal de usuario. Así, la técnica SC-FDMA es una candidata mejor que OFDM para las comunicaciones por satélite, además de que presenta la ventaja de que es compatible con los transmisores basados en OFDM. También utiliza un prefijo cíclico y también la igualación se realiza en el dominio de la frecuencia. Esta igualación puede eliminar completamente las interferencias (Zero Forcing, ZF) o bien reducirlas pero limitando el ruido (Minimum Mean Square Error, MMSE).

SC-FDMA puede verse como OFDM con una precodificación en el transmisor a través de una transformada de Fourier discreta (Discrete Fourier Transform, DFT) previa al bloque que implementa la transformada inversa de Fourier para la transmisión OFDM. Con esta DFT, la energía de los símbolos modulados se reparte entre un conjunto de portadoras. Este mapeo puede realizarse a portadoras contiguas (Localized SC-FDMA, LFDMA) o equiespaciadas en todo el ancho de banda (Interleaved SC-FDMA, IFDMA) [9].

Para aliviar los desvanecimientos inherentes a las comunicaciones móviles, muchos sistemas hacen uso de técnicas de diversidad espacial [10] como la combinación máxima (Maximal Ratio Combining, MRC) o igual (Equal Gain Combining, EGC) entre antenas. En MRC, las señales que llegan a las antenas se pesan y combinan para obtener la relación señal a ruido (Signal to Noise Ratio, SNR) máxima mientras que un combinador EGC únicamente corrige la fase de las señales para evitar que se cancelen y directamente las combina.

El indicador de rendimiento usado más habitualmente es la tasa binaria de error (Bit Error Rate, BER) para una cierta modulación. En los últimos años, la modulación en cuadratura (Quadrature Amplitude Modulation, QAM) ha sido la constelación más empleada.

Para mejorar la capacidad del sistema, la velocidad binaria y la cobertura, la señal

transmitida a o desde un usuario puede ser modificada continuamente para seguir las variaciones de la calidad de la señal a través de un proceso habitualmente conocido como modulación adaptativa (Adaptive Modulation and Coding, AMC). Así es posible adaptar el esquema de modulación a las condiciones del canal para cada usuario (requiriendo, por supuesto, un canal de realimentación y cierta reducción de la velocidad de transmisión debida a la señalización necesaria). Aquellos usuarios con condiciones buenas del canal consiguen mayores órdenes de modulación (por ejemplo, 64 QAM) mientras se reservan las modulaciones más robustas para los usuarios con peores condiciones para mantener la BER por debajo de un cierto objetivo. En este caso, la eficiencia espectral (en bits por segundos por hertzio) es la métrica de interés.

En canales por satélite, el modelo de canal de Loo [18] es el más ampliamente aceptado y empleado en la literatura para canales móviles (Land Mobile Satellite, LMS). Este modelo asume que la envolvente del canal sigue la distribución de Rice con una componente de visión directa que, a su vez, es aleatoria y sigue una distribución lognormal. En [19] se propone un modelo más simple y analíticamente tratable que considera que la línea de visión directa sigue una distribución de Nakagami. Este modelo de Rice-Nakagami se ajusta de manera similar al de Loo a los datos experimentales.

La bibliografía considera diferentes niveles de desvanecimientos para las comunicaciones por satélite, comúnmente llamadas como sombreado ligero, medio y fuerte. El último se refiere a un canal muy cercano a uno de Rayleigh mientras un sombreado ligero asume una línea de visión directa potente con componentes multicamino débiles.

Al tratarse de una transmisión de banda ancha, aparece la interferencia entre símbolos debido a que la duración del símbolo es corta comparada con el ensanchamiento del retardo. El perfil de potencia del canal define la correlación entre las respuestas del canal a diferentes subportadoras ya que el mecanismo puede también verse como selectividad en frecuencia. La igualación con fuerce a cero (ZF) aplica entonces la inversa de la respuesta del canal. MMSE es también una igualación lineal pero al canal se le añade una constante antes de la inversión para evitar un aumento del ruido incontrolado.

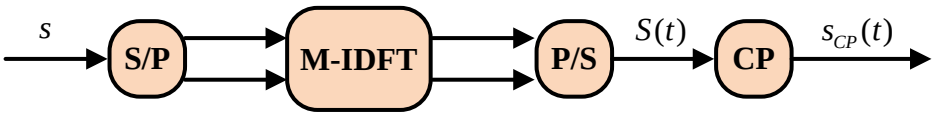

Figure A.1: Transmisor OFDMA

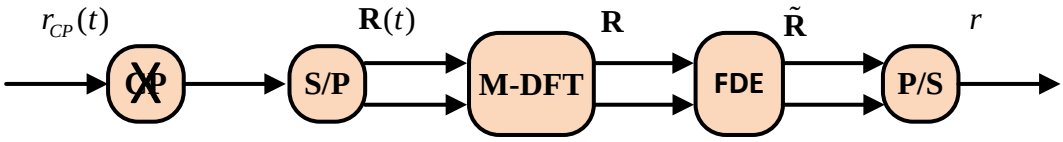

Figure A.2: Receptor OFDMA

A.2 Descripción de OFDM y SC-FDMA

En OFDM [22], el ancho de banda disponible se divide entre subportadoras que son ortogonales en el sentido de que el pico de una portadora coincide con los nulos de las otras, evitando así el uso de guardas en frecuencia y aumentando la eficiencia espectral. Normalmente, como el ancho de banda de la señal transmitida sobre cada portadora es menor que el ancho de banda de coherencia del canal, la respuesta puede considerarse plana, y el canal puede modelarse entonces como un conjunto de canales de banda estrecha, cada uno de ellos monoportadora.

El diagrama de bloques del transmisor y del receptor de un sistema OFDM se presentan en las figuras A.1 y A.2, respectivamente. Aunque no se muestra en la figura, en primer lugar la secuencia de bits se mapea a una secuencia de símbolos complejos de acuerdo al esquema de modulación usado, típicamente QAM. Los símbolos complejos s se transmiten en paralelo empleando una transformada inversa de Fourier de tamaño M. Para eliminar la dispersión temporal y la interferencia entre símbolos, se añade como guarda una extensión cíclica de longitud mayor que la respuesta del canal. Esta extensión transforma la convolución lineal entre los símbolos OFDM en el dominio del tiempo y la respuesta del canal en una convolución circular que, en el dominio de la frecuencia, se presenta como una multiplicación entre los símbolos en cada suportadoras y la respuesta en frecuencia del canal. De esta forma, es posible realizar la igualación en el dominio de la frecuencia. En el receptor, es elimina el prefijo cíclico y la trasformada discreta de Fourier devuelve el símbolo OFDM al dominio

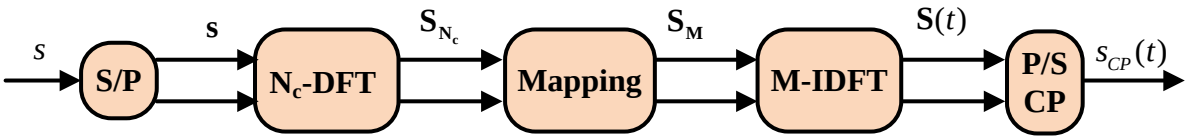

Figure A.3: Esquema de transmisión en SC-FDMA

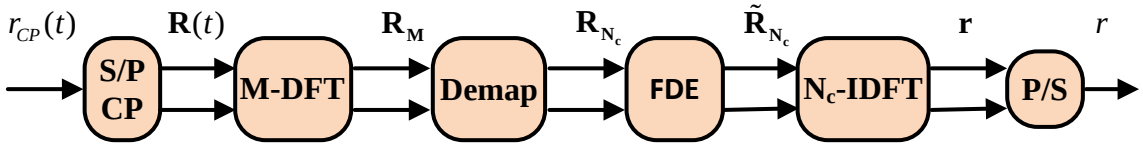

Figure A.4: Esquema de recepción en SC-FDMA

de la frecuencia. La versión ruidosa de la señal transmitida se entrega al igualador en el dominio de la frecuencia y, finalmente, al detector para recuperar los datos transmitidos.

SC-FDMA y OFDMA usan los mismos bloques de transmisión, con la diferencia de que se incluye una trasformada de Fourier más en el transmisor (y su equivalente inversa en el receptor).

En el modo entrelazado de SC-FDMA (Interleaved SC-FDMA, IFDMA) los símbolos se sitúan equiespaciados en todo el ancho de banda del canal. En el modo localizado (Localized SC-FDMA, LFDMA), los símbolos se asignan a un grupo de portadoras adyacentes. OFDM y SC-FDMA pueden transmitir la misma cantidad de símbolos en el mismo periodo pero en SC-FDMA la transmisión es monoportadora aunque distribuida en el ancho de banda asignado.

Las figuras A.3 y A.4 muestran la cadena de transmisión-recepción para SC-FDMA. Como paso previo, la secuencia de bits a transmitir se mapean en símbolos complejos usando QAM. El vector complejo resultante de longitud N_c es precodificado por una transformada discreta de Fourier (Discrete Fourier Transform, DFT) antes de ser mapeado en un subconjunto de subportadoras asignadas. Los símbolos precodificados son entonces mapeados al subconjunto de portadoras por usuario, N_c de las M portadoras, contiguas o entrelazadas. Las portadoras no empleadas se fuerzan a cero. Desde este punto, la transmisión es similar a la de OFDMA.

En el receptor, después del demapeo de las subportadoras, la igualación puede hacerse ZF o MMSE. Finalmente, los símbolos vuelven al dominio del tiempo con una transformada discreta de Fourier inversa y son entregados al detector.

A.3 Modelos de canal

A.3.1 Modelo de canal LMS Rice sombreado

En un canal LMS ideal, hay una línea de visión directa clara entre el satélite y el usuario terrestre, de manera que la envolvente no es aleatoria. Sin embargo, existe un desvanecimiento producido en los caminos que no tienen línea de visión directa, de manera que finalmente el canal puede considerarse que el canal sigue una distribución de Rice. Además, que la línea se bloquee parcialmente hace aleatoria también la componente de visión directa. El equivalente paso bajo de la envolvente del canal puede finalmente escribirse como:

$$z(t) = A(t)\exp\left(j\alpha(t)\right) + B(t)\exp(j\alpha_0) \tag{A.3.1}$$

donde $\alpha(t)$ es la fase aleatoria que se distribuye uniformemente en $[0, 2\pi)$, y α_0 es la fase de la componente de visión directa. Los procesos estacionarios independientes $A(t)$ y $B(t)$, que también son independientes de $\alpha(t)$, representan las amplitudes de la componente multicamino y de visión directa respectivamente. El modelo propuesto en [19] usa una distribución de Rayleigh para $A(t)$ y de Nakagami para $B(t)$ cuyas funciones de densidad de probabilidad (Probability Density Function, PDF) pueden escribirse como:

$$f_A(a) = \frac{a}{b_0}\exp\left(\frac{-a^2}{2b_0}\right) \tag{A.3.2}$$

$$f_B(b) = \frac{2m^m}{\Gamma(m)\Omega^m} b^{2m-1}\exp\left(\frac{-mb^2}{\Omega}\right) \tag{A.3.3}$$

donde $2b_0 = E[A^2]$ es la potencia media de la componente multicamino, $\Gamma(\ )$ es la función gamma, $m = \dfrac{E\left[B^2\right]}{Var\left[B^2\right]} \geq 0$ es el parámetro de Nakagami con $Var[\ ]$ como la varianza y $\Omega = E\left[B^2\right]$ es la potencia media de la componente de visión directa.

La PDF de una distribución de Rice sombreada para la envolvente de la señal $Z = |z(t)|$

en un canal LMS puede escribirse como [19]:

$$f_Z(z) = \left(\frac{2b_0 m}{2b_0 m + \Omega}\right)^m \frac{z}{b_0}\, exp\left(-\frac{z^2}{2b_0}\right)\, {}_1F_1\left(m, 1, \frac{\Omega z^2}{2b_0(2b_0 m + \Omega)}\right). \tag{A.3.4}$$

Valores diferentes de m modelan distintos entornos. Mientras $m = 0$ corresponden a áreas con obstrucción completa de la línea de visión directa, cualquier valor $0 < m < \infty$ representa áreas con obstrucción parcial. Los valores comúnmente considerados se presentan en la Tabla A.1.

Table A.1: Parámetros para los canales con desvanecimientos considerados [19]

Tipo de sombreado	b_0	m	Ω
Ligero	0.158	19.4	1.29
Fuerte	0.063	0.739	8.97×10^{-4}
Medio	0.126	10.1	0.835

A.3.2 Modelos de respuesta en frecuencia

La respuesta en frecuencia del canal, representada por la matriz diagonal $\mathbf{H_M}$ de tamaño $M \times M$, es la transformada de Fourier de la respuesta al impulso variable del canal. Se han empleado dos modelos para la dependencia entre las respuestas en frecuencia del canal en las subportadoras asignadas, $\mathbf{h} = diag(\mathbf{P}^H \mathbf{H_M} \mathbf{P})$, con $\mathbf{P}$ la matriz de mapeo.

Como primer modelo, se han supuesto independientes e idénticamente distribuidos los elementos de $\mathbf{h}$. Cada uno de ellos sigue la distribución de Rice ensombrecida dada por la ec. A.3.4. La PDF de la potencia instantánea en cada subportadora, $|h_j|^2$, puede escribirse como (ec. (6) in [19]):

$$f_{|h_j|^2}(q) = \left(\frac{2b_0 m}{2b_0 m + \Omega}\right)^m \frac{1}{2b_0} exp\left(-\frac{q}{2b_0}\right)\, {}_1F_1\left(m, 1, \frac{\Omega q}{2b_0(2b_0 m + \Omega)}\right). \tag{A.3.5}$$

Como segundo modelo, se ha empleado un modelo en banda ancha formado por varios ecos retrasados una cantidad diferente. El primer eco se asume que sigue el modelo de Rice sombreado descrito anteriormente mientras que el resto de ecos siguen una distribución de Rayleigh, es decir, no presentan línea de visión directa. Con este modelo, es fácil mostrar que

h sigue también una distribución Rice ensombrecida pero, en este caso, hay cierta correlación entre elementos de **h** . Específicamente, se ha empleado un perfil de potencia exponencial, habitual en canales satelitales [27], de manera que la potencia recibida para el eco l-ésimo es:

$$p_l = \frac{1}{\tau_{avg}} exp\left(-\frac{\tau_l}{\tau_{avg}}\right). \tag{A.3.6}$$

En el caso de entornos rurales, valores típicos de τ_{avg} son menores de $1\mu s$ y menores de $2\mu s$ para áreas suburbanas [32]. El valor de τ_{avg} usado en esta tesis ha sido $1.17\mu s$. Los parámetros seleccionados para la extensión cíclica de SC-FDMA deberían ser tales que la mayor parte de la energía de la respuesta al impulso del canal quede dentro de la extensión cíclica.

A.3.3 Modelo de canal para diversidad de antenas en recepción

En este caso, el canal de un sistema con N_R antenas en el receptor se representa por un canal vector:

$$\mathbf{h} = [h_j] \tag{A.3.7}$$

donde h_j es el coeficiente del canal entre la antena transmisora y la j-ésima antena receptora. Además, h_j se puede describir habitualmente como un canal con múltiples ecos como el de la sección anterior.

En general, existe cierta correlación entre antenas, expresada a través del coeficiente de correlación ρ, que toma valores entre 0 y 1. El modelo del canal correlado **H** viene dado por

$$\mathbf{H} = \mathbf{R}_r^{1/2} \mathbf{H}_w \mathbf{R}_t^{1/2} \tag{A.3.8}$$

donde $\mathbf{R}_t$ y $\mathbf{R}_r$ son las matrices de correlación entre antenas transmisoras y receptoras, respectivamente. $\mathbf{H}_w$ nota las ganancias independientes entre antenas. Para el caso de una única antena transmisora y dos receptoras (Single Input Multiple Output, SIMO) el modelo de canal se simplifica a:

$$\mathbf{H} = \mathbf{R}_r^{1/2} \mathbf{H}_w \tag{A.3.9}$$

A.4 Probabilidad binaria de error para canales LMS

A.4.1 Modelo de sistema

Las figuras A.3 y A.4 muestran la cadena de transmisión para SC-FDMA. Como paso previo, la secuencia de bits a transmitir se mapean en símbolos complejos usando Binary Phase Shift Keying (BPSK), Quadrature Phase Shift Keying (QPSK) o 16 Quadrature Amplitude Modulation (QAM). El vector complejo resultante $\mathbf{s}$ de longitud N_c es precodificado por una transformada discreta de Fourier (Discrete Fourier Transform, DFT) antes de ser mapeado en un subconjunto de N_c subportadoras asignadas. El vector columna $\mathbf{S}_{N_c}$ es entonces mapeado al subconjunto de portadoras por usuario, N_c de las M portadoras, contiguas o entrelazadas. Las portadoras no empleadas se fuerzan a cero. El mapeo entonces puede escribirse en términos de la matriz $\mathbf{P}$ de tamaño $M \times N_c$ tal que $\mathbf{P_{i,j}} = 1$ si el símbolo j se transmite sobre la portadora i y cero en caso contrario.

El símbolo en el dominio de la frecuencia puede escribirse como $\mathbf{S}_M = \mathbf{P}\mathbf{S}_{N_c}$. Desde este punto, la transmisión es similar a la de OFDMA: una operación M-IDFT convierte cada símbolo en el dominio de la frecuencia en un símbolo en el dominio del tiempo y se añade la extensión cíclica.

Tras la transmisión por el canal LMS, se suprime el prefijo cíclico y una operación M-DFT convierte cada símbolo en el dominio del tiempo al dominio de la frecuencia $\mathbf{R}_M$. Tras aplicar la matriz hermítica de $\mathbf{P}$, $\mathbf{P}^H$, para demapear la asignación de portadoras, la señal en el receptor $\mathbf{R}_{N_c}$ puede expresarse como

$$\mathbf{R}_{N_c} = \mathbf{P}^H\mathbf{H}_M\mathbf{P}\mathbf{F}\mathbf{s} + \mathbf{P}^H\boldsymbol{\eta}_M, \tag{A.4.1}$$

donde $\boldsymbol{\eta}_M$ es el vector de ruido cuyas entradas son gaussianas complejas independientes e idénticamente distribuidas (i.i.d.) $\mathcal{CN}(0, N_0)$. $\boldsymbol{\eta} = \mathbf{P}^H\boldsymbol{\eta}_M$ son las muestras de ruido en las subportadoras asignadas a la transmisión. La respuesta en frecuencia del canal para cada subportadora viene representada por la matriz diagonal de tamaño $M \times M$ $\mathbf{H}_M$, cuyas características ya han sido descritas.

Como en OFDM, la adición del prefijo cíclico en SC-FDMA también transforma la

convolución lineal en el dominio del tiempo entre los símbolos OFDMA y la respuesta del canal en una convolución circular. En el dominio de la frecuencia, esto se convierte en una multiplicación punto a punto entre los símbolos asignados en cada subportadora y la respuesta en frecuencia del canal. De esta forma, es posible realizar la igualación en el dominio de la frecuencia simplemente multiplicando $\mathbf{R}_{N_c}$ por una matriz de igualación $\mathbf{W}$ de tamaño $N_c \times N_c$. El diseño de $\mathbf{W}$ se puede realizar como Zero Forcing (ZF) o Minimum Mean Square Error (MMSE) Frequency Domain Equalization (FDE), lo que conduce a que

$$\widetilde{\mathbf{R}}_{\mathbf{N_c}} = \mathbf{W}\mathbf{R}_{N_c} = \mathbf{WHFs} + \mathbf{W}\boldsymbol{\eta}. \tag{A.4.2}$$

donde $\mathbf{H} = \mathbf{P}^H\mathbf{H}_M\mathbf{P}$ es una matriz diagonal de tamaño $N_c \times N_c$ cuyos términos $\mathbf{h} = diag(\mathbf{H}) = [h_1 \dots h_{N_c}]$ son la respuesta en frecuencia del canal para cada subportadora asignada, y $\boldsymbol{\eta} = \mathbf{L}^H\boldsymbol{\eta}_M$ es un vector cuyos elementos son valores de ruido complejo.

Antes de la detección, se realiza una precodificación inversa por medio de una transformada discreta inversa de Fourier:

$$\mathbf{r} = \mathbf{F}^H\mathbf{R}_{N_c} = \mathbf{F}^H\mathbf{WHFs} + \mathbf{F}^H\mathbf{W}\boldsymbol{\eta} \tag{A.4.3}$$

A.4.2 Análisis de la SINR

Como se ha obtenido en la sección previa, para SC-FDMA el ruido efectivo a la entrada del detector $\boldsymbol{\eta}$ es una combinación del ruido recibido y las respuestas del canal en el conjunto de subportadoras asignadas a través de la matriz de igualación $\mathbf{W}$. Además, si se aplica MMSE, se verá que también existe una componente de interferencia en el ruido efectivo [33].

ZF FDE

La igualación en la ec. (A.4.2) puede diseñare con el objetivo de eliminar completamente la interferencia entre portadoras. En ese caso, $\mathbf{W}$ se aplica como

$$\mathbf{W}^{ZF} = (\mathbf{H}^H\mathbf{H})^{-1}\mathbf{H}^H, \tag{A.4.4}$$

y la expresión para el símbolo recuperado en frecuencia tras la igualación lleva a

$$\mathbf{r} = \mathbf{F}^H(\mathbf{H}^H\mathbf{H})^{-1}\mathbf{H}^H\mathbf{HFs} + \mathbf{F}^H(\mathbf{H}^H\mathbf{H})^{-1}\mathbf{H}^H\boldsymbol{\eta}. \tag{A.4.5}$$

Así, la expresión para el k-ésimo símbolo viene dado por

$$r_k = s_k + \sum_{j=1}^{N_c} \frac{F_{j,k}^*}{h_j}\eta_j = s_k + \sum_{j=1}^{N_c} \hat{\eta}_{j,k} = s_k + \tilde{\eta}_k \tag{A.4.6}$$

donde $\hat{\eta}_{j,k} = \dfrac{F_{j,k}^*\eta_j}{h_j}$.

Como se muestra en la ec. (A.4.6), el ruido efectivo en ZF-DFE es el resultado de añadir un término de ruido elemental $\hat{\eta}_{j,k}$ para cada subportadora asignada. Condicionado a la respuesta en frecuencia del canal $\mathbf{h} = [h_1 \dots h_{N_c}]$, el ruido efectivo $\tilde{\eta}_k$ en la ec. (A.4.6) sigue una distribución gaussiana compleja con media cero y varianza $\dfrac{N_0}{E_S}\beta^{ZF}$ con la variable aleatoria β^{ZF} definida como [14]

$$\beta^{ZF} = \frac{1}{N_c}\sum_{j=1}^{N_c}\frac{1}{|h_j|^2} = \sum_{j=1}^{N_c}\beta_j^{ZF}. \tag{A.4.7}$$

Cada término β_j de la suma es una variable aleatoria que depende del desvanecimiento del canal. Para el modelo Rice sombreado, su PDF puede calcularse como

$$f_{\beta_j^{ZF}}(s) = \left(\frac{2b_0 m}{2b_0 m + \Omega}\right)^m \frac{1}{2b_0}\frac{1}{N_c s^2} exp\left(-\frac{1}{2b_0 N_c s}\right) {}_1F_1\left(m, 1, \frac{\Omega}{2b_0 N_c s(2b_0 m + \Omega)}\right). \tag{A.4.8}$$

Si puede asumirse independencia entre portadoras, la función característica (Characteristic Function, CHF) de la suma en la ec. (A.4.8) puede escribirse como

$$\Phi_{\beta^{ZF}}(\omega) = \left(\Phi_{\beta_j^{ZF}}(\omega)\right)^{N_c}. \tag{A.4.9}$$

con la CHF de β_j dada por

$$\Phi_{\beta_j^{ZF}}(\omega) = \int_0^\infty f_{\beta_j^{ZF}}(s) e^{\imath s\omega} ds \tag{A.4.10}$$

Hasta donde conocen la autora, no es posible obtener una expresión analítica de la CHF de β_j si bien es posible realizar el cálculo numérico, por ejemplo, por computaciones sucesivas de la ec. (A.4.8). Posteriormente, es posible evaluar la CDF de β^{ZF} usando el teorema de inversión de Gil-Peláez [34] que puede particularizarse como

$$F_{\beta^{ZF}}\left(\beta^{ZF}\right) = \frac{1}{2} - \frac{1}{2\pi}\int_0^\infty \left(\frac{\Phi_{\beta^{ZF}}(\omega)}{\imath\omega} e^{-\imath\beta^{ZF}\omega} - \frac{\Phi_{\beta^{ZF}}(-\omega)}{\imath\omega} e^{\imath\beta^{ZF}\omega}\right) d\omega. \tag{A.4.11}$$

Una vez se ha caracterizado β^{ZF}, se podría usar para evaluar la SNR instantánea condicionada al canal ya que se relacionan como

$$\gamma^{ZF} = \frac{E_S/N_0}{\beta^{ZF}}. \tag{A.4.12}$$

MMSE FDE

Si se pretende evitar el aumento del ruido que la igualación ZF introduce, el diseño de $\mathbf{W}$ puede realizarse con el criterio MMSE:

$$\mathbf{W}^{MMSE} = \left(\frac{N_0}{E_S}\mathbf{I} + \mathbf{H}^H\mathbf{H}\right)^{-1}\mathbf{H}^H, \tag{A.4.13}$$

donde E_S y N_0 son las potencias de señal y de ruido, respectivamente. En este caso, el símbolo recuperado es

$$\mathbf{r} = \mathbf{F}^H\left(\frac{N_0}{E_S}\mathbf{I} + \mathbf{H}^H\mathbf{H}\right)^{-1}\mathbf{H}^H\mathbf{H}\mathbf{F}\mathbf{x} + \mathbf{F}^H\left(\frac{N_0}{E_S}\mathbf{I} + \mathbf{H}^H\mathbf{H}\right)^{-1}\mathbf{H}^H\boldsymbol{\eta}. \tag{A.4.14}$$

Cada símbolo recibido puede escribirse como el símbolo transmitido modificado y contaminado por ruido e interferencia:

$$r_k = T_{k,k}s_k + \sum_{\substack{l\neq k\\ l=1}}^{N_c} s_l T_{k,l} + \sum_{j=1}^{N_c}\frac{F_{j,k}^* h_j^*}{|h_j|^2 + N_0/E_S}\eta_j \tag{A.4.15}$$

Los elementos de $\mathbf{T} = \mathbf{F}^H\mathbf{W}^{MMSE}\mathbf{H}\mathbf{F}$ pueden expresarse como:

$$T_{k,l} = \sum_{j=1}^{N_c}\frac{F_{j,k}^* F_{j,l}\,|h_j|^2}{|h_j|^2 + N_0/E_S}. \tag{A.4.16}$$

Específicamente, el término $T_{k,k}$, que multiplica la señal transmitida, viene dado por:

$$T_{k,k} = \sum_{j=1}^{N_c}\frac{|F_{k,j}|^2\,|h_j|^2}{|h_j|^2 + N_0/E_S} = \frac{1}{N_c}\sum_{j=1}^{N_c}\frac{|h_j|^2}{|h_j|^2 + N_0/E_S}. \tag{A.4.17}$$

Se observa en el resultado que $T_{k,k}$ es independiente de k, es decir, todos los símbolos se reciben con la misma potencia. Tras compensar este término, el símbolo transmitido se obtiene como:

$$r_k = s_k + T_{k,k}^{-1}\sum_{\substack{l\neq k\\ l=1}}^{N_c} s_l T_{k,l} + T_{k,k}^{-1}\sum_{j=1}^{N_c}\frac{F_{j,k}^* h_j^*}{|h_j|^2 + N_0/E_S}\eta_j = s_k + \sum_{\substack{l\neq k\\ l=1}}^{N_c}\delta_{l,k} + \sum_{j=1}^{N_c}\tilde{\eta}_{j,k}, \tag{A.4.18}$$

es decir, el símbolo transmitido está contaminado por el ruido equivalente $\tilde{\eta}_k$ y la interferencia δ_k:

$$r_k = s_k + \delta_k + \tilde{\eta}_k = s_k + \xi_k. \tag{A.4.19}$$

El término ξ_k reúne el efecto del ruido y de la independencia, aunque ambos son inherentemente independientes [14]. Cuando la respuesta del canal es tal que $\frac{N_0}{E_S} \ll |h_j|^2$, el efecto del término de la interferencia decrece y el término de ruido es igual al de Z en la ec. (A.4.6).

La densidad del ruido $\tilde{\eta}_k$ condicionado a la respuesta del canal $\mathbf{h} = [h_1 \dots h_{N_c}]$ es la suma de N_c términos, gaussiano cada uno de ellos. El total sigue, por tanto, también una distribución gaussiana

$$p\left(\tilde{\eta}_k/\mathbf{h}\right) \sim \mathcal{CN}\left(0, \sigma_{\tilde{\eta}}^2\right), \tag{A.4.20}$$

cuya varianza $\sigma_{\tilde{\eta}}^2$, igual para todos los símbolos, puede obtenerse teniendo en cuenta que $|F_{j,k}^*| = 1$ y que las muestras de ruido son independientes:

$$\sigma_{\tilde{\eta}}^2 = \frac{N_0}{(T_{k,k})^2} \frac{1}{N_c} \sum_{j=1}^{N_c} \left(\frac{|h_j|}{|h_j|^2 + N_0/E_S} \right)^2. \tag{A.4.21}$$

En cuanto al término de interferencia, condicionado al canal, podemos asumir que sigue una distribución gaussiana circularmente simétrica [14]:

$$p\left(\delta_k/h\right) \sim \mathcal{CN}\left(0, \sigma_{\delta}^2\right). \tag{A.4.22}$$

Esto sólo se cumple si los símbolos transmitidos son independientes y con igual energía E_S, y será más realista cuantas más subportadoras se empleen. En este caso, σ_{δ}^2 puede expresarse como:

$$\sigma_{\delta}^2 = \frac{E_S}{(T_{k,k})^2} \sum_{\substack{l=1 \\ l \neq k}}^{N_c} |T_{k,l}|^2, \tag{A.4.23}$$

Como ruido e interferencia son independientes, su suma puede modelarse con otra gaussiana compleja de media cero y varianza dada por:

$$\sigma_{\xi}^2 = \sigma_{\delta}^2 + \sigma_{\tilde{\eta}}^2, \tag{A.4.24}$$

puede escribirse como

$$\sigma_\xi^2 = \frac{\frac{N_0}{N_c}\sum_{j=1}^{N_c}\left(\frac{|h_j|}{|h_j|^2+No/Es}\right)^2 + \frac{Es}{N_c}\sum_{j=1}^{N_c}\left(\frac{|h_j|^2}{|h_j|^2+No/Es}\right)^2 - Es\left(\frac{1}{N_c}\sum_{j=1}^{N_c}\frac{|h_j|^2}{|h_j|^2+No/Es}\right)^2}{\left(\frac{1}{N_c}\sum_{j=1}^{N_c}\frac{|h_j|^2}{|h_j|^2+No/Es}\right)^2} \tag{A.4.25}$$

Se nota como β^{MMSE} a

$$\beta^{MMSE} = \frac{1}{N_c}\sum_{j=1}^{N_c}\frac{1}{|h_j|^2 + N_0/E_S} = \sum_{j=1}^{N_c}\beta_j^{MMSE}. \tag{A.4.26}$$

Con esta definición, el rango de β^{MMSE} está limitada a $0 \leq \beta^{MMSE} \leq \frac{E_s}{N_0}$.

Manipulando las ecuaciones, se puede escribir:

$$\sigma_\xi^2 = E_S\frac{\frac{N_0}{E_S}\beta^{MMSE}}{1-\frac{N_0}{E_S}\beta^{MMSE}}, \tag{A.4.27}$$

La PDF de β_j^{MMSE} puede obtenerse por un procedimiento similar al empleado en ZF para llegar a:

$$f_{\beta_j^{MMSE}}(s) = \left(\frac{2b_0m}{2b_0m+\Omega}\right)^m \frac{1}{2b_0}\frac{1}{N_cs^2}exp\left(-\frac{1-sN_cN_0/E_S}{2b_0N_cs}\right)\ {}_1F_1\left(m,1,\frac{\Omega(1-sN_cN_0/E_S}{2b_0(2b_0m+\Omega)N_cs}\right). \tag{A.4.28}$$

Si se compara esta expresión con la de ZF de la ec. (A.4.8), se pueden observar que ambas son equivalentes para $N_0 = 0$.

Como en el caso anterior, si se asume independencia entre las respuestas a distintas frecuencias, la función característica de β^{MMSE} se puede calcular a partir de la de β_j, que puede obtenerse con métodos numéricos desde su PDF.

En el caso de MMSE, la SNR puede expresarse desde ec. (A.4.27) como

$$\gamma^{MMSE} = \frac{E_s}{\sigma_\xi^2} = \frac{\frac{E_s}{N_0}}{\beta^{MMSE}} - 1 \tag{A.4.29}$$

y su CDF se puede evaluar como:

$$F_\gamma^{MMSE}(g) = 1 - F_\beta^{MMSE}\left(\frac{E_s/N_0}{g+1}\right). \tag{A.4.30}$$

A.4.3 Resultados

Para ambos igualadores, la tasa binaria de error puede calcularse como la media de la BER condicionada a β, es decir,

$$BER \doteq \int BER(\beta) f_\beta(\beta) d\beta \tag{A.4.31}$$

con $BER(\beta)$ evaluada a partir de la BER de QAM sobre canales AWGN [14]. Para codificación Gray y QAM cuadrada, puede evaluarse esta BER [35] como:

$$BER(\gamma) = \frac{2}{\sqrt{M} log_2 \sqrt{M}} \sum_{k=1}^{log_2 \sqrt{M}} \sum_{i=0}^{(1-2^{-k})(\sqrt{M}-1)} \left\{ (-1^{\lfloor \frac{i2^{k-1}}{\sqrt{M}} \rfloor} \left(\frac{i2^{k-1}}{\sqrt{M}} + \frac{1}{2} \right) Q \left(\sqrt{\frac{6(2i+1)^2}{2(M-1)} \gamma} \right) \right\} \tag{A.4.32}$$

simplemente sustituyendo γ por β como se describen en las ecuaciones (A.4.12) o (A.4.29) para ZF y MMSE FDE, respectivamente.

Table A.2: Parámetros de simulación para SC-FDMA en canales LMS.

Parámetro	Valor
Número total de subportadoras M	1024
Longitud del prefijo cíclico	144
Valor por defecto de E_s/N_0 (dB)	10
Δf	$15KHz$
τ_{avg} (perfil de potencia de retardo exponencial)	$1.17\mu s$

CDF de β

Se han seguido dos aproximaciones diferentes para evaluar la PDF de β dependiendo del modelo de canal.

Para respuestas en frecuencia independientes, la CDF de β puede evaluarse numéricamente siguiendo el procedimiento descrito previamente. Los resultados se muestran en la figura A.5 para un desvanecimiento fuerte y SNR media 10 dB. Por su parte, cuando se considera el perfil exponencial de la ec. (A.3.6), la existencia de correlación impide usar que la CHF de la suma es el producto de la de cada término por separado. En ese caso, se ha seguido una aproximación semianalítica al problema: desde los valores de **h** se ha

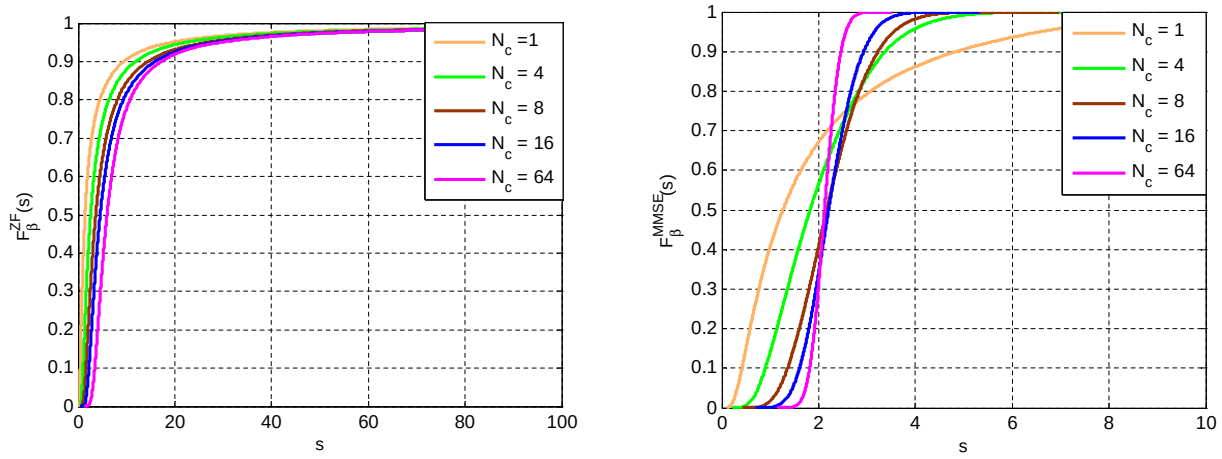

Figure A.5: CDF of β para respuestas en frecuencia independientes entre subportadoras con sombreado fuerte para ZF (izquierda) y MMSE (derecha)

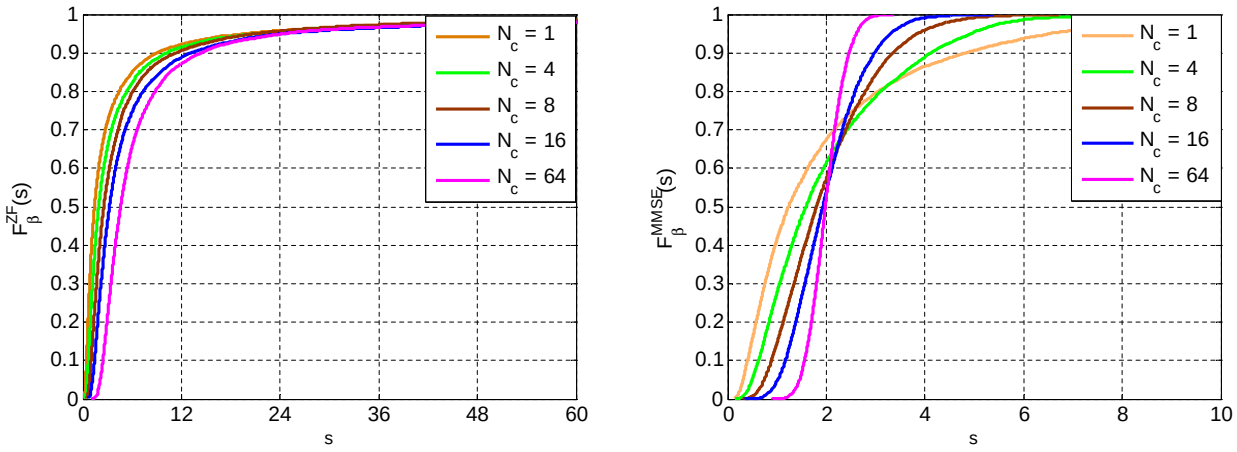

Figure A.6: CDF of β para respuestas en frecuencia correladas entre subportadoras con sombreado fuerte para ZF (izquierda) y MMSE (derecha) con IFDMA

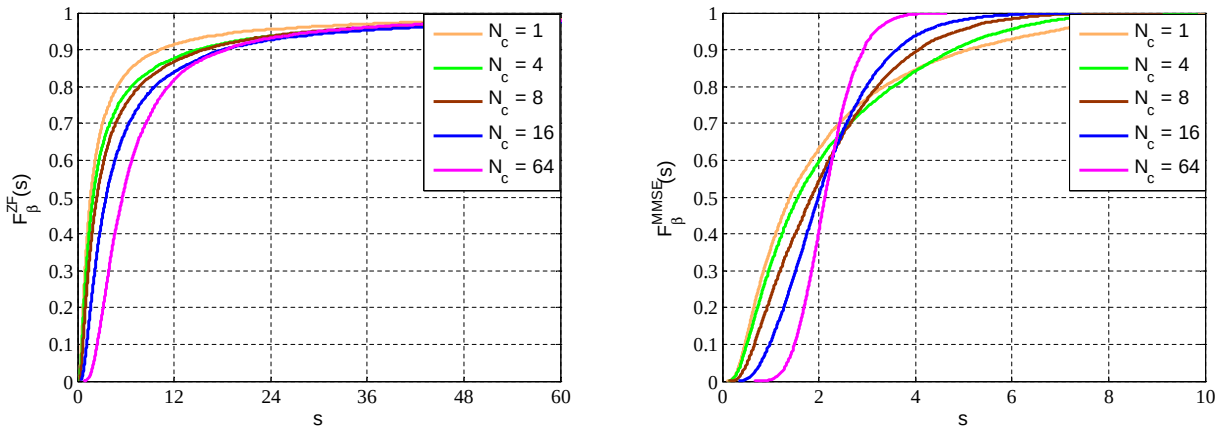

Figure A.7: CDF of β para respuestas en frecuencia correladas entre subportadoras con sombreado fuerte para ZF (izquierda) y MMSE (derecha) con LFDMA

evaluado los de β con (A.4.7) o eq. (A.5.8). Usando la condición de ergodicidad, su CDF se evalúa a partir del histograma. Los resultados en este caso se muestran en las figuras A.6 y A.7. Además, β toma estadísticamente valores menores que para el desvanecimiento medio o suave.

Desde estos resultados para subportadoras independientes, está claro que para la igualación ZF β puede alcanzar valores más altos debido al aumento del ruido por valores bajos de ganancia del canal. Por el contrario, la igualación MMSE fuerza un valor máximo de β. Esto también se observa en el comportamiento tan diferente para la igualación ZF y MMSE según N_c. Con la igualación ZF, reducir el número de subportadoras reduce el valor de β^{ZF} por lo que los valores para OFDM ($N_c = 1$) son menores. Por otra parte, en el caso de la igualación MMSE, el efecto es el contrario.

El efecto de la correlación en frecuencia puede verse comparando A.5, A.6 y A.7. Sólo se observan diferencias pequeñas para MMSE. Por el contrario, el uso de igualación ZF cuando hay mucha correlación en frecuencia, como en LFDMA, reduce el rango de β, forzado por la subportadora más desvanecida.

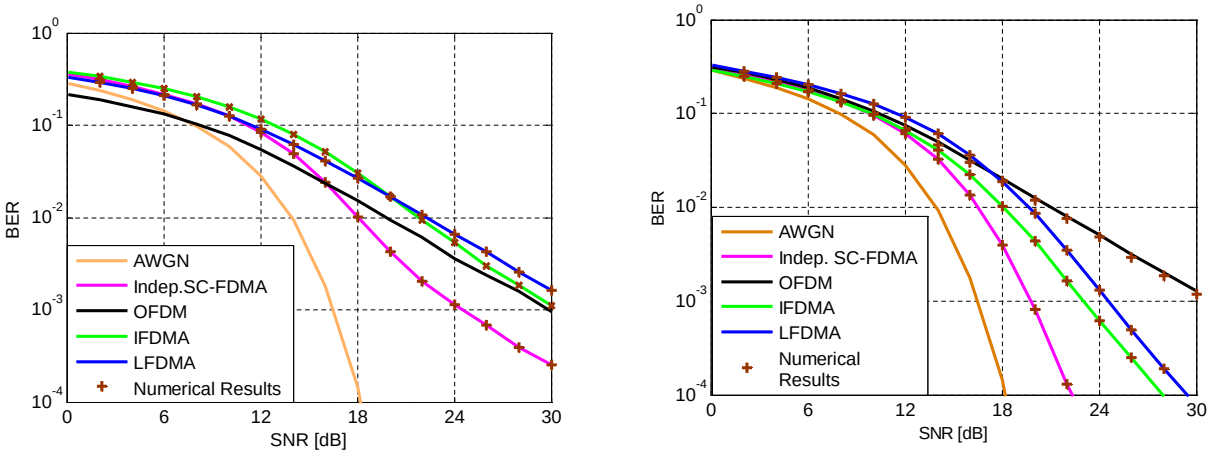

Figure A.8: BER para 16QAM para respuestas en frecuencia independientes entre subportadoras con sombreado suave, $N_c = 64$ e igualación ZF (izquierda) y MMSE (derecha)

Resultados de BER

La figura A.8 permite comparar la BER en canales con sombreado suave para igualación ZF y MMSE. Como se ha descrito anteriormente, para ZF, el valor de SNIR γ es siempre menor que el de OFDM y, como consecuencia, la BER es peor. En el caso de MMSE, la BER es, por el contrario, más pequeña para SC-FDMA. La correlación en frecuencia mejora el comportamiento de ZF mientras empeora el de MMSE.

La figura A.9 permite analizar el efecto del número de subportadoras. Se observa que aumentar el número de portadoras asignadas mejora el comportamiento para MMSE pero no así para ZF, limitada por la peor subportadora.

A.5 Eficiencia espectral de SC-FDMA para el canal LMS

La técnica de modulación y codificación adaptativa (Adaptive Modulation and Coding, AMC) se emplea en la mayor parte de los sistemas de comunicaciones actuales para mitigar la selectividad temporal. Básicamente, la modulación adaptativa sigue el canal de manera que, cuando su calidad es peor, se emplean esquemas con constelaciones/codificaciones más robustas. Por otra parte, si la calidad del canal mejora, crece la velocidad de transmisión a

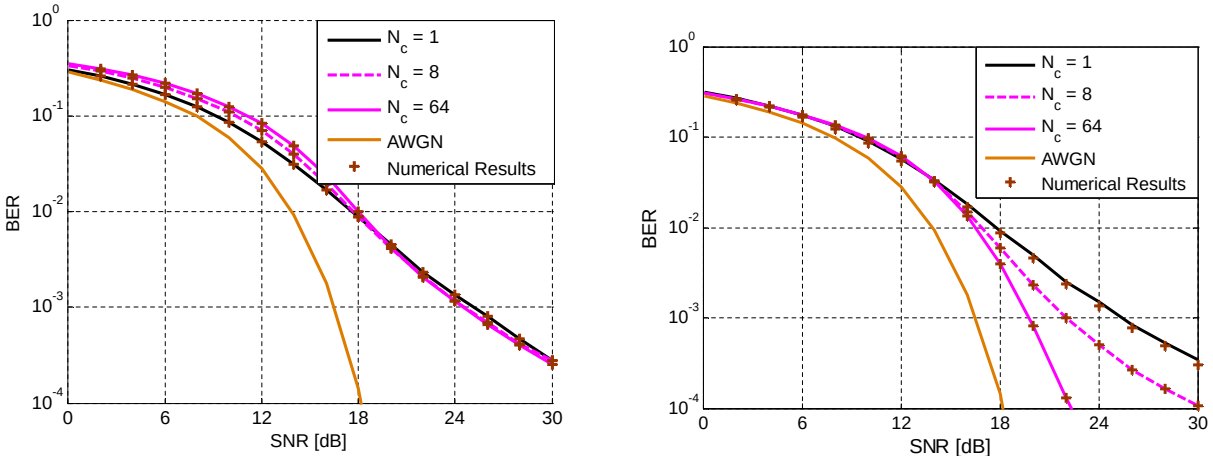

Figure A.9: BER para 16QAM para respuestas en frecuencia independientes entre subportadoras con sombreado suave, diferentes N_c e igualación ZF (izquierda) y MMSE (derecha)

coste de cómo de protegidos están los bits transmitidos.

A.5.1 Revisión de la modulación adaptativa

Se considera una modulación adaptativa con potencia constante y con un conjunto de constelaciones limitadas cuyos tamaños son $R_0 = 0$, $R_1 = 2$, and $R_i = 2^{2(i-1)}$, i=2 .. N.

Pueden emplearse varios criterios para asociar una constelación a cada SNR γ en la modulación adaptativa. En esta tesis se ha discretizado el nivel de desvanecimientos de tal manera que la BER se mantiene siempre bajo una objetivo, BER_T, que es un parámetro de diseño. Como se muestra en la figura A.10, el rango de γ se divide en N regiones $\Re_i = \{\gamma_i, \gamma_{i+1}\}$, $i = 0, 1, 2, ...N-1$ con $\gamma_0 = 0$ y $\gamma_N = \infty$. En la región $\Re_i$ se emplea una constelación QAM con R_i bits/símbolo. Para valores de SNR por debajo de un umbral mínimo (es decir, condiciones de canal muy pobres), hay un estado en el que no hay transmisión de datos. Los umbrales se han diseñado para maximizar la eficiencia espectral bajo la limitación de que la BER sea menor que BER_T. Dado que la BER es monótona decreciente con la SNR, los umbrales son aquellos valores que hacen la BER exactamente igual a la objetivo.

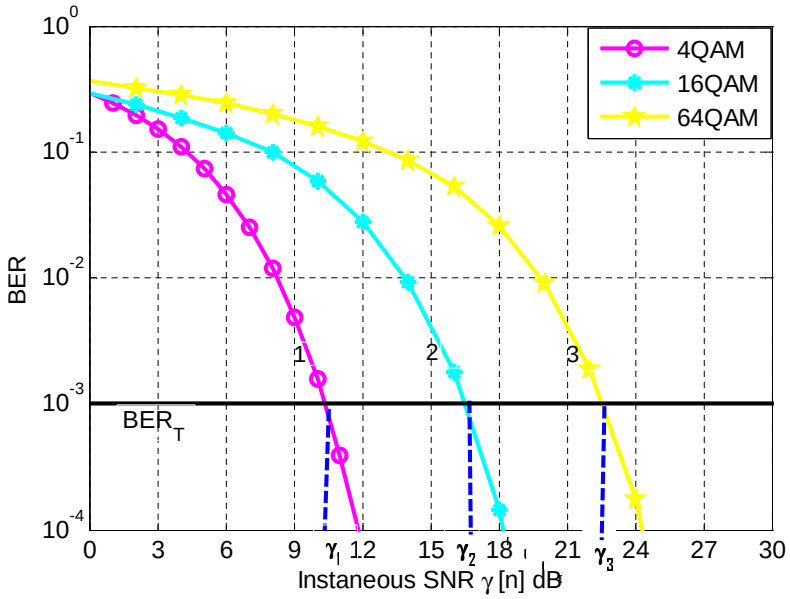

Figure A.10: Ejemplos de regiones de modulación adaptativa para QAM sin codificación

Sea cual sea el criterio tomado, la eficiencia espectral media puede escribirse como:

$$\frac{R}{B} = \sum_{i=1}^{L-1} \log_2 (M_i)\, Pr\{\gamma_{i-1} < \gamma \leq \gamma_i\}. \tag{A.5.1}$$

Valores más estrictos de BER_T implican eficiencias espectrales menores.

Para llevar a cabo la adaptación, la SNR instantánea tiene que ser estimada en el receptor, que determina la región de modulación $\Re_i$ e informa al transmisor. Ambas SNRs, media e instantáneas, se suponen perfectamente conocidas en el transmisor y en el receptor.

A.5.2 Análisis de la eficiencia espectral

ZF

Como se ha obtenido anteriormente, la SNR instantánea en el receptor para SC-FDMA con igualación ZF viene dada por

$$\gamma^{ZF} = \frac{E_S}{\beta^{ZF} N_0}, \tag{A.5.2}$$

donde β^{ZF} se definió como

$$\beta^{ZF} = \frac{1}{N_c} \sum_{k=1}^{N_c} \frac{1}{|h_k|^2}. \tag{A.5.3}$$

Para OFDM la misma expresión es válida haciendo $N_c = 1$. En ambos casos, la constelación correspondiente a la i-ésima región se aplica entre los umbrales, es decir,

$$\gamma_i < \frac{E_s}{\beta^{ZF} N_0} < \gamma_{i+1} \tag{A.5.4}$$

Puede reescribirse la ecuación anterior en función de unos umbrales para β^{ZF}:

$$\beta_{i+1}^{ZF} = \frac{1}{\gamma_{i+1}} \frac{E_S}{N_0} < \beta^{ZF} < \frac{1}{\gamma_i} \frac{E_S}{N_0} = \beta_i^{ZF} \tag{A.5.5}$$

donde β_i^{ZF} and β_{i+1}^{ZF} son los umbrales. Puede observarse que los umbrales así descritos dependen de E_s/N_0.

La eficiencia espectral puede promediarse entonces como:

$$\frac{R}{B} = \sum_{i=1}^{N-1} \log_2 (M_i) \left[F_{\beta^{ZF}} \left(\beta_i^{ZF} \right) - F_{\beta^{ZF}} \left(\beta_{i+1}^{ZF} \right) \right]. \tag{A.5.6}$$

donde N es el número de regiones de modulación. Obsérvese que sólo es necesaria la CDF $F_{\beta^{ZF}}(\beta^{ZF})$ dada por la ec. (A.4.11).

Análisis para MMSE

Para MMSE, el valor de la SNR en el receptor viene determinada por la ec. (A.4.29), repetida aquí por conveniencia:

$$\gamma^{MMSE} = \frac{E_s}{\sigma_\xi^2} = \frac{\frac{E_s}{N_0}}{\beta^{MMSE}} - 1. \tag{A.5.7}$$

donde

$$\beta^{MMSE} = \frac{1}{N_c} \sum_{j=1}^{N_c} \frac{1}{|h_j|^2 + N_0/E_S} = \sum_{j=1}^{N_c} \beta_j^{MMSE}. \tag{A.5.8}$$

El parámetro β^{MMSE} determina la SNR y la constelación que usar, esto es,

$$\beta_{i+1}^{MMSE} = \frac{1}{\gamma_{i+1}} \frac{E_S}{N_0} < \beta^{MMSE} < \frac{1}{\gamma_i} \frac{E_S}{N_0} = \beta_i^{MMSE} \tag{A.5.9}$$

con β_i^{MMSE} and β_{i+1}^{MMSE} , los umbrales modificados que, de nuevo, dependen de la SNR. La eficiencia espectral puede calcularse como

$$\frac{R}{B} = \sum_{i=1}^{N-1} \log_2 (M_i) \left[F_{\beta^{MMSE}} \left(\beta_i^{MMSE} \right) - F_{\beta^{MMSE}} \left(\beta_{i+1}^{MMSE} \right) \right]. \tag{A.5.10}$$

que, de nuevo, solo requiere la CDF $F_{\beta^{MMMSE}}(\beta^{MMSE})$.

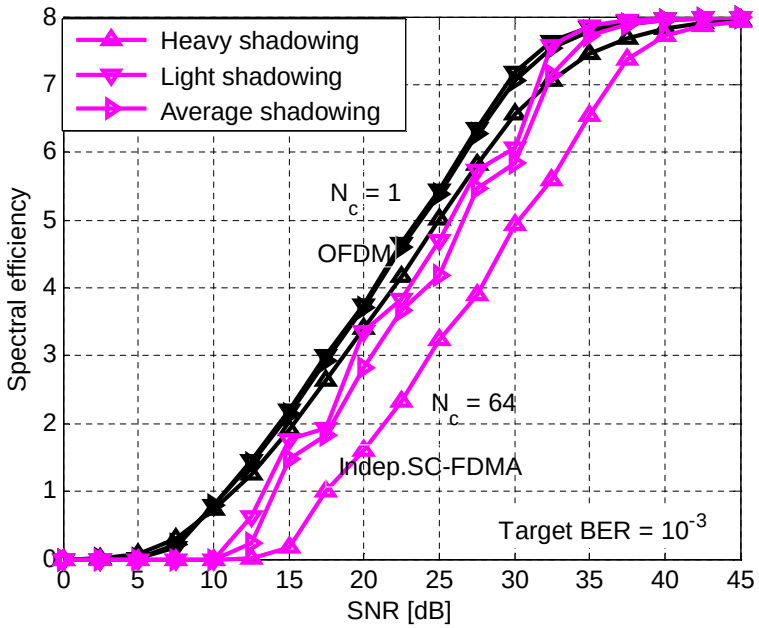

Figure A.11: Eficiencia espectral de OFDM y SC-FDMA para respuestas en frecuencia independiente entre subportadoras y diferentes sombreados con igualador ZF

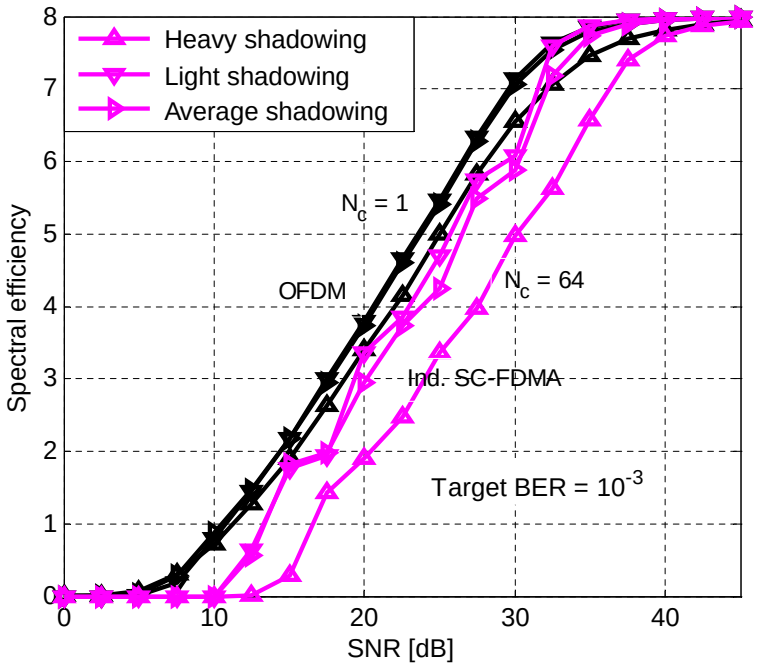

Figure A.12: Eficiencia espectral de OFDM y SC-FDMA para respuestas en frecuencia independientes entre subportadoras y diferentes sombreados con igualador MMSE

Table A.3: Umbrales entre regiones de modulación de SNR y eficiencia espectral por constelación

$\gamma_i(dB)$	9 .7980	16.5290	22.5510	28.4170
$log_2(M_i)$	2	4	6	8

A.5.3 Resultados

Los resultados presentados aquí se refieren a una BER de referencia $BER_T = 10^{-3}$. Valores más estrictos implican menor eficiencia espectral. El conjunto de umbrales $\{\gamma_i,\ i = 1, .., N-1\}$ se presenta en la tabla A.3.

Las figuras A.11 y A.12 muestran la eficiencia espectral de OFDM y SC-FDMA para respuestas en frecuencia independientes entre subportadoras y diferentes sombreados para los igualadores ZF y MMSE, respectivamente. El resultado para $N_c = 1$ se refiere a OFDM. Se observa que un aumento del número de subportadoras reduce la eficiencia espectral en SC-FDMA.

En cuanto a la forma que presentan las figuras, se observa que parecen escalones. Este comportamiento se nota más para un sombreado suave. La razón para esto puede encontrarse en el comportamiento de la pdf de β, que es muy estrecha. Esto implica que la mayor parte del tiempo se emplea un único esquema de modulación. En el caso de OFDM ($N_c = 1$), la pdf de β ocupa un rango más amplio, lo que, a través del promediado, resulta en un crecimiento más suave de la eficiencia espectral.

A.6 Rendimiento de SC-FDMA para técnicas de diversidad en recepción

A.6.1 Técnicas de diversidad en recepción

Esta tesis doctoral se centra en dos técnicas habituales de diversidad en recepción: combinación por selección (Selection Combining, SC) y combinación de máximo cociente (Maximal Ratio Combining, MRC). Para las dos técnicas, la meta es encontrar un conjunto de pesos para cada antena tal que el impacto de los desvanecimientos sea mínima para el usuario mientras se limita la complejidad tanto por la estimación como por el procesado. Se

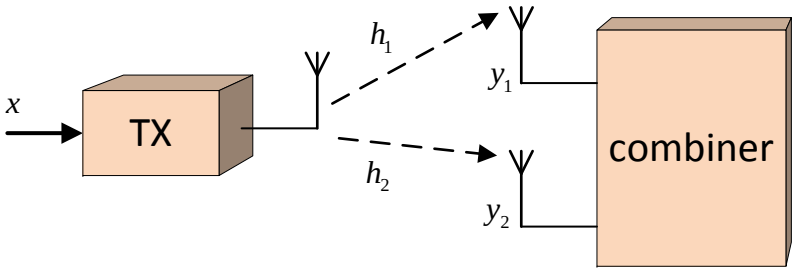

Figure A.13: Esquema de combinación de diversidad en recepción.

ha asumido que el receptor conoce de forma exacta el canal vector **h**.

Se considera un receptor con N_R antenas como muestra la figura A.13. Como se describió anteriormente, el canal puede expresarse como

$$\mathbf{h} = [h_1,\ h_2, .., h_{N_R}]^T. \tag{A.6.1}$$

La correlación entre antenas se expresa como el coeficiente de correlación ρ.

El conjunto de señales recibidas $\mathbf{R} = [R_1,\ R_2, .., R_{N_R}]^T$ puede entonces escribirse como

$$\mathbf{R} = \sqrt{\frac{E_s}{N_0}}\mathbf{h}x + \mathbf{n} \tag{A.6.2}$$

siendo x la única señal transmitida. El vector **n** está formado por muestras de ruido blanco. Cada término del vector de señales recibidas puede escribirse como

$$R_n = \sqrt{\frac{E_s}{N_0}}h_n x + n_n \tag{A.6.3}$$

y la SNR γ_n en la rama n-ésima rama viene dada por:

$$\gamma_n = \frac{E_s}{N_o}|h_n|^2. \tag{A.6.4}$$

Todas las ramas se combinan como una suma con ciertos pesos:

$$R^{COMB} = \mathbf{W}^T\mathbf{R} \tag{A.6.5}$$

donde $\mathbf{W} = [W_1\ W_2\ ..W_{N_R}]^T$ es el vector de pesos. Tras cierta manipulación, la señal combinada puedes escribirse como

$$R^{COMB} = \sqrt{\frac{E_s}{N_0}}x\sum_{n=1}^{N_R}W_n h_n + \sum_{n=1}^{N_R}W_n n_n. \tag{A.6.6}$$

La potencia media de la señal y del ruido vienen dadas, respectivamente, por

$$P_s = E_x\left[\left(\sqrt{\frac{E_s}{N_0}}\mathbf{W}^T\mathbf{h}x\right)^2\right] = \frac{E_s}{N_0}|\mathbf{W}^T\mathbf{h}|^2 \tag{A.6.7}$$

y

$$P_z = E_n\left[\left(\mathbf{W}^T\mathbf{n}\right)^2\right] = ||\mathbf{W}||^2, \tag{A.6.8}$$

con $||\cdot||$ la norma del vector. La SNR puede entonces escribirse como:

$$\gamma = \frac{P_S}{P_Z} = \frac{E_s}{N_0}\frac{|\mathbf{W}^T\mathbf{h}|^2}{||\mathbf{W}||^2}. \tag{A.6.9}$$

Maximal Ratio Combining (MRC)

MRC diseña el vector de pesos que maximiza la SNR γ. Invocando la desigualdad de Cauchy-Schwartz,

$$|\mathbf{W}^T\mathbf{h}|^2 \leq ||\mathbf{W}||^2||\mathbf{h}||^2. \tag{A.6.10}$$

La igualdad sólo se alcanza para un cierto vector (excepto constantes):

$$\mathbf{W}_{MRC} = \mathbf{h}^* \tag{A.6.11}$$

La SNR máxima es entonces:

$$\gamma^{MRC} = \frac{E_S}{N_o} \tag{A.6.12}$$

Equal Gain Combining (EGC)

En este caso, se simplifica el vector de pesos para evitar el escalado de amplitud. Aún hay que poner en fase todas las entradas antes de combinar [43] para evitar la cancelación de las señales.

A.6.2 Modelo de sistema SC-FDMA SIMO

Mientras el transmisor SC-FDMA no se modifica, el receptor con N_R antenas se presenta en la figura A.14.

Como se ha comentado anteriormente, la respuesta en frecuencia del canal en la j-ésima rama puede representarse por el vector $\mathbf{H}_j = [h_{i,j}]^T$, con $h_{i,j}$ el coeficiente entre la antena

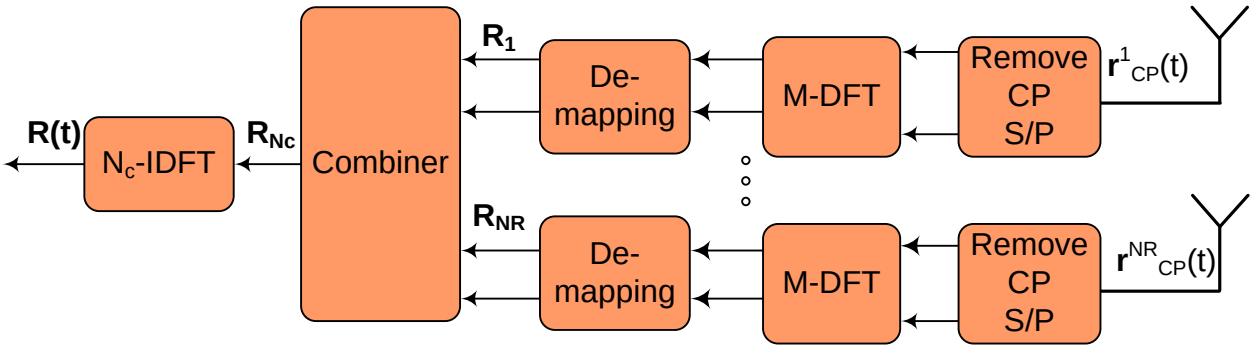

Figure A.14: Esquema de recepción SIMO SC-FDMA

transmisora y la j-ésima antena receptora en la subportadora i-ésima subportadora. $\mathbf{H}_j$ sigue cualquier modelo en frecuencia descrito anteriormente.

Las respuestas en frecuencia del canal para cada subportadora puede escribirse a su vez como un vector con las respuestas en cada camino, $\mathbf{h}_i = [h_{i,j}]^T, j = 1..N_R$. Estas se combinan como muestra la figura A.14. El prefijo cíclico es suprimido y la transformada de Fourier discreta transfiere el símbolo al dominio de la frecuencia. Posteriormente, se demapeo la señal recibida en cada antena. El vector de señales en la portadora i-ésima puede escribirse como:

$$\mathbf{R}_i = \mathbf{h_i} s_i + \mathbf{n} \tag{A.6.13}$$

donde $\mathbf{n}$ es un vector de ruido cuyas entradas son gaussianas complejas $CN(0, N_0)$ i.i.d. Las N_R señales se combinan en frecuencia usando el vector de pesos $\mathbf{W_i} = [W_{i,j}]$ y normalizado para permitir la detección. Específicamente, el resultado de MRC se obtiene con el vector de pesos $W_{i,j} = h^*_{i,j}$, de manera que el vector de señales puede escribirse como:

$$R_i^{MRC} = \frac{\sum_{j=1}^{N_R} R_{i,j} h^*_{i,j}}{\sum_{j=1}^{N_R} |h_{i,j}|^2}. \tag{A.6.14}$$

Para EGC [46], las N_R señales se combinan compensando la fase pero sin modificar la amplitud:

$$R_i^{EGC} = \frac{\sum_{j=1}^{N_R} R_{i,j} \exp\left(-\jmath \cdot angle(h_{i,j})\right)}{\sum_{j=1}^{N_R} |h_{i,j}|}. \tag{A.6.15}$$

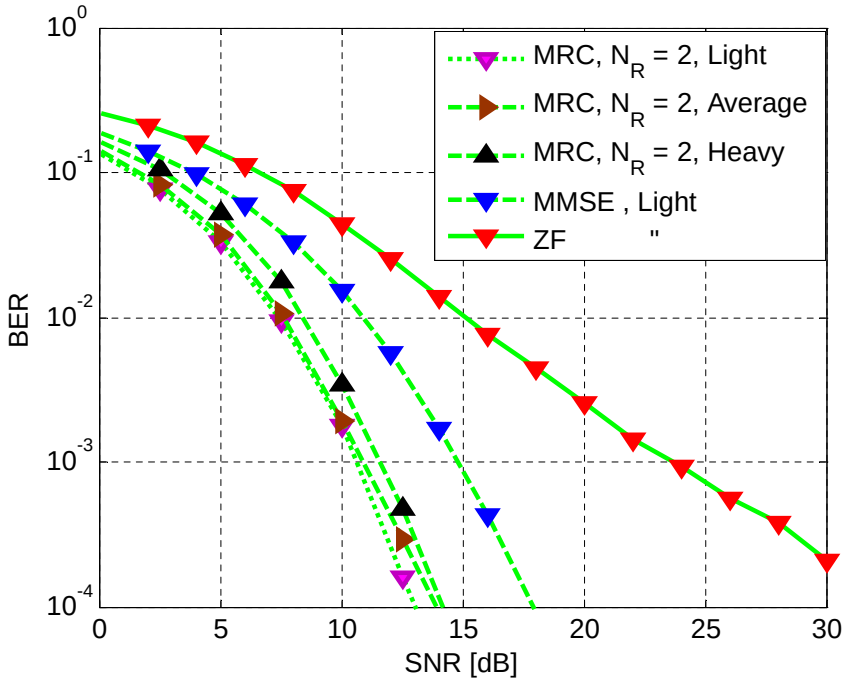

Figure A.15: BER para SIMO MRC y SISO con igualación MMSE y ZF para IFDMA con QPSK, 64 subportadoras

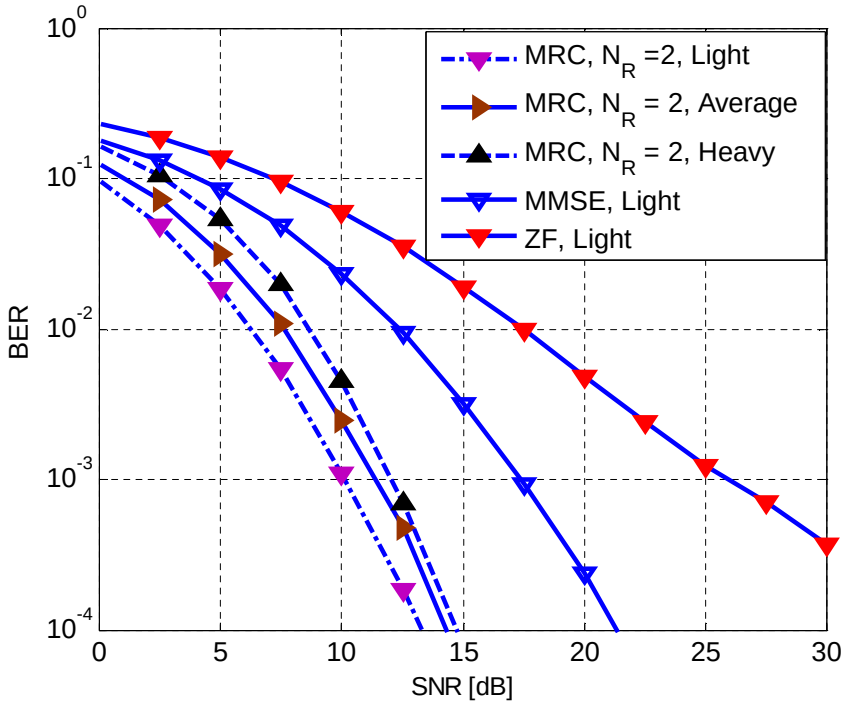

Figure A.16: BER para SIMO MRC y SISO con igualación MMSE y ZF para LFDMA con QPSK, 64 subportadoras, con diversos sombreados en el canal

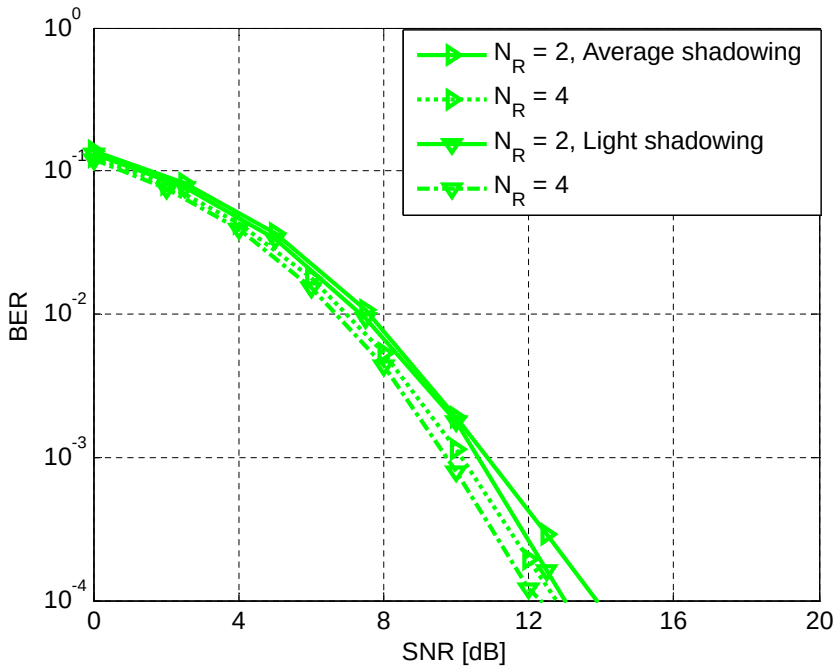

Figure A.17: BER para MRC IFDMA con diferente número de antenas receptoras (N_R) para QPSK, 64 subportadoras, con diversos sombreados en el canal

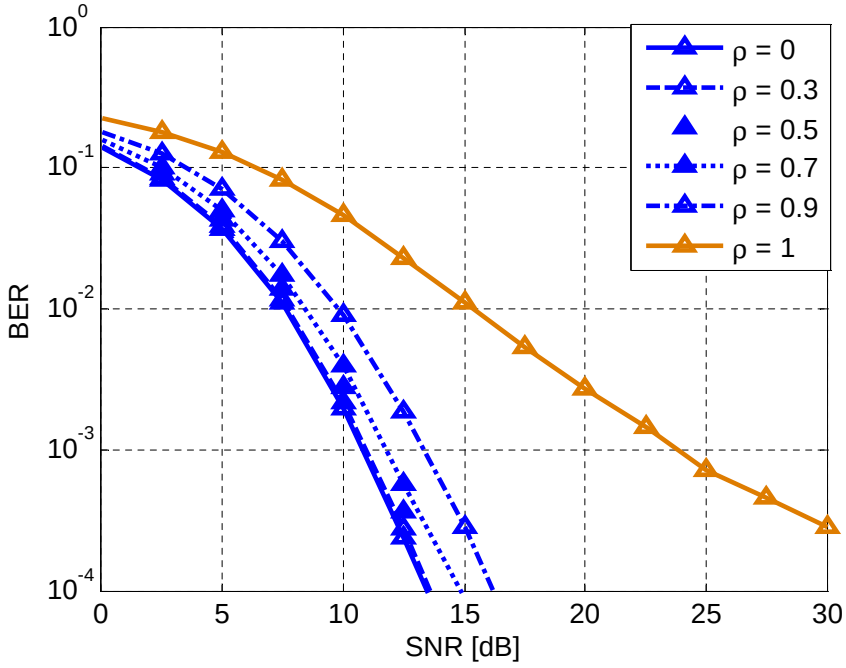

Figure A.18: BER para SIMO MRC LFDMA con diferente correlación entre antenas (ρ) para QPSK, 64 subportadoras, con sombreado fuerte

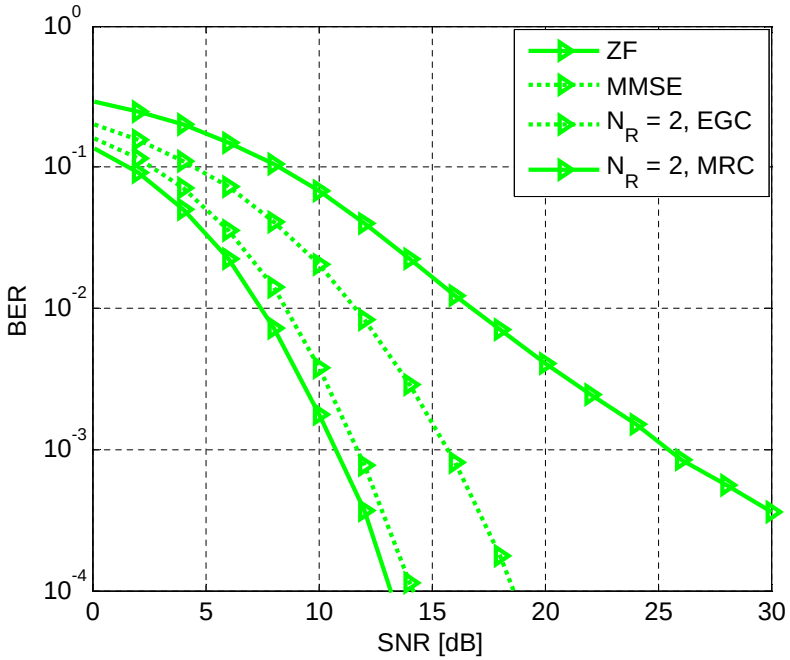

Figure A.19: BER para SIMO EGC y MRC junto a la de SISO con igualación MMSE y ZF para IFDMA con QPSK, 64 subportadoras, sobre sombreado medio

A.6.3 Resultados

Los parámetros usados para el modelado del canal se mostraron en la tabla A.1. Los parámetros para SIMO SC-FDMA se muestran en la tabla A.4.

Las figuras A.15 y A.16 comparan la probabilidad de error binaria para SIMO y SISO en varios escenarios para SF-FDMA entrelazada (IFDMA) y localizada (LFDMA), respectivamente. Los resultados se muestran para dos antenas receptoras, $N_R = 2$, excepto que se explicite de otra forma. En ambos casos, el rendimiento de IFDMA con MRC es mejor que el de una única antena receptora para ambas técnicas de igualación, ZF and MMSE ya que SIMO MRC es capaz de explotar la diversidad de ambas antenas.

El efecto del número de antenas en el receptor puede observarse en la figura A.17. Como era de esperar, un aumento del número de antenas mejora la BER. Sin embargo, se observa que la mayor parte de la ganancia se obtiene con el uso de una segunda antena.

Los resultados anteriores se habían obtenido asumiendo independencia entre señales recibidas en distintas antenas. La figura A.18 muestra la BER de LFDMA en función del

Table A.4: Parámetros de simulación para SIMO SC-FDMA

Tamaño de la FFT	1024
Esquema de modulación	QPSK
Frecuencia de portadora	2.00 GHz
Ancho de banda del sistema	20.00 MHz
Modelo de canal	LMS con perfil exponencial
Número de antenas	$2 por defecto, 4$
Técnicas de diversidad	MRC, EGC
τ_{avg}	$1.17 \mu s$

factor de correlación para varios canales. Se observa que, a medida que crece el factor de correlación, la BER crece. La razón es que existe menos diversidad.

Se muestra en la figura A.19 una comparación entre EGC y MRC con dos antenas receptoras. EGC es ligeramente peor que MRC pero, aun así, mejor que la igualación con una única antena.

A.7 Conclusiones y líneas futuras

En esta tesis, se ha presentado el trabajo desarrollado para el análisis de rendimiento en términos de BER, eficiencia espectral y diversidad de un receptor SC-FDMA para el canal sombreado Rice móvil terrestre por satélite (LMS). En primer lugar, se han introducido las tecnologías de capa física utilizadas y diferentes tipos de modelos de canal para llevar a cabo análisis anterior mencionado. A continuación, se ha evaluado el rendimiento de SC-FDMA para canales con sombreado fuerte, medio y ligero con igualación ZF y MMSE. Se ha analizado también la eficiencia espectral de SC-FDMA, y se ha estudiado la ganancia por usar varias antenas receptoras. Los resultados obtenidos se compararon con los de OFDMA.

Algunas líneas futuras posibles son estas:

- Análisis de SC-FDMA en canales LMS con la línea de visión directa siguiendo una distribución lognormal.

Table A.4: Parámetros de simulación para SIMO SC-FDMA

Tamaño de la FFT	1024
Esquema de modulación	QPSK
Frecuencia de portadora	2.00 GHz
Ancho de banda del sistema	20.00 MHz
Modelo de canal	LMS con perfil exponencial
Número de antenas	2 por defecto, 4
Técnicas de diversidad	MRC, EGC
τ_{avg}	1.17μs

factor de correlación para varios canales. Se observa que, a medida que crece el factor de correlación, la BER crece. La razón es que existe menos diversidad.

Se muestra en la figura A.19 una comparación entre EGC y MRC con dos antenas receptoras. EGC es ligeramente peor que MRC pero, aun así, mejor que la igualación con una única antena.

A.7 Conclusiones y líneas futuras

En esta tesis, se ha presentado el trabajo desarrollado para el análisis de rendimiento en términos de BER, eficiencia espectral y diversidad de un receptor SC-FDMA para el canal sombreado Rice móvil terrestre por satélite (LMS). En primer lugar, se han introducido las tecnologías de capa física utilizadas y diferentes tipos de modelos de canal para llevar a cabo análisis anterior mencionado. A continuación, se ha evaluado el rendimiento de SC-FDMA para canales con sombreado fuerte, medio y ligero con igualación ZF y MMSE. Se ha analizado también la eficiencia espectral de SC-FDMA, y se ha estudiado la ganancia por usar varias antenas receptoras. Los resultados obtenidos se compararon con los de OFDMA.

Algunas líneas futuras posibles son estas:

- Análisis de SC-FDMA en canales LMS con la línea de visión directa siguiendo una distribución lognormal.

- Análisis de SC-FDMA con varias antenas transmisoras y receptoras.
- SC-FDMA con diversidad en transmisión.
- SC-FDMA para un canal multiestado LMS.
- SC-FDMA con muchas antenas transmisoras y receptoras (Massive MIMO).
- Capacidad de SC-FDMA.

Bibliography

[1] P. Falcone, F. Colone, C. Bongioanni, and P. Lombardo, "Experimental results for OFDM Wi-Fi based passive bistatic radar," 2010 IEEE Radar Conference, pp. 516-521, Washington DC, USA, 10-14 May 2010

[2] M. Vijayalakshmi, S.R. Puranik, and L. Kulkarni, "A cross layer scheduling algorithm in IEEE 802.16e WiMAX standard to support PS traffic class," 2014 Fourth International Conference on Communication Systems and Network Technologies (CSNT), pp. 347-351, Bhopal, India, 7-9 April 2014

[3] 3^{rd} Generation Partnership Project (3GPP), "Evolved universal terrestrial radio access (E-UTRA)," Tech. Rep. 3GPP TR 36.942, January 2009 [Online]. Available: http://www.etsi.org

[4] ETSI, "Digital video broadcasting (DVB): Frame structure channel coding and modulation for a second generation digital terrestrial television broadcasting system (DVB-T2)," Tech. Rep. EN 302 755 V1.1.1, September 2009 [Online]. Available http://www.dvb.org/technology/dvbt2

[5] ETSI EN302 583, "Digital video broadcasting (DVB): Frame structure channel coding and modulation for Satellite Services to Handheld devices (DVB-SH) below 3 GHz," March 2008, Technical Report EN 302 583 V1.1.3, June 2010 [Online]. Available: http://etsi.org

[6] ETSI EN 302, 304, V1.1.1, "Digital video broadcasting (DVB); Transmission a system for handheld terminals (DVB-H)," 2004-2011

[7] S. Cioni, G.E. Corazza, M. Neri, and A. Vanelli-Corall, "On the use of OFDM Radio Interface for satellites digital multimedia broadcasting systems," International Journal for Satellite Communications and Networking, vol. 24, no. 2, pp. 153-167, March-April 2006

[8] S.C. Thompson, A.U. Ahmed, J.G. Proakis, J.R. Zeidler, and M.J. Geile, "Constant envelope OFDM," IEEE Transactions on Communications, vol. 56, no. 8, pp. 1300-1312, August 2008

[9] H.G. Myung, J. Lim, and D.J. Goodman, "Single carrier FDMA for uplink wireless transmission," IEEE Vehicular Technology Magazine, vol. 1, pp. 30-38, September 2006

[10] G.L. Stuber, Principles of mobile communications, Norwell, M.A. Kluwer Academic Publisher, 1996

[11] S. Janaaththanan, C. Kasparis, and B.G. Evans, "Comparison of SCFDMA and HSUPA in the return-link of evolved S-UMTS architecture", Proceedings of 2007 International Workshop on Satellite and Space Communications (IWSSC'07), pp. 56-60, Salzburg, Austria, 13-14 September 2007

[12] V. Dalakas, P.T. Mathioloulos, F. Di Cecca, and G. Galliano, "A comparative study between SC-FDMA and OFDMA schemes for satellite uplinks," IEEE Transactions on Broadcasting, vol. 58, no. 3, pp. 370-378, 2012

[13] H.G. Myung, "Single carrier orthogonal multiple access techniques for broadband wireless communications," Ph.D.Dissertation, Polytechnic University, Brooklyn, USA, January 2007

[14] M. Nisar, H. Nottensteiner, and T. Hindelang, "On performance limits of DFT spread OFDM systems," in 16^{th} IST Mobile and Wireless Communications Summit, pp. 1- 4, Budapest, Hungary, 1-5 July 2007

[15] J.J. Sánchez-Sánchez, M.C .Aguayo-Torres, and U.Fernández-Plazaola, "BER analysis for zero-forcing SC-FDMA over Nakagami-m fading channels," IEEE Transactions on Vehicular Technology, vol. 60, no. 8, pp. 4077 - 4081, 2011

[16] J.J. Sánchez-Sánchez, M.C. Aguayo-Torres, and U. Fernández-Plazaola, "Spectral efficiency of adaptive interleaved SC-FDMA over Nakagami-m fading channels," IEEE Transactions on Vehicular Technology, vol. 62, no. 8, pp. 3663-3670, October 2013

[17] S. Rosati, G.E.Corazza, A. Vanelli-Coralli, "Coded SC-FDMA for broadband satellite return links," 6th Advanced Satellite Multimedia Systems Conference (ASMS) and 12^{th} Signal Processing for Space Communications Workshop (SPSC), 2012

[18] C. Loo, "A statistical model for a land mobile satellite link," IEEE Transactions on Vehicular Technology, vol. VT-34, pp. 122-127, 1985

[19] A. Abdi, W.C. Lau, M. Alouini, and M. Kaveh, "A new simple model for land mobile satellite channels: first- and second-order statistics," IEEE Transactions on Wireless Communications, vol. 2, no. 3, May 2003

[20] S. Hara and R. Prasad, "Multicarrier Techniques for 4G Mobile Communications," Universal Personal Communications, Artech House, 2003

[21] K. Fazel, S. Kaiser, Multicarrier spread spectrum systems, Chapter 5: Applications, Willey, 2003

[22] R. Nee, R. Prasad, OFDM for wireless multimedia communications, Artech House, Inc., Norwood, USA, 2000

[23] J. van de Beek, P.Odling, S. Wilson and P. Borjesson, Review of Radio Science, 1996-1999, Orthogonal Frequency Divison Multiplexing (OFDM), Wiley, 2002

[24] M. Ergen, Mobile Broadband Including WiMAX and LTE, Springer Science+Business Media, LLC, 1^{st} edition, 2009, ISBN: 0387681892

[25] H.G. Myung and D.J. Goodman, Single-Carrier FDMA: a new air interface for long term evolution, Wiley Series on Wireless Communications and Mobile Computing, John Wiley and Sons, October 2008

[26] B. Sklar, Digital Communications: Fundamentals and Applications, Prentice Hall, 2002

[27] F.P. Fontan, M.V. Castro, C. Enjamio Cabado, J. Pita Garcia and E.Kubista, "Statistical modeling of the LMS channel," IEEE Transactions on Vehicular Technology, vol. 50, no. 6, November 2001

[28] J.V. Evans, "Satellite systems for personal communications," Proceedings of IEEE, vol. 86, pp. 1325-1341, July 1998

[29] G.E. Corazza and F. Vatalaro, "A statistical model for land mobile satellite channels and its application to nongeostationary orbit system," IEEE Transactions on Vehicular Technology, vol. 43, no. 3, August 1994

[30] R.L. Campbell, R. Estus, "Attenuated direct and scattered wave propagation on simulated land mobile satellite service path in the presence of trees," in Proceedings of Mobile Satellite Conference, pp. 101-106, Pasadena, USA, May 1988

[31] M. Abramowitz and I.A. Stegun, Handbook of mathematical functions with formulas, graphs, and mathematical tables, Dover, New York, 1964

[32] J.V. Rees, "Measurements of the wide band radio channel characteristics for rural, residential, and suburban areas," IEEE Transactions on Vehicular Technology, vol. 36, pp. 2-6, February 1987

[33] J.G. Proakis, Digital Communications, Mc-Graw-Hill, New York, 2000

[34] J. Gil-Peláez, "Note on the inversion theorem'," Biometrika, vol. 38, no. 3/4, pp. 481-482, 1951

[35] F. López-Martínez, E. Martos-Naya, J. Paris, U. Fernández Plazaola, "Generalized BER analysis of QAM and its application to MRC under imperfect CSI and interference in Ricean fading channels," IEEE Transactions on Vehicular Technology, vol. 59, no. 5, pp. 2598-2604, June 2010

[36] J.R. Gangane, M.C. Aguayo-Torres, J.J. Sánchez-Sánchez, and U. Fernández Plazaola, "SC-FDMA Performance over Rician Channel," Proceedings of 6^{th} IEEE International Conference on Broadband and Biomedical Communications (IB2Com), Melbourne, Australia, November 21-24, 2011

[37] A. Goldsmith, Wireless Communications, Cambridge University Press, 2005

[38] J.J. Sánchez-Sánchez, M.C. Aguayo-Torres, and U. Fernández Plazaola, "Analysis of SC-FDMA Spectral Efficiency over Rayleigh Fading Channels", in Workshop on Broadband Single-Carrier and Frequency Domain Communications at IEEE GLOBECOM 2010, Miami, USA, 6-10 December 2010

[39] W. Bai, D. Yan, Y. Xiao, and L. Shaoqian, "Performance evaluation of MIMO SC-FDMA system with FDE receiver," International Conference on Wireless Communications and Signal Processing (WCSP), pp. 1-5, Nanjing, China, 13-15 November 2009

[40] D. Tse, P. Viswanath, Fundamentals of Wireless Communications, Cambridge University Press, New York 2005

[41] M.K. Simon, M.S. Alouini, Digital communication over fading channels, Wiley Series in Telecommunications and Signal Processing, John Wiley and Sons, 2005

[42] Y.S. Cho, J. Kim, W.Y. Yang, and C.G. Kang, MIMO-OFDM wireless communications with MATLAB. John Wiley and Sons, 2010

[43] A. Annamalai, C. Tellambura, and V.K. Bhargava, "Equal-gain diversity reciver performance in wireless channels," IEEE Transactions on Communications, vol. 48, pp. 1732-1745, October 2000

[44] N.C. Beaulieu and A.A. Abu-Dayya, "Analysis of Equal Gain Diversity on Nakagami fading channels," IEEE Transactions on Communications, vol. 39, no .2, pp. 225-234, February 1991

[45] J. Zang, L.L.Yang, and L. Hanzo, "Multiuser performance of the amplify and forward single relay assisted SC-FDMA uplink," IEEE Vehicular Technology Conference 2009 Fall, 20-23 September 2009

[46] J.R. Gangane, M.C. Aguayo-Torres, J.J. Sánchez-Sánchez, and S. Wagh, "Equal Gain Combining (EGC) SC-FDMA Performance over Land Mobile Satellite (LMS) Rice Fading Channel," IEEE International Conference on Computational Intelligence and Computing Research (IEEE ICCIC), Coimbatore, India, 20-22 December 2012

[47] J.R. Gangane, M.C. Aguayo-Torres, and J.J. Sánchez-Sánchez, "Maximal Ratio Combining SC-FDMA Performance over Correlated Rician Channels," Eighth International Conference on Wireless and Mobile Communications (ICWMC), Venice (Italy), June 2012